

**SPATIAL FOLIAGE DISTRIBUTION MODELS  
FOR WESTERN LARCH (*LARIX OCCIDENTALIS*)**

A Thesis

Presented in Partial Fulfillment of the Requirements for the

Degree of Master of Science

with a

Major in Natural Resources

in the

College of Graduate Studies

University of Idaho

by

Geoffrey Michael Williams

Major Professor: Andrew Nelson, Ph.D.

Committee Members: Mark Coleman, Ph.D.; Randy Brooks, Ph.D.

Department Administrator: Randy Brooks, Ph.D.

August 2017

**AUTHORIZATION TO SUBMIT**

This thesis of Geoffrey Michael Williams, submitted for the degree of Master of Science with a Major in Natural Resources and titled “SPATIAL FOLIAGE DISTRIBUTION MODELS FOR WESTERN LARCH (*LARIX OCCIDENTALIS*),” has been reviewed in final form.

Permission, as indicated by the signatures below, is now granted to submit final copies to the College of Graduate Studies for approval.

Major Professor: \_\_\_\_\_ Date: \_\_\_\_\_

Andrew Nelson, Ph.D.

Committee Members: \_\_\_\_\_ Date: \_\_\_\_\_

Mark Coleman, Ph.D.

\_\_\_\_\_ Date: \_\_\_\_\_

Randy Brooks, Ph.D.

Department

Administrator: \_\_\_\_\_ Date: \_\_\_\_\_

Randy Brooks, Ph.D.

## ABSTRACT

Western larch (*Larix occidentalis* Nutt.) provides high-value lumber and wildlife habitat but is threatened by fire suppression and climate change. Crown foliage allocation was studied to enrich knowledge of western larch production ecology. Analysis of spatial models revealed that western larch produces foliage in an increasingly diffuse distribution as the crown lengthens. Unlike other conifers, foliar biomass increased linearly with DBH, indicating significant constraints on crown volume-filling. Specific leaf area (SLA) increased on the south side of the crown. Leaf area peaked closer to the bole in the southwest quadrant. Intrinsic variables accounted for less variance in horizontal foliage distribution compared to vertical distribution. The characteristic intrinsic dynamics of spatial foliage distribution and SLA variation are consistent with a hypothesis of plasticity to hydraulic and light conditions. The amount and distribution of foliar biomass and leaf area reflect the mesic site preference, deciduous habit, and shade intolerance of western larch.

## ACKNOWLEDGEMENTS

I am grateful for the opportunity to complete a graduate degree at the University of Idaho. Completion of this thesis would simply not have been possible without support and guidance of the faculty, research staff, and support staff in the College of Natural Resources. I am indebted to Andrew Nelson, who agreed to mentor me with short notice, knowing I had little background in the field of silviculture. The dedicated confidence he put in me as his student was indispensable. It would have been impossible for me to complete this work without his guidance. Dave Affleck of the University of Montana provided the majority of the data used in Chapter 2, thereby permitting a truly representative sample of western larch foliage. Jon Cherico, Gus Reely, and Michael Skandalis put in many hours over the summer of 2016 to harvest trees in the field. The combined assistance of Sundee Lamb and Ella Salkeld in the processing of foliage in the lab within a short timeframe ultimately permitted the completion of the present thesis.

Randy Brooks and Mark Coleman have both provided support and friendly advice. Over the course of my short time at the University of Idaho, Dan Johnson imparted valuable ecophysiology knowledge innumerable times, which was particularly helpful in interpreting the results in Chapter 3. I also owe Dave Tank for his professional encouragement, and course instructors including Jack Sullivan, Audrey Fu, Sanford Eigenbrode, and Lori Carris for countless memorable lessons that will serve me for many years to come. Mina Ashkannejhad generously copyedited a large portion of this manuscript. Most of all, I owe immeasurable gratitude to every person who challenged me to trust in my own abilities, to think harder, to be resourceful, and to work on improving myself and the world around me.

## **DEDICATION**

To my family for their support, encouragement, and example.

## TABLE OF CONTENTS

AUTHORIZATION TO SUBMIT THESIS .....	ii
ABSTRACT .....	iii
ACKNOWLEDGEMENTS .....	iv
DEDICATION .....	v
TABLE OF CONTENTS .....	vi
LIST OF FIGURES .....	viii
LIST OF TABLES .....	ix
I BACKGROUND ON WESTERN LARCH AND CROWN MODELING .....	1
1.1 Western larch: autecology and management considerations .....	1
1.1.1 Autecology and silvics of western larch .....	1
1.1.2 Management of larch forests in the INW .....	4
1.2 Crown biomass modeling, applications, and previous studies of <i>Larix</i> spp .....	7
1.2.1 Historical review of the theoretical foundations of crown modeling.....	7
1.2.2 Applications of tree crown models .....	11
1.3 Spatial foliage distribution modeling.....	14
1.3.1 Rationale and applications .....	14
1.3.2 Statistical methods for modeling spatial foliage distribution.....	16
1.4 Works cited .....	22
II VERTICAL DISTRIBUTION OF FOLIAR BIOMASS IN WESTERN LARCH.....	29
2.1 Abstract .....	29
2.2 Introduction .....	29
2.3 Materials and methods .....	33
2.3.1 Study site and data collection.....	33
2.3.2 Branch foliar mass models .....	34
2.3.3 Crown foliar mass models.....	36
2.3.4 Vertical distribution of foliage in the crown.....	39
2.4 Results .....	41
2.4.1 Branch foliar mass model .....	41

2.4.2 Crown foliar mass model .....	43
2.4.3 Vertical distribution of foliage in the crown .....	44
2.5 Discussion .....	51
2.5.1 Branch foliar mass.....	51
2.5.2 Crown foliar mass .....	52
2.5.3 Vertical distribution of foliage in the crown .....	54
2.5.4 Conclusions .....	56
2.6 Works cited .....	59
<b>III SPATIAL VARIATION IN SPECIFIC LEAF AREA AND HORIZONTAL</b>	
<b>DISTRIBUTION OF LEAF AREA IN JUVENILE WESTERN LARCH .....</b>	<b>64</b>
3.1 Abstract .....	64
3.2 Introduction .....	64
3.3 Materials and methods .....	67
3.3.1 Study site and data collection.....	67
3.3.2 Specific leaf area models .....	70
3.3.3 Horizontal distribution of leaf area along branches .....	71
3.4 Results .....	73
3.4.1 Specific leaf area model .....	73
3.4.2 Horizontal distribution of leaf area along branches .....	75
3.5 Discussion .....	83
3.5.1 Specific leaf area .....	83
3.5.2 Horizontal distribution of leaf area along branches .....	86
3.5.3 Conclusions .....	88
3.6 Works cited .....	91
<b>IV APPENDIX .....</b>	<b>96</b>

## LIST OF FIGURES

2.1	Sites where <i>L. occidentalis</i> were harvested for the study .....	34
2.2	Branch foliar mass predicted by Equation [2.1].....	42
2.3	Crown foliar mass predicted by Equation [2.2] .....	44
2.4	Crown foliar mass of <i>L. occidentalis</i> compared to other species.....	45
2.5	Error and absolute bias of Weibull bin FM predictions by tree size.....	46
2.6	Predicted vertical foliar mass distribution for representative trees by height class .....	48
2.7	Predicted vertical foliar mass distribution for representative trees by TH and CL.....	49
2.8	Predicted vertical foliar mass distribution by TH, CL and DBLC quartile .....	50
3.1	Predicted specific leaf area by quadrant and RPAB, HMC and HIC quartile .....	74
3.2	Root mean squared error and mean absolute bias for binning schemes and PDFs.....	76
3.3	RMSE and MAB of fitted Weibull distribution by RPAB with 13 bins.....	76
3.4	Correlation between absolute bias and leaf area averaged across trees for each bin....	76
3.5	Predicted horizontal distribution of LA density for SW versus other quadrants .....	78
3.6	Fitted Weibull curve and actual foliage from four branches from the tallest tree .....	79
3.7	Fitted Weibull curve and actual foliage from four branches from intermediate tree....	80
3.8	Predicted horizontal distribution of LA density by RDIC, HBLC and TBL quartile ...	81
3.9	Predicted horizontal distribution for by RDIC quartile for correlated TBL and BD....	82

## LIST OF TABLES

1.1	Previously published models used to estimate branch foliage.....	19
1.2	Previously published models used to estimate total crown foliage.....	20
1.3	Previously published models used to estimate foliage distribution parameters.....	20
2.1	Variables tested to fit branch and tree level foliage models .....	35
2.2	Branches sampled for branch foliage models .....	37
2.3	Trees used to fit vertical foliar distribution models .....	38
2.4	Parameter estimates for branch and crown FM models .....	43
2.5	Fit statistics for PDFs .....	46
2.6	Parameter estimates for models of vertical foliage distribution kurtosis and skew .....	47
2.7	Fit statistics for models selected to estimate FM and its distribution .....	48
3.1	Summary of trees destructively harvested for leaf area study .....	68
3.2	Summary of branches harvested for leaf area study .....	68
3.3	Variables tested in model fitting .....	70
3.4	Parameter estimates for spatial SLA model .....	75
3.5	Fit statistics for PDFs .....	76
3.6	Fit statistics for SLA and horizontal LA distribution parameter models .....	77
3.7	Parameter estimates for horizontal Weibull skew and kurtosis models.....	78
A1	Summary of branches used to estimate CFM and fit vertical distribution models .....	96
A2	Models evaluated for goodness of fit to branch foliar mass .....	97
A3	Models evaluated for goodness of fit to total crown foliar mass .....	101
A4	Models evaluated for goodness of fit to Weibull kurtosis parameter estimates .....	102
A5	Models evaluated for goodness of fit to Weibull skew parameter estimates .....	103
B1	Summary of branch segments sampled for foliar mass .....	104
B2	Summary of branch segments sampled for specific leaf area .....	105
B3	Models evaluated for goodness of fit to specific leaf area.....	108
B4	Models evaluated for goodness of fit to Weibull kurtosis parameter estimates .....	112
B5	Models evaluated for goodness of fit to Weibull skew parameter estimates .....	115

## Chapter I

### BACKGROUND ON WESTERN LARCH AND CROWN MODELING

#### 1.1 Western larch: autecology and management considerations

##### 1.1.1 Autecology and silvics of western larch

Western larch (*Larix occidentalis* Nutt.) is an important forest tree species found in the Inland Northwest (INW) and the largest species in the genus *Larix*. The native range of *L. occidentalis* traverses British Columbia, Alberta, Washington, Oregon, Idaho, and Montana, where it is found on mesic, mid-elevation sites in the northern Rocky Mountains west of the continental divide, along the eastern slopes of the Cascades, and in the Wallowa and Blue Mountains. As of the early 1990s, *L. occidentalis*-dominated forests covered 2.3 million acres in the United States and 3% of forested areas in Washington, Oregon, Idaho, and Montana. *L. occidentalis* accounted for an estimated 6.0 billion cubic feet in timber volume in the US, and was expected to increase in volume by 1.7% annually (Conner and O'Brien 1992). Projected by twenty-five years, the Conner and O'Brien estimates would bring volume to approximately 9.5 billion cubic feet in the US in 2017. However, mortality and harvesting can fluctuate from one year to the next due to insects, disease, disturbance, and market pressures.

Temperature and precipitation appear to be the most significant factors restricting the natural range of *L. occidentalis*. The preferred habitat of *L. occidentalis* is cool mesic sites, particularly northern aspects, valleys, and drainage bottoms (Schmidt and Shearer 1990). Based on a model fit to data from 185,000 Forest Inventory and Analysis (FIA) plots in the INW, *L. occidentalis* most strongly prefers sites where a greater portion of total annual precipitation occurs in the summer and winters are milder (Rehfeldt and Jaquish 2010). The

preference of *L. occidentalis* for mesic sites is likely related to its high rates of stomatal water conductance and relative insensitivity of stomata to changes in vapor pressure deficit and water potential (Higgins et al. 1987). *Larix* spp. generally have lower water-use efficiency than evergreen conifers, but have a high capacity for water uptake from the roots (Gower and Richards 1990; Anfodillo et al. 1998; Oberhuber et al. 2015).

*L. occidentalis*, and its higher-elevation counterpart subalpine larch (*Larix lyallii* Parl.), are the only deciduous species among INW conifers. Historically it was hypothesized that annual net carbon gain should be higher in evergreens than sympatric deciduous conifers in milder climates due to a longer growing season (Waring and Franklin 1979). It has since been demonstrated that total aboveground production is similar between larch and evergreens (Gower and Richards 1990). Since *L. occidentalis* prefers milder sites, its ability to match evergreens in annual productivity despite needle shedding and dormancy could be due to higher rates of photosynthesis (Higgins 1987), higher specific leaf area (SLA), and/or overall lower investment cost for needle production and thus less loss to respiratory demands (Fry and Phillips 1977; Gower et al. 1989; Gower and Richards 1990). Needle arrangement and crown architecture, however, are also important factors in determining productivity.

In addition to turnover of annually deciduous foliage, other factors contribute to plasticity in crown development in *L. occidentalis*. Self-pruning and epicormic sprouting can lead to the eventual replacement of the entire crown over the course of the lifespan of older trees (Lanner 1992). Higher rates of foliage and branch turnover may partly explain the low incidence of disease in larch forests. *L. occidentalis* also differs from most other sympatric conifers in its capacity for sustained, indeterminate annual branch growth (Parent et al. 2008).

*L. occidentalis* is the most shade-intolerant conifer in the northern Rocky Mountains (Schmidt and Shearer 1990). *Larix* spp. are generally extremely shade-intolerant. In an out-planting study, *L. occidentalis* had a significantly lower survival rate when subjected to low light conditions, but SLA, shoot-to-root ratio, and height growth were not plastic to light level (Chen and Klinka 1998). These findings partly account for the preference of *L. occidentalis* for disturbed sites, and indicate inflexibility to acclimate to changes in light conditions such as shifts in social position during stand development. *L. occidentalis* is a pioneer species, but can be long-lived (Schmidt and Shearer 1976). On open and disturbed sites, newly-established seedlings quickly overtop other species through superior height growth.

On mesic sites where *L. occidentalis* grows, climax communities may include more shade-tolerant species such as Douglas-fir [*Pseudotsuga menzeisii* var. *glauca* (Beissn.) Franco], grand fir [*Abies grandis* (Dougl. ex D. Don) Lindl.], western redcedar (*Thuja plicata* Donn ex D. Don), and western hemlock [*Tsuga heterophylla* (Raf.) Sarg.]. Alternatively, when not overtopped by shade-tolerant successors, *L. occidentalis* can persist as a co-dominant species on drier sites with other shade intolerant species such as lodgepole pine (*Pinus contorta* Dougl. ex Loud.) and ponderosa pine (*P. ponderosa* Dougl. ex Laws.). *L. occidentalis* can live 500-1000 years if conditions remain favorable (Arno et al. 1997).

Fire exclusion is a primary factor that promotes transition in stand composition from *L. occidentalis* to more shade-tolerant species. With its thick bark, *L. occidentalis* is the most fire-resistant tree species in the northern Rocky Mountains (Schmidt and Shearer 1990). Historically *L. occidentalis* forests typically experienced regular fire return intervals of approximately 25 years (Arno et al. 1997). Under favorable conditions, *L. occidentalis* produces a large volume of small seeds that only germinate on the bare mineral soils typical

of recent fire disturbance events (Schmidt and Shearer 1976). However, the phenology of seed production is climatically dependent. Early spring warm spells followed by late spring freezes frequently lead to sporadic, unreliable cone crops in Idaho (Parent et al. 2008).

### *1.1.2 Management of western larch forests in the INW*

*Larix occidentalis* is ecologically and aesthetically valuable from a variety of perspectives. As a fire-adapted species, *L. occidentalis* is arguably central to public agencies' collective effort to restore natural fire cycles to the INW. Dead larch trees become persistent snags that are favored by cavity-nesting birds (McClelland et al. 1979). Medium-sized larch is preferred over other trees for juicy phloem by bears during summer months when food is limiting (Parent et al. 2008). The range of *L. occidentalis* is restricted geographically and climatically compared to most sympatric conifers, making *L. occidentalis* forests and associated flora an important, endemic component of INW plant communities. Culturally *L. occidentalis* is valued as a historic component of the landscape, as well as for its displays of senescent bright yellow foliage in the fall. In terms of ecosystem services, relatively high rates of carbon assimilation and storage can be expected given superior growth rates, making *L. occidentalis* important in biogeochemical cycling and climate change mitigation.

*L. occidentalis* is also highly valuable from an economic perspective. *L. occidentalis* is the fastest growing conifer by height increment in the northern Rocky Mountains (Schmidt and Shearer 1990). It also has the densest wood of sympatric conifers, by comparison of specific gravity (Kretschmann 2010). Larch gum is an important product in the industrial biochemical industry (Parent et al. 2008). As a fast- and tall-growing tree with dense wood

and a typically long, very straight and branch-free bole, *L. occidentalis* is useful as a source of high-value construction-grade lumber.

In recognition of its demonstrable ecological, economic, and cultural value, and the combined threats of fire repression and climate change to its continued presence in the region, *L. occidentalis* has been targeted as a focal species for future forest planning goals (Scott et al. 2013). Efforts to restore natural *L. occidentalis* forests in the inland INW will require renewed attention of researchers to the relative effects of management choices. It is known that fire repression has negatively impacted *L. occidentalis* within the native range. In the absence of fire disturbance, mesic sites have shifted to grand fir, western red cedar, and western hemlock. Over the last 100 years, a 67% reduction of fire frequency has led to understory invasion of old-growth Ponderosa-Larch sites by Douglas-fir and groundcover replacement of grasses with Ericaceous plants (Arno et al. 1997). Arno et al. (1997) also concluded that historical establishment of mixed-age and old-growth larch stands depended on pre-Colombian anthropogenic burning, further highlighting the importance of active management to the sustainability of INW forests.

In addition to the pressure from changing fire regimes, changing temperatures and moisture regimes are expected to shift the future suitable geographic range of *L. occidentalis* out of the US INW and further north into Canada in the coming decades (Rehfeldt and Jaquish 2010). Effort on the part of public agencies to aid the imminent range-shift of *L. occidentalis* will require regeneration strategies that employ seed selection informed by provenance testing (Rehfeldt 1995).

*L. occidentalis* shows different responses to thinning treatments depending on stand age. In a survey across sites, diameter growth was 50% lower in un-thinned stands, but

response to release was delayed in stands aged 30-50 or older due to crown reduction from overstocking (Schmidt and Shearer 1990). These observations are consistent with differences in lag time in response to thinning and release treatments observed across life histories and growing conditions (Oliver and Larson 1990). Long-term silvicultural and provenance research may not produce practical and needed results in the timeframe demanded by the imminent threats to *L. occidentalis*. By taking advantage of the influence of biomass allocation on light interception and growth potential (Horn 1971), short-term morphological responses can be used to predict long-term shifts in growth and stand structure (Buckley et al. 1997). An improved understanding of *L. occidentalis* crown structure and its plasticity to growing conditions will inform efforts to optimize management and restoration of larch forests in the INW.

The present study is motivated by the general goal of improving management techniques for timber production as well as restoring western forests to a more natural composition, structure, and disturbance regime. The future health of larch forests is of economic, aesthetic, and ecological importance to managers, public agencies, recreators, and the biosphere. Due to the demand for larch and threats from anthropogenic factors such as fire suppression and climate change, more information is needed on how *L. occidentalis* responds to changing stand conditions in pure and mixed stands if it is to be targeted for timber production, conservation, or regeneration in new, current, or past habitats. There is currently little or no information available on above-ground biomass allocation and spatial distribution for *L. occidentalis*. In order to establish a framework for silvicultural studies on crown development and response to treatments and to infer intrinsic biomass allocation strategies, baseline analysis of crown allometry and foliage distribution are needed for *L. occidentalis*.

## 1.2 Crown biomass modeling, applications, and previous studies of *Larix* spp.

### 1.2.1 Historical review of the theoretical foundations of crown modeling

Many decades of forestry research have been devoted to developing and testing empirical models for the estimation of the above ground structure of trees. Biometric models explain crown development through relations to tree and stand-level characters such as stem diameter. Ordered from early to contemporary, empirical crown development models include pipe-model theory (Shinozaki et al. 1964), profile theory (a modified pipe-model theory; Osawa et al. 1991), and allometric biomass scaling (Vose et al. 1994; Lacoïnte 2000). Hybrid empirical-process based theories include metabolic scaling (Duursma et al. 2010) and fractal space-filling (Ford 1985; Enquist et al. 1999). These models demonstrate that components of crown biomass scale with stem diameter in a predictable and quantifiable site-, species-, and age-dependent manner that can be related back to species life history strategy and growing environment.

The pipe-model theory relates stem diameter at a given height to the integral of foliar mass above that height via a direct proportionality (Shinozaki et al. 1964). The rationale for the pipe model theory is that each increment of stem cross-sectional mass is dedicated to a proportional unit of foliage above the location of the cross-section. The continued expansion of the bole below the crown is explained by the disuse of “unit pipes,” or dedicated portions of cross-sectional area, when branches above are shed. “Specific pipe length” is the proportionality constant between stem cross-sectional biomass and integrated foliage above unique to a given species. In contrast to *Abies* and *Picea* which had respective specific pipe lengths of 192 and 176, *Larix leptolepis* Sieb. & Zucc. had a specific pipe length of 70, much closer to that of deciduous and evergreen angiosperms such as *Betula* and *Ficus* than to

evergreen conifers. Lower specific pipe-length of *L. leptolepis* compared to evergreen conifers could indicate much higher wood density, lower rates of volume filling in the crown, and/or greater growth efficiency as defined by unit growth per unit foliage (Waring 1983).

As a modification to pipe-model theory, the profile theory predicts stem growth over time, and growth efficiency (stem increment divided by total foliage) from distribution of foliage mass above (Osawa et al. 1991). The profile theory assumes no change in vertical distribution of foliage mass within the crown and a constant upward shift of the entire crown distribution as the stem grows. The model was tested on a number of species of conifers and angiosperms native to Japan including *Larix kaempferi* Sarg. and compared to a base model that estimated stem growth from stem diameter at the base of the crown (Chiba et al. 1988). In contrast to other species, the Chiba et al. (1988) model did not fit data for stem growth and neither model fit data for growth efficiency in *L. kaempferi*. A better fit was obtained for *L. kaempferi* by relaxing the assumptions of 1) constant height growth over time, and 2) constant proportionality between stem increment at a position and the foliage above. The pipe model and profile theory studies illustrate the distinctly different patterns of biomass accumulation and distribution characteristic of *Larix* when compared to other genera.

By introducing an exponent, allometry accounts for more nuanced relationships between stem growth and foliar biomass than pipe model theory. Empirical allometry typically fits nonlinear models to the relationships between structural dimensions and biomass components, which may take on functional meaning through interpretation (Lacointe 2000). Because empirical allometric models are based on *a priori* knowledge (data), they require local validation. Variation between sites can be attributed to environmental factors in the form of site-specific parameterization, which in turn can be considered functionally significant.

Classically, allometric models take on the form of a multiplicative power function; for example,  $z = ax^by^c$  where  $z$ ,  $x$  and  $y$  are measurable values describing components of biomass or spatial dimensions of tree organs such as branch or crown foliar biomass, branch or trunk sapwood area, and branch length or height to the middle of the crown, and  $a$ ,  $b$ , and  $c$  are parameters that are optimized to fit the model to the data (Marchand 1983; Long and Smith 1989; Smith and Long 1989; Monserud and Marshall 1999). Such models can also be linearized via logarithmic transformation, as in the expression  $\ln LAI = \ln a + b \ln DBH$ , where  $a$  and  $b$  are parameters, LAI is leaf area index, and DBH is stem diameter measured at a height of 1.3 m (Vose et al. 1994).

Theories of fractal space-filling were posited to relate overall above-ground structure of trees to their growth potential. Early work by Horn (1971) related growth rates to overall crown shape, shade-tolerance, and successional status. Horn also related successional life history strategy to wood density and water-use efficiency. Later work by Ford (1985) proposed the concept of branch bifurcation ratio, a simple proportionality constant relating the average number of branches of a given order within the crown to the average number in the next lowest order. Needle-bearing evergreens had a branch bifurcation ratio of 5.1 compared to deciduous broadleaf trees with a ratio of 3.2, and thus develop a more vertically-stratified distribution of foliage (e.g., the multilayer, Horn 1971) with lower maximum order of branches. In contrast, shade-tolerant broad-leaf trees support a vertical foliage distribution concentrated in the upper portion of the crown (e.g., the monolayer, Horn 1971). As deciduous conifers, where *Larix* spp. fall along the continuum between mono and multilayered crown structure relative to other species is of interest.

Metabolic scaling has been proposed as a functional framework to justify the allometric relationships between biomass allocation to different plant organs. A central inconsistency in functional models that estimate biomass is whether biomass is measured by proxy as volume or as mass. Enquist et al. (1999) applied the previously established  $3/4$  power rule of scaling metabolism with the mass of supporting fractal networks by treating foliar mass  $Y$  as a proxy for metabolism in the relation  $Y = a_0 M^{3/4}$ , where  $M$  is the total mass of the organism (Niklas 1994). The  $3/4$  power scaling rule fit data from 45 species of tropical forest trees from a range of life histories. Thus, metabolism scaled with mass independent of wood density, suggesting that fast and slow-growing trees (e.g., pioneers and climax species) produce biomass at similar rates. Extending the investigation, Duursma et al. (2010) estimated the scaling exponent between foliar mass and diameter for a large dataset of conifer species. The fractal dimension of foliar mass ranged between 2 and 3, which was interpreted to indicate scaling of foliar mass with a dimension somewhere between that of crown surface area and total crown volume, respectively. Thus, branching and foliage production in conifers is less than volume-filling, presumably due to self-shading or hydraulic limitations.

In conclusion, over the course of several decades and multiple lines of reasoning, empirically based investigations have successfully modeled crown structure in relation to total biomass and identified trends across large numbers of species (Horn 1971; Ford 1985; Enquist et al. 1999; Duursma et al. 2010). Building on early models that related foliage directly to stem cross-sectional mass (Shinozaki et al. 1964), more sophisticated models allowed relationships between crown structure and growth to be quantified and compared across species and life history strategies (Horn 1971; Osawa et al. 1991). The allometric scaling of body biomass with foliage mass expressed algebraically as a power series function has been interpreted as a

functional consequence of the fractal scaling of metabolism with organismal biomass, where foliar mass is treated as a proxy for metabolism (Enquist et al. 1999). Considering the findings of Duursma et al. (2010), differences in life history should be quantifiable in terms of the constraints placed by efficiency of light and water use on fractal scaling of metabolism, which vary with and translate to species growth potential differences across niche space.

### *1.2.2 Applications of tree crown models*

The study of crown structure and morphology has multiple applications in forest ecology and silviculture. Plasticity in crown morphology of a particular species can be used by managers as a monitoring tool to assess the potential long-term effects of silvicultural treatments on future stand composition and structure, and to identify mechanisms to explain those effects (Buckley et al. 1997). Allometric equations are useful as guides for stocking and density management (Seymour and Smith 1987; Jack and Long 1996). To be useful, models need to be parameterized for different species and locations.

Light interception is the primary determinant of gross photosynthesis and depends on leaf area and its distribution in the crown. Beer's law, which describes attenuation of direct solar radiation in the atmosphere, can be adapted to describe the penetration of light into a known distribution of photosynthetic organs (Nilson 1971). Horn (1971) distinguished between optimal light conditions of a multilayer, which has competitive advantage in full sun, relative to that of a monolayer, which has competitive advantage in the understory.

Differences in allometry reveal different carbon allocation strategies in larch relative to associated tree species at a given site, even within ostensibly similar life history classes. *P. menzeisii* and *P. contorta* co-occur with *L. occidentalis*. As a shade-intolerant, fast-growing,

early successional species, *P. contorta* closely matches the life history of *L. occidentalis*. *P. contorta* of a given diameter has a similar rate of stem wood allocation to *L. occidentalis*, but *L. occidentalis* supports less total foliage by mass while still allocating more carbon to current foliage, and has a greater ratio of leaf area to stem cross-sectional area (Gower et al. 1987). The more shade-tolerant, relatively slower-growing *P. menzeisii* has a greater ratio of leaf area to stem cross sectional area (Gower et al. 1987) than either of the other two species, and denser wood than *P. contorta* but less dense wood than *L. occidentalis* (Kretschmann 2010). The above relationships may be the combined result of the annually deciduous habit, higher specific leaf area, and higher growth efficiency of *L. occidentalis* relative to *P. contorta* (Waring 1983; Gower and Richards 1990).

Alternately, *L. occidentalis* may allocate biomass more efficiently. Crown structure and form can be used to predict wood production. A basic rationale for applying crown models to predict wood production potential follows from consideration of a simple inversion of the pipe-model hypothesis of stem diameter-leaf area proportionality. This relationship, however, is overly simple. The balance of area for photosynthesis and respiratory demand of supporting tissues determines the amount of carbon available for height, and finally, lateral growth. Thus, the efficiency of growth depends dually on the amount of light interception and whole-plant respiration. A literature review found consistent support for the hypothesis that high ratio of crown height to width was associated with higher growth efficiency (Stenberg et al. 1994). A narrower crown presumably supports similar amounts of foliage, but with less respiratory loss to supporting branch biomass. Even tree species with similar crown morphologies may still have differing levels of shade tolerance as well as differing intrinsic patterns of allocation and distribution of foliage within the crown (Goudie et al. 2016).

Structural complexity in the stand and relative position of the crown in the canopy have been assessed empirically as modulators of the effect of crown structure and form on growth efficiency. Because relative position within the canopy is correlated with tree size, the effect of relative canopy position on efficiency further involves the tradeoff between the light competition advantage afforded by greater relative height within the stand and optimization of the ratio of leaf area to respiring biomass (Ryan 1989). As trees accumulate a large amount of respiring tissue through secondary and lateral growth, it becomes increasingly difficult to produce the corresponding marginal increase in photosynthetic area required to offset increases in respiratory demand, and growth begins to slow. In a study testing the hypothesis that leaf area more strongly affected growth efficiency in suppressed relative to canopy-level *Abies lasiocarpa* (Hook.) Nutt., Roberts and Long (1992) found an inverse relationship between total leaf area and the amount of foliar mass per unit stem, and that the most efficient trees were the largest trees with less than maximum leaf area for their height class.

Allometric models of biomass allocation often require local validation. The findings of Gower et al. (1987) conflicted with previous studies on the variation of leaf area with stem cross sectional area in *L. occidentalis*. A study of three other *Larix* species (*L. laricina*, *L. decidua*, and *L. decidua* × *L. leptolepis*) estimated significantly different values across sites (Maine, Minnesota, and Austria) for parameter estimates in a height-crown length equation and a diameter-crown radius equation (Gilmore 2001). Taken together and with evidence that site and species effects on crown allometric relationships may be confounded (Weiskittel et al. 2009), the findings of Gower et al. (1987) and Gilmore (2001) highlight the need for both site- and species-specific validation of allometric models of biomass allocation in forest trees

and for *Larix* spp. in particular. Species- and site-dependent changes in spatial distribution of foliage are important as indicators of future tree growth and mixed stand development.

### **1.3 Spatial foliage distribution modeling**

#### *1.3.1 Rationale and applications*

Light interception and photosynthesis both depend on light penetration. In turn, light penetration depends on horizontal and vertical distribution of foliage within the crown. After radiation is attenuated by the highest or outermost layers of foliage, penumbral, transmitted, and reflected light may still be photosynthetically active as it penetrates deeper into the crown. Penumbrae, the portion of a shadow where the light source is not completely blocked, are greater in crowns with greater inter-whorl space, and greater in trees with narrow leaves such as conifers (Stenberg et al. 1994). Based on the crude baseline compensation point of 20% of full light to balance photosynthesis and respiration and a calculation of the vanishing point of light emanating from the sun, Horn (1971) empirically derived optimal spacing distances of foliage in a multilayered tree crown. Leaf area (LA), which quantifies the amount of area exposed to light, foliar mass (FM), which quantifies the total amount of photosynthetic capacity, and specific leaf area, which relates LA and FM, have been treated as response variables in spatial distribution models in many previous studies.

The variation of specific leaf area (SLA), the ratio of projected area to dry mass of individual leaves, defines the difference between the distributions of FM and LA within the crown. SLA also quantifies the amount of area available for carbon assimilation per unit photosynthetic capacity by mass, and is negatively correlated with maximum photosynthetic rate across tree species (Jurik 1986; Oren et al. 1986; Ellsworth and Reich 1993; Reich et al.

1997) and within the genus *Larix* (Higgins et al. 1987). Similar to leaf area, the characteristic patterns of spatial distribution of SLA within the crown are correlated with life history. Shade-intolerant, early successional species are adapted to grow on open sites and have multilayered canopies with low SLA and high rates of growth and photosynthesis, whereas shade-tolerant, late successional species tend to have higher SLA and allocate foliage in a single layer near the top of the crown to maximize surface area exposed to high levels of photosynthetically active radiation in light gaps (Horn 1971; Niinemets and Kull 1994).

Because water status has been theoretically and experimentally demonstrated to influence cell expansion and SLA (Tardieu et al. 1999; Phillips and Riha 1993; Ibrahim et al. 1998; Myers et al. 1998), observed species differences in spatial distribution of SLA may be due to differences in water conservation strategy. In support of a hypothetical relationship between SLA and stomatal regulation, a proxy for ratio of conductance to photosynthesis ( $\delta^{13}\text{C}$ ) was positively correlated with SLA in *P. ponderosa* (Weiskittel et al. 2008), an isohydric and intermediately drought-tolerant, shade-intolerant species. Thus, differences observed between species in components of SLA variance and their relative degree of influence may be due to different light and moisture requirements.

Changes in distribution of foliage can be quantified and assessed in response to silvicultural treatments such as fertilization, thinning, release, and/or regeneration (Wang et al. 1990; Kantola and Mäkelä 2004; Nelson et al. 2015), or stand level variables such as density and social position (Maguire and Bennet 1996). The development of models for economically important species will directly benefit the field of forestry by facilitating optimization of management and providing resources for future research.

### 1.3.2 Statistical methods for modeling spatial foliage distribution

Probability density functions (PDFs) provide reliable approximations of foliage distributions across vertical and horizontal dimensions of the crown. Early models of vertical distribution of foliage used the normal (Gaussian) distribution or even more basic algebraic functions such as the quadratic. In what is considered the first vertical foliage distribution model, Stephens (1969) fit a normal distribution to foliar mass in *Pinus resinosa* Ait. The normal distribution also fits stand-level vertical distribution of leaf area in the canopy (Beadle et al. 1982).

Subsequent studies employed more sophisticated PDFs to model vertical foliage distributions. The Weibull, truncated Weibull, Johnson's  $S_B$ , and  $\beta$ -distributions are superior to the normal distribution for describing profiles of vertical foliage distributions for two reasons: they accommodate greater levels of plasticity, and the ends of the distribution can be truncated or fixed to define the distribution over a finite distance (e.g., from 0 to 1), unlike the asymptotic ends of the normal distributions and hyperbolic functions (Schreuder and Swank 1974). To standardize comparisons between individual trees and improve model fit, foliage distributions are typically plotted across a relative rather than an absolute vertical dimension of the crown, such as vertical position in the crown divided by crown length (Gillespie et al. 1994; Weiskittel et al. 2009; Nelson et al. 2014). Relative positions can then be converted back to absolute distances if desired (Garber and Maguire 2005; Nelson et al. 2015).

Two contrasting approaches and an intermediate approach may be employed when fitting PDFs to vertical biomass distribution in tree crowns. The most labor-intensive method requires measuring biomass from the entire crown and fitting the models to a complete, exhaustive dataset (Stephens 1969; Schreuder and Swank 1974; Wang et al. 1990). A less intensive method is to collect data from a random sample of branches from regularly spaced

strata within the canopy and to fit distributions to the incomplete sample (Vose et al. 1988; Massman 1982). In a hybrid method employed by many studies, branch models are first fit to the foliage data from a subsample of branches, and then used to estimate the foliage for the rest of the branches (Maguire and Bennett 1996; Nelson et al. 2015). Allometric equations can be used to estimate total branch-level foliage (Table 1.1; Ek 1979). These models may express total branch foliage as a linear, quadratic, root-transformed, power-series, exponential, or mixed function of branch- and tree-level variables. Branch-level foliage models may also include random effects to account for variation at the level of tree, plot, and location. Similar formulations have also been applied to model total foliage in the crown (Table 1.2).

Variables that may influence crown morphology and foliage allocation may be intrinsic or extrinsic. Intrinsic variables are physical dimensions or attributes and include metrics such as tree height (TH), crown length (CL), and age. Extrinsic variables correspond to the environmental component of phenotype, and include indexes of site quality, stand density, and management history. When PDFs are used to model vertical distribution of total foliage, the parameters estimated for the PDFs, which define the relative shape of the distribution for each individual tree, can then be modeled as functions of tree-level variables (Table 1.3). Thus, by fitting functions of tree- and stand-level variables to the PDF parameter estimates for a number of trees in a study, the influence of intrinsic and extrinsic variables on the relative pattern of vertical foliage allocation within the tree crown can be inferred from the behavior of the model (Kantola and Mäkelä 2004; Jerez et al. 2005; Utsugi et al. 2006; Maguire and Bennet 1996; Weiskittel et al. 2009; Nelson et al. 2015).

The two-parameter  $\beta$ -distribution has been applied to foliar mass and area in *Abies*, *Pinus*, *Pseudotsuga*, and *Picea*. For data from 27 *P. menzeisii*, Maguire and Bennet (1996)

assessed linear and power series models of total branch LA from combinations of eight different branch- and tree-level variables. The parameters for the  $\beta$ -distributions for both leaf mass and leaf area were expressed as functions of CL, DBH, and TH. Garber and Maguire (2005) modeled the  $\beta$ -distribution parameters for vertical distribution of leaf area of three species at multiple sites as functions of DBH, CL, ratio of crown length to tree height (CLR), relative height in the stand, stand species composition, and stand basal area. Also applying the  $\beta$ -distribution function, Schneider et al. (2011) included site, TH, CL, and DBH as intrinsic explanatory variables in a model of vertical variation in the proportion of nodal to intermodal foliage of jack pine (*Pinus banksiana* Lamb.). Jerez et al. (2005) fit the Johnson's  $S_B$  function to the vertical foliage distribution in loblolly pine (*Pinus taeda* L.), using a two percentile method to estimate the kurtosis ( $\gamma$ ) and skew ( $\delta$ ) parameters (Knoebel and Burkhar 1991). The location of foliage distribution percentiles  $x_{50}$  and  $x_{15}$  were modeled as exponential functions of TH, vertical height to the middle of the crown (HMC), CLR, and tree age.

Weibull distributions sometimes fit vertical leaf data slightly better when tested alongside other PDFs. In a study applied to the leaf area of multiple species, truncated Weibull distributions yielded a marginally better fit with lower root mean squared error (RMSE) than Johnson's  $S_B$  or the  $\beta$ -distribution for conifer and angiosperm species (Nelson et al. 2014; Nelson et al. 2015). Weiskittel et al. (2009) constructed a model for vertical leaf area distributions using the Weibull distribution. They included species and site in their model by using dummy variables as fixed effects for each species included in their study and random effects for site. Inclusion of species only marginally improved fit, whereas random effects from site and tree within site were substantial. This suggests differences in model parameters attributed to species in other studies where species were modeled separately may have been

**Table 1.1** Previously published models used to estimate total branch foliage.

Species <sup>a</sup>	Var <sup>b</sup>	Class <sup>c</sup>	Branch Model Formula	Citation
PISY	FM	Quad	$BA(a_0RDIC + a_1RDIC^2 + a_2) + a_3$	Mäkelä and Vanninen 2001
TSCA	LA	Other	$(a_0 + a_1\sqrt[3]{BA} + a_2\sqrt[3]{RDIC})^3$	Kenefic and Seymour 1999
PITA	FM	Power	$BD^{a_1}DIC^{a_2}$	Gillespie et al. 1994
Multiple	LA/BM /FM	Power	$a_0DIC^{a_1}BA^{a_3}$	Monserud and Marshall 1999
POTR	FM/BM	Power	$a_0BD^{a_1}DIC^{a_2}\left(\frac{TH}{BD}\right)^{a_3}$	Ek 1979
PISY	FM	Power	$a_0RDIC^{a_1}RHIC^{a_2}BA^{a_3}$	Mäkelä and Vanninen 2001
PITA	FM	Mixed	$a_0BD^{a_1}e^{a_2RHIC^{a_3}}$	Xu and Harrington 1998
PIRU	LA	Mixed	$e^{a_0}BD^{a_1}RDIC^{a_2}e^{a_3RDIC}$	Maguire et al. 1998
PSME	LA/FM	Mixed	$a_0BD^{a_1}RDIC^{a_2-1}e^{a_3RDIC^{a_4}}$	Maguire and Bennet 1996
ABGR	LA	Mixed	$a_0BD^{a_1}RDIC^{a_2-1}e^{-(a_3RDIC)^{a_2}}$	Garber and Maguire 2005
PICO				Maguire 2005
PIAB	FM/BM	Mixed	$RDIC^{a_1}BA^{a_2}e^{a_3RDIC^{a_4}}e^{a_5}$	Kantola and Mäkelä 2004
PIPO	LA	Mixed	$(a_0 - \varphi_i)BD^{a_1}RDIC^{a_2-1}e^{-(a_3RDIC)^{a_2}}$	Garber and Maguire 2005
Multiple	LA	Mixed	$BD^{a_1}RDIC^{a_2-1}e^{-(a_3+\varphi_i)RDIC^{a_2}}$	Nelson et al. 2014 <sup>†</sup>
Multiple	LA	Mixed	$a_0BD^{a_1}RDIC^{a_2-1}e^{((a_3+\varphi_i+\omega_{ij})RDIC^{a_2})^2}$	Weiskittel et al. 2009

<sup>a</sup> PSME = *Pseudotsuga menzeisii* var. *menzeisii*, PITA = *Pinus taeda*, ABGR = *Abies grandis*, PICO = *Pinus contorta*, PIPO = *Pinus ponderosa*, POTR = *Populus* × *Tristis*, PIAB = *Picea abies*, PISY = *Pinus sylvestris*; TSCA = *Tsuga canadensis*; <sup>b</sup> LA = leaf area, FM = foliar biomass, BM = branch biomass; <sup>c</sup> Power = power series, Quad = quadratic, Mixed = mixed power series and exponential; <sup>†</sup>Nelson et al. accounted for branch angle in the original model, but *L. occidentalis* has near 90° branch angles, so we present a model where RDIC replaces distance to branch tip and to start of foliage on the branch in the power and exponential portions of the original model, respectively.

**Table 1.2** *Previously published models used to estimate crown foliage.*

Species <sup>a</sup>	Var <sup>b</sup>	Class <sup>c</sup>	Crown Model Formula	Citation
TSCA	LA	Mixed	$b_0 DBH^{b_1 + b_2 CL + b_3 (TH/DBH)}$	Weiskittel et al. 2009
PSME	FM	Mixed	$b_0 CL^{b_1} e^{b_2 DBH/TH}$	Maguire and Bennet 1996
Multiple	LA	Mixed	$b_0 DBH^{b_1} e^{(b_2 + \varphi_i) \left(\frac{DBH}{CL}\right)}$	Nelson et al. 2014
PSME PIPO PIMO	FM/ LA/BM	Power	$b_0 DBH^{b_1} CLR^{b_2} CL^{b_3}$	Monserud and Marshall 1999 <sup>†</sup>
TSCA	LA	Linear	$b_0 + b_1 (DBH + MCLR)$	Kenefic and Seymour 1999 <sup>‡</sup>
CHOB	LA	Power	$b_0 DBH^{b_1}$	Utsugi et al. 2006
PITA	LA	Power	$\frac{1}{HMC} \left(\frac{DBH}{b_1}\right)^{b_2}$	Jerez et al. 2005

<sup>a</sup> PSME = *Pseudotsuga menzeisii*, PITA = *Pinus taeda*, PIPO = *Pinus ponderosa*, PIMO = *Pinus monticola*, TSCA = *Tsuga canadensis*, CHOB = *Chamaecyparis obtusa*; <sup>b</sup> LA = leaf area, FM = foliar biomass, BM = branch biomass; <sup>c</sup> Function classes: Power = power series, Mixed = mixed power series and exponential; <sup>†</sup> Modified from the original published version which also included sapwood area and crown competition factor; <sup>‡</sup> Original regression was weighted by DBH.

**Table 1.3** *Previously published models used to estimate foliage distribution parameters.*

Species <sup>a</sup>	Var <sup>b</sup>	Function	Parameter Model Formulas <sup>c</sup>	Citation
TSCA	FM/LA	Beta	$c = g_0 + g_1 CFM$ $d = g_2 TH^{g_3} e^{g_3 CR + g_4 TH}$	Maguire and Bennet 1996
Multiple	LA	Weibull	$\eta = g_0 CL^{g_1 + g_2 CLA}$ $\beta = g_3 CL^{g_4 + g_5 CLA + g_6 TH}$	Weiskittel et al. 2009
CHOB	LA	Weibull	$\eta = g_0 + g_1 CLA + g_2 TH,$ $\beta = g_3 + g_4 CLA + g_5 TH$	Utsugi et al. 2006

<sup>a</sup> TSCA = *Tsuga Canadensis*, CHOB = *Chamaecyparis obtusa*; <sup>b</sup> LA = leaf area, FM = foliar biomass; <sup>c</sup> CLA = total crown leaf area, CFM = total crown foliar biomass.

confounded with unquantified site-level effects. However, interactions between dummy variables for species and other factors are not accounted for in the Weiskittel et al. (2009) model, and thus differences in species responses to such factors cannot be inferred.

Horizontal distributions of foliage in branches have been modeled in the published literature less frequently than vertical distributions, but essentially the same approaches are applicable to horizontal distribution along individual branches or radial distances within vertical sections of the crown as those applicable to vertical distribution. Because foliage is concentrated in the outer shells of the crown, an asymmetric PDF such as the Weibull,  $\beta$ -distribution, or Johnson's  $S_B$  function fit horizontal foliage distribution data well.

Stenberg et al. (1993) treated secondary shoots and higher order shoots as the photosynthetic organ, and fit a  $\beta$ -distribution to their horizontal distribution. Kershaw and Maguire (1996) fit Weibull,  $\beta$ -distribution, normal, and Johnson's  $S_B$  functions to horizontal distribution of foliage within vertical sections of crowns of *A. grandis*, *T. heterophylla*, and *P. menzeisii*. Moment-derived parameters were treated as response variables in allometric functions of branch diameter (BD), absolute depth into the crown of the supporting branch (DIC), and length of the green portion of the branch. Xu and Harrington (1998) fit a Weibull function to horizontal distribution of LAI in *Pinus taeda* (L.) and the kurtosis ( $\beta$ ) and skew ( $\eta$ ) parameters were modeled as functions of branch, tree, and stand-level variables. Weibull skew was fit to a linear function of CLR and relative dominance of the tree defined as height divided by the mean height of dominant and codominant trees in the stand. Weibull kurtosis was fit to a linear function of BD, DIC, and CLR.

The form of allometric and foliage distribution models and the sign and magnitude of the parameters estimated for the models provide useful information about the species being

modeled. Model building proceeds by first comparing the relative explanatory power of candidate variables on biomass allocation to different crown components, and then by successively testing additional variables for a significant improvement in the amount of variation accounted for by a simpler base model. The intrinsic autecological traits underlying the life histories and adaptive strategies of species may be inferred through analysis of the form and parameter estimates of allometric and foliage distribution models and comparison between species and studies. By accounting for the intrinsic autecological behavior of foliage allocation of a species, the extrinsic factors influencing foliage allocation, and thus growth potential, can be better identified, thereby adding to knowledge of its production ecology.

#### 1.4 Works cited

1. Anfodillo, T., Rento, S., Carraro, V., Furlanetto, L., Urbinati, C., and Carrer, M. 1998. Tree water relations and climatic variations at the alpine timberline: seasonal changes of sap flux and xylem water potential in *Larix decidua* Miller, *Picea abies* (L.) Karst. and *Pinus cembra* L. *Ann. Sci. Forest.* **55**(1-2): 159-172.
2. Arno, S.F., Smith, H.Y., and Krebs, M.A. 1997. Old Growth Ponderosa Pine and Western Larch Stand Structures: Influence of Pree-1900 Fires and Fire Exclusion. USDA For. Serv. Res. Pap. INT-RP-495.
3. Beadle, C.L., Talbot, H., and Jarvis, P.G. 1982. Canopy structure and leaf area index in a mature Scots pine forest. *Forestry* **55**(2): 105-123.
4. Buckley, D.S., Zasada, J.C., Tappeiner, J.C., II, and Stone, D.M. 1997. Plant morphological characteristics as a tool in monitoring response to silvicultural activities. *In* Communicating the role of silviculture in managing the national forests: Proceedings of the National Silviculture Workshop. Warren, PA, 19-22 May 1997. UDSA For. Serv. Gen. Tech. Rep. NE-238: 37-41.
5. Chen, H.Y., and Klinka, K. 1998. Survival, growth, and allometry of planted *Larix occidentalis* seedlings in relation to light availability. *Forest Ecol. Manag.* **106**(2): 169-179.
6. Chiba, Y., Fujimori, T., and Kiyono, Y. 1988. Another interpretation of the profile diagram and its availability with consideration of the growth process of forest trees. *J. Jpn. For. Soc.* **70**(6): 245-254.

7. Connor, R.C., and O'Brien, R.A. Distribution and volume of larch forests in the Western United States. *In Ecology and Management of Larix Forests: Proceedings of an International Symposium, Whitefish, MT., 5-9 October 1992. Edited by W.C. Schmidt and K.J. McDonald. USDA For. Serv. Gen. Tech. Rep. GTR-INT-319. pp. 147-150.*
8. Duursma, R.A., Mäkelä, M., Reid, D.E.B., Jokela, E.J., Porte, A.J., and Roberts, S.D. 2010. Self-shading affects allometric scaling in trees. *Funct. Ecol.* **24**: 723 -730.
9. Ek, A.R. 1979. Notes: a model for estimating branch weight and branch leaf weight in biomass studies. *Forest Sci.* **25**(2): 303-306.
10. Ellsworth, D.S., and Reich, P.B. 1993. Canopy structure and vertical patterns of photosynthesis and related leaf traits in a deciduous forest. *Oecologia* **96**(2): 169-178.
11. Enquist, B.J., West, G.B., Charnov, E.L., and Brown, J.H. 1999. Allometric scaling of production and life history variation in vascular plants. *Nature* **401**: 907-911
12. Ford, E.D. 1985. Branching, crown structure and the control of timber production. *In Attributes of trees as crop plants. Edited by M.G.R. Cannell and J.E. Jackson. Abbotts Ripton, Institute of Terrestrial Ecology, Huntingdon, England. pp. 228-252.*
13. Fry, D.J., and Phillips, I.D.J. 1977. Photosynthesis of conifers in relation to annual growth cycles and dry-matter production. 2. Seasonal photosynthetic capacity and mesophyll ultrastructure in *Abies grandis*, *Picea sitchensis*, *Tsuga heterophylla* and *Larix leptolepis* growing in south west England. *Physiol. Plant.* **40**(4): 300-306.
14. Garber, S.M., and Maguire, D.A. 2005. The response of vertical foliage distribution to spacing and species composition in mixed conifer stands in central Oregon. *Forest Ecol. Manag.* **211**: 341-355.
15. Gillespie, A.R., Allen, H.L., and Vose, J.M. 1994. Amount and vertical distribution of foliage of young loblolly pine trees as affected by canopy position and silvicultural treatment. *Can. J. For. Res.* **24**(7): 1337-1344.
16. Gilmore, D.W. 2001. Equations to describe crown allometry of *Larix* require local validation. *Forest Ecol. Manag.* **148**: 109-116.
17. Goudie, J.W., Parish, R., and Antos, J.A. 2016. Foliage biomass and specific leaf area equations at the branch, annual shoot and whole-tree levels for lodgepole pine and white spruce in British Columbia. *Forest Ecol. Manag.* **361**: 286-297.
18. Gower, S.T., and Richards, J.H. 1990. Larches: Deciduous Conifers in an Evergreen World. *BioScience.* **40**(11): 818-826.

19. Gower, S.T., Grier, C.C., and Vogt, K.A. 1989. Aboveground production and N and P use by *Larix occidentalis* and *Pinus contorta* in the Washington Cascades, USA. *Tree Physiol.* **5**(1): 1-11.
20. Gower, S.T., Grier, C.C., Vogt, D.J., and Vogt, K.A. 1987. Allometric relations of deciduous (*Larix occidentalis*) and evergreen conifers (*Pinus contorta* and *Pseudotsuga menziesii*) of the Cascade Mountains in central Washington. *Can. J. For. Res.* **17**: 630-634.
21. Higgins, S.S., Black, R.A., Rademaker, G.K., and Bidlake, W.R. 1987. Gas exchange characteristics and water relations of *Larix occidentalis*. *Can. J. For. Res.* **17**(11): 1364-1370.
22. Horn, H.S. 1971. *The Adaptive Geometry of Trees*. Princeton University Press, Princeton, N.J.
23. Ibrahim, L., Proe, M.F., and Cameron, A.D. 1998. Interactive effects of nitrogen and water availabilities on gas exchange and whole-plant carbon allocation in poplar. *Tree Physiol.* **18**: 481-487.
24. Jack, S.B., and Long, J.N. 1996. Linkages between silviculture and ecology: an analysis of density management diagrams. *Forest Ecol. Manag.* **86**(1): 205-220.
25. Jerez, M., Dean, T.J., Cao, Q.V., and Roberts, S.D. 2005. Describing Leaf Area Distribution in Loblolly Pine Trees with Johnson's SB Function. *Forest Sci.* **51**(2): 93-101.
26. Jurik, T.W. 1986. Temporal and spatial patterns of specific leaf weight in successional northern hardwood tree species. *Am. J. Bot.* **73**(8): 1083-1092.
27. Kantola A., and Mäkelä, A. 2004. Crown development in Norway spruce [*Picea abies* (L.) Karst.]. *Trees* **18**: 408-421.
28. Kenefic, L.S., and Seymour, R.S. 1999. Leaf area prediction models for *Tsuga canadensis* in Maine. *Can. J. For. Res.* **29**(10): 1574-1582.
29. Knoebel, B.R., and Burkhart, H.E. 1991. A bivariate distribution approach to modeling forest diameter distributions at two points in time. *Biometrics* **47**: 241-253.
30. Kretschmann, D.E. 2010. Mechanical properties of wood (Chapter 5). *In Wood Handbook: Wood as an Engineering Material*. USDA For. Serv. Gen. Tech. Rep. FPL-GTR 190.
31. Lacointe, A. 2000. Carbon allocation among tree organs: A review of basic processes and representation in functional-structural models. *Ann. Forest Sci.* **57**:251-533.
32. Lanner, R.M. 1995. The Role of Epicormic Branches in the Life History of Western Larch. *In Ecology and Management of Larix Forests: Proceedings of an*

- International Symposium, Whitefish, MT., 5-9 October 1992. *Edited by* W.C. Schmidt and K.J. McDonald. USDA For. Serv. Gen. Tech. Rep. GTR-INT-319. pp. 323-326.
33. Long, J.N., and Smith, J.N. 1989. Estimating leaf area in *Abies lasiocarpa* across ranges of stand density and site quality. *Can. J. For. Res.* **19**: 930-932.
  34. Maguire, D.A., Brissette, J.C., and Gu, L. 1998. Crown structure and growth efficiency of red spruce in uneven-aged, mixed-species stands in Maine. *Can. J. For. Res.* **28**(8), 1233-1240.
  35. Maguire, D.A., and Bennett, W.S. 1996. Patterns in vertical distribution of foliage in young coastal Douglas-fir. *Can. J. For. Res.* **16**: 1991-2005.
  36. Mäkelä, A., and Vanninen, P. 2001. Vertical structure of Scots pine crowns in different age and size classes. *Trees* **15**: 385-392.
  37. Marchand, P.J. 1984. Sapwood area as an estimator of foliage biomass and projected leaf area for *Abies balsamea* and *Picea rubens*. *Can. J. For. Res.* **14**(1): 85-87.
  38. Massman, W.J. 1982. Foliage distribution in old-growth coniferous tree canopies. *Can. J. For. Res.* **12**(1): 10-17.
  39. McClelland, B.R., Frissell, S.S., Fischer, W.C., and Halvorson, C.H. 1979. Habitat management for hole-nesting birds in forests of western larch and Douglas-fir. *J. Forest.* **77**(8): 480-483.
  40. Monserud, R.A., and Marshall, J.D. 1999. Allometric crown relations in three northern Idaho conifer species. *Can. J. For. Res.* **29**(5): 521-535.
  41. Myers, B.J., Benyon, R.G., Theiveyanathan, S., Criddle, R.S., Smith, C.J., and Falkner, R.A. 1998. Response of effluent-irrigated *Eucalyptus grandis* and *Pinus radiata* to salinity and vapor pressure deficits. *Tree Physiol.* **18**: 565-573.
  42. Nelson, A.S., Wagner, R.G., Weiskittel, A.R., and Saunders, M.R. 2015. Effects of species composition, management intensity, and shade tolerance on vertical distribution of leaf area index in juvenile stands in Maine, USA. *Eur. J. Forest Res.* **134**: 281-291.
  43. Nelson, A.S., Weiskittel, A.R., and Wagner, R.G. 2014. Development of branch, crown, and vertical distribution leaf area models for contrasting hardwood species in Maine, USA. *Trees* **28**: 17-30.
  44. Niinemets, Ü., and Kull, K. 1994. Leaf weight per area and leaf size of 85 Estonian woody species in relation to shade tolerance and light availability. *For Ecol. Manag.* **70**: 1-10.

45. Niklas, K.J. 1994. Plant Allometry: The Scaling of Form and Process. The University of Chicago Press, Chicago, IL.
46. Nilson, T. 1971. A theoretical analysis of the frequency of gaps in plant stands. *Agr. Meteorol.* **8**: 25-38.
47. Oberhuber W., Kofler, W., Schuster, R., and Wieser, G. 2015. Environmental effects on stem water deficit in co-occurring conifers exposed to soil dryness. *Int. J. Biometeor.* **59**: 417-426.
48. Oliver, C.D., and Larson, B.C. 1990. Forest stand dynamics. McGraw-Hill, NY, NY.
49. Oren, R., Schulze, E.D., Matyssek, R., and Zimmermann, R. 1986. Estimating photosynthetic rate and annual carbon gain in conifers from specific leaf weight and leaf biomass. *Oecologia* **70**(2), 187-193.
50. Osawa A., Ishizuka, M., and K. Yoichi. 1991. A profile theory of tree growth. *Forest Ecol. Manag.* **41**:33-63.
51. Parent, D.R., Mahoney, R.L., and Barkley, Y.C.. 2008. Western Larch: A Deciduous Conifer in an Evergreen World. Available from the University of Idaho Forest, Wildlife and Range Experiment Station, Moscow, ID. Bulletin No. 90.
52. Phillips, J.G., and Riha, S.J. 1993. Canopy development and solar conversion efficiency in *Acacia auriculiformis* under drought stress. *Tree Physiol.* **12**: 137–149.
53. Rehfeldt, G.E. 1995. Genetic variation, climate models and the ecological genetics of *Larix occidentalis*. *Forest Ecol. Manag.* **78**: 21-37.
54. Rehfeldt, G.E., and Jaquish, B.C. 2010. Ecological impacts and management strategies for western larch in the face of climate-change. *Mitig. Adapt. Strat. Gl.* **15**: 283-306.
55. Reich, P.B., Walters, M.B., & Ellsworth, D.S. 1997. From tropics to tundra: Global convergence in plant functioning. *PNAS* **94**(25): 13730-13734.
56. Roberts, S.D., and Long, J.N. 1992. Production efficiency of *Abies lasiocarpa*: influence of vertical distribution of leaf area. *Can. J. For Res.* **22**: 1230-1324.
57. Ryan, M.G. 1989. Sapwood volume for three subalpine conifers: predictive equations and ecological implications. *Can J. For. Res.* **19**(11): 1397-1401.
58. Schmidt, W.C. and Shearer, R.C. 1976. Ecology and silviculture of western larch forests. USDA For. Serv. Tech. Bull. No. 1520.
59. Schmidt, W.C. and Shearer, R.C. 1990. Western larch (*Larix occidentalis*). In *Silvics of North America: Vol 1. Conifers. Edited by R.M. Burns and B. Honkala.* USDA For. Serv. Ag. Hand. No. 654.

60. Schneider, R., Fortin, M., Berninger, F., Ung, C. H., Swift, D.E., and Zhang, S.Y. 2011. Modeling Jack Pine (*Pinus banksiana*) Foliage Density Distribution. *Forest Sci.* **57**(3): 180-188.
61. Schreuder, H.T., and Swank, W.T. 1974. Coniferous stands characterized with the Weibull distribution. *Can. J. For. Res.* **4**(4): 518-523.
62. Scott, G., Mahalovich, M.F., Rinehart, S., and Krueger, J. 2013. Reforestation-Revegetation Climate Change Primer for the Norther Region: Incorporating Climate Change Impacts into Reforestation and Revegetation Prescriptions. USDA For. Serv. Available from [http://ecoadapt.org/data/documents/Reforestation-Revegetation\\_Primer\\_Final.pdf](http://ecoadapt.org/data/documents/Reforestation-Revegetation_Primer_Final.pdf) [accessed 18 April 2017].
63. Seymour, R.S., and Smith, D.M. 1987. A new stocking guide formulation applied to eastern white pine. *Forest Sci.* **33**(2): 469-484.
64. Shinozaki, K., Yoda, K., Hozumi, K. and Kira, T. 1964. A quantitative analysis of plant form: the pipe model theory. 1. Basic analyses. *Jap. J. Ecol.* **14**(3): 97-105.
65. Smith, F.W., and Long, J.N. 1989. The influence of canopy architecture on stemwood production and growth efficiency of *Pinus contorta* var. *latifolia*. *J. Appl. Ecol.* **26**: 681-691.
66. Stenberg, P., Kuuluvainen, T., Kellomäki, S., Grace, J.C., Jokela, E.J., and Gholz, H.L. 1994. Crown Structure, Light Interception and Productivity of Pine Trees and Stands. *Ecol. Bull.* **43**: 20-34.
67. Stenberg, P., Smolander, H., and Kellomäki, S. 1993. Description of crown structure for light interception models: angular and spatial distribution of shoots in young Scots pine. *Stud. For. Suec.* **191**: 43-50.
68. Stephens, G.R. 1969. Productivity of Red Pine, 1. Foliage distribution in tree crown and stand canopy. *Agr. Meteorol.* **6**: 275-82.
69. Tardieu, F., Granier, C., and Muller, B. 1999. Modelling leaf expansion in a fluctuating environment: are changes in specific leaf area a consequence of changes in expansion rate? *New Phytol.* **143**: 33-43.
70. Utsugi, H., Araki, M., Kawasaki, T., and Ishizuka, M. 2006. Vertical distributions of leaf area and inclination angle, and their relationship in a 46-year-old *Chamaecyparis obtusa* stand. *Forest Ecol. Manag.* **225**(1): 104-112.
71. Vose, J.M. 1988. Patterns of leaf area distribution within crowns of nitrogen-and phosphorus-fertilized loblolly pine trees. *Forest Sci.* **34**(3): 564-573.
72. Vose, J.M., Dougherty, P.M., Long, J.N., Smith, F.W., Gholz, H.L., and Curran, P.J. 1994. Factors influencing the amount and distribution of leaf area of pine stands. *Ecol. Bull.* **43**: 102-114.

73. Wang, Y.P., Jarvis, P.G., and Benson, M.L. 1990. Two-dimensional needle-area density distribution within the crowns of *Pinus radiata*. *Forest. Ecol. Manag.* **32**:217-237.
74. Waring, R.H., and Franklin, J.F. 1979. Evergreen coniferous forests of the Pacific Northwest. *Science* **204**: 1380-1386.
75. Waring, R.H. 1983. Estimating forest growth and efficiency in relation to canopy leaf area. *Adv. Ecol. Res.* **13**: 327-354.
76. Weiskittel, A.R., Kershaw, J.A., Hofmeyer, P.V., and Seymour, R.S. 2009. Species differences in total and vertical distribution of branch- and tree-level leaf area for the five primary conifer species in Maine, USA. *Forest Ecol. Manag.* **258**: 1695-1703.
77. Weiskittel, A.R., Temesgen, H., Wilson, D.S., and Maguire, D.A. 2008. Sources of within- and between-stand variability in specific leaf area of three ecologically distinct conifer species. *Ann. Forest Sci.* **65**:103.
78. Xu, M., and Harrington, T.B. 1998. Foliage biomass distribution of loblolly pine as affected by tree dominance, crown size, and stand characteristics. *Can. J. For. Res.* **28**: 887-892.

## Chapter II

### VERTICAL DISTRIBUTION OF FOLIAR BIOMASS IN WESTERN LARCH

#### 2.1 Abstract

Western larch (*Larix occidentalis* Nutt.) is an endemic pioneer species in the Inland Northwest (INW) and unique as a deciduous conifer and the most shade-intolerant, fastest-growing, and most fire-resistant species in the region. To better understand its production ecology, we used a multilevel modeling approach to analyze the intrinsic dynamics of western larch vertical foliage distribution compared with other species. We found that western larch allocates foliage into a more diffuse distribution as the crown lengthens, whereas shade-tolerant evergreens concentrate foliage into a more monolayered distribution higher within the crown as it lengthens. Crown foliar biomass scaled linearly with DBH, indicating western larch does not fill volume in the crown with foliage at an increasing rate like other species. Based on our model, foliar shade-intolerance and water stress appear to jointly influence foliage allocation in this deciduous species. These results also highlight intrinsic foliage distribution as a character contributing to the inability of western larch to survive light-limiting conditions. The models developed here provide a base framework that may be built upon to study the morphological response of western larch to modified stand conditions such as disturbance and silvicultural treatment.

#### 2.2 Introduction

Characterization of the vertical distribution of foliage in the crown is essential to understand ontogenic changes and underlying response of trees to modified stand conditions. The vertical distribution of foliage is the primary factor determining the distribution of photosynthetically

active light intercepted by foliage (Horn 1971; Stenberg et al. 1994; Vose et al. 1995) and thus has a strong influence on growth. Therefore, a strong understanding of the differences in the response of vertical foliage distributions across species to changes in intrinsic (e.g., diameter, height, and age) and extrinsic variables (e.g., stand density, social position, and disturbance) will facilitate the optimization of management strategies. To enrich general knowledge of forest ecology, a mechanistic framework to explain observations may then be proposed by relating contrasting foliage allocation strategies back to species traits such as relative shade or drought tolerance.

Vertical foliage distributions are also useful in applied forestry. Morphological changes provide a useful substitute for long-term growth responses to management (Buckley et al. 1997). Changes in crown morphology and leaf distribution can be used to predict growth response insofar as they directly reflect the expected overall carbon budget of the tree. Growth efficiency of lodgepole pine (*Pinus contorta* Dougl. ex Loud.) defined by stem increment per unit height per unit foliage was inversely proportional to the vertical length of the crowns, such that higher efficiency could be attributed to less respiring branch biomass per unit foliage in more condensed crowns (Smith and Long 1989). However, crown length provides only a crude surrogate for foliar density and no specific information about foliage distribution.

The character and degree of plasticity of tree species' vertical foliage distributions to light and hydraulic conditions defines their ability to adapt to disturbance, management, and competition (Oliver and Larson 1990). Effects of treatments, environmental factors, intrinsic traits, and their interactions on vertical foliage distributions may be inferred through analysis of empirical models (Jerez et al. 2005; Garber and Maguire 2005). Probability density functions (PDFs) include at their most basic the Gaussian distribution and at their more

complex a wide array of families of functions such as the Weibull and Johnson distributions. PDFs provide good approximations of vertical foliage distributions. PDFs may be fit to foliage measurements such as leaf area or biomass across absolute or relative dimensions such as distance along the main stem from the base of the crown toward the stem apex. Using a PDF framework, empirical vertical foliage distribution models may be further parameterized with intrinsic explanatory variables like crown length, height, the ratio of crown length to height, and age (Maguire and Bennet 1996; Utsugi et al. 2006; Weiskittel et al. 2009).

Using the PDF framework, the form and characteristic dynamics of vertical foliage distributions have been found to vary across shade-tolerance level, across hardwood species, between hardwoods and conifers, and within species or populations (Nelson et al. 2014; Nelson et al. 2015). Shade-tolerant conifer vertical foliage distributions peak at a lower relative stratum within the crown relative to shade-intolerant species (Mäkelä and Vanninen 2001; Goudie et al. 2016). Vertical foliage distributions also change with respect to extrinsic factors such as social position (Xu and Harrington 1998; Kantola and Mäkelä 2004). The relative magnitude and direction of a shift in vertical foliage distribution in response to changing growing conditions may be influenced by leaf anatomy, mode of physiological response to hydrological stress, level of epinastic control during crown development, and other ecophysiological characters (Horn 1971; Oliver and Larson 1990).

North American larches (*Larix* spp.) are unique among sympatric conifers for their annually deciduous foliage, indeterminate annual growth, and high rate of epicormic branch replacement (Gower and Richards 1990; Lanner 1992), which together should allow for a high level of temporal plasticity in biomass allocation within the crown. Previous studies of vertical distribution of biomass in *Larix* spp. have been limited to the whole-canopy level or

to wood biomass, and did not measure crown foliage distribution (Bidlake and Black 1989; Li et al. 2004). However, *Larix* spp. exhibit substantial spatial variation in foliage density, and previous studies suggest a high level of plasticity of biomass allocation to immediate growing conditions, especially light availability (Kurachi et al. 1986; Osawa et al. 1990; Zhao and Wang 2004). It is not known whether shade intolerance is a factor in and/or a function of the unique aspects of *Larix* crown development. In addition to contributing to general knowledge, the development of baseline models of vertical foliage distribution in the crown of *Larix* spp. will provide a framework to study its response and to optimize silvicultural treatments.

Western larch (*Larix occidentalis* Nutt.) has the highest wood density and is the fastest-growing and most fire-resistant conifer species in the Inland Northwest (INW), where it is endemic (Schmidt and Shearer 1990; Kretschmann 2010). *L. occidentalis* prefers mesic sites, especially drainages and northern aspects. Decline of *L. occidentalis* has been linked to fire suppression and climate change (Arno et al. 1997; Rehfeldt and Jaquish 2010). In addition to making it a valuable wood commodity, the high wood density and rapid growth of *L. occidentalis* also provide the ecosystem service of carbon storage. Dead *L. occidentalis* snags are rot resistant and preferred over other species by cavity-nesting birds (McClelland et al. 1979). Improved knowledge of the production ecology of *L. occidentalis* is tantamount to the sustainability of the cultural, economic, and ecological value of INW forests, and particularly to the long-term goal of restoration of more natural fire regimes to the region.

In this study, we employ a multilevel modeling approach to characterize the behavior of vertical foliage distribution in *L. occidentalis* with respect to intrinsic factors. The specific objectives of the study were: A) to develop allometric models for foliar mass at the branch and tree levels; B) to evaluate the fit of PDFs to vertical distribution of foliage; and C) to

characterize how vertical foliage distributions change with respect to intrinsic variables. In addition to providing a modeling framework for optimizing *L. occidentalis* management strategies, the present study will also seek to answer the question of whether the behavior of the vertical foliage distribution in *L. occidentalis* is driven by or is a function of its shade intolerance and deciduous habit.

## **2.3 Materials and methods**

### *2.3.1 Study site and data collection*

A total of 64 *L. occidentalis* trees were destructively sampled from 20 locations across the northern Rocky Mountains in northern Idaho and western Montana between 2011 and 2016 (Figure 2.1). Mean average temperature at the sites ranged from 3.8°C to 9.3°C and mean annual precipitation ranged from 312 mm to 837 mm. Elevation ranged from 957 m to 2051 m. Latitude ranged from 44°45'13''N to 48°52'58''N.

For every tree at each location, diameter at breast height (DBH), diameter at the base of the live crown (DBLC), total height (TH), and vertical distance along the stem from the base of the bole to the base of the live crown (HBLC) were measured. For every branch on every tree, the vertical distance along the stem from the base of the bole to the center of the branch at the junction with the stem (HIC) and the diameter of the branch approximately 5 cm from the junction of the branch and the stem (BD) were measured. Additional tree- and branch-level variables were calculated, including branch cross sectional area (BA) and relative positions of the branches within the crown (Table 2.1).

At each location, a subset of between 1 and 8 branches per tree were randomly selected for measurement of total branch foliage biomass (Table 2.2). Branch segments were

placed in an oven and allowed to dry for at least 72 hours at 65°C. After drying to eliminate moisture weight, foliage was removed from each segment and weighed on a balance for total dry biomass.

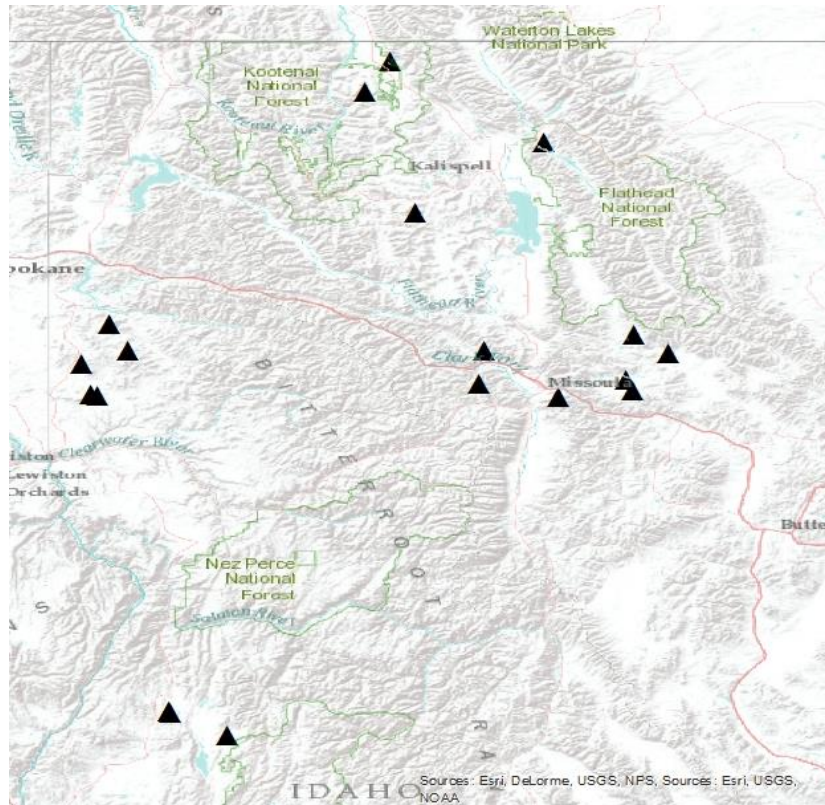


**Figure 2.1** Sites where *L. occidentalis* were harvested for the study

### 2.3.2 Branch foliar mass models

Foliar mass measurements of 312 branches from 64 trees (Table 2.2) were used to fit models to estimate foliar mass as a function of branch- and tree-level variables. A range of equation forms and combinations of predictive variables have been employed for estimation of branch foliage mass (FM), branch leaf area (LA), and branch woody biomass (BM) in past studies (Table 1.1). In addition to previous models used to predict FM, model forms previously used to estimate LA and BM were also adapted and tested for their ability to estimate FM in *L. occidentalis*. Variation due to unmeasured tree-level factors such as age and social position

were accounted for by including random effects for site and tree within site (Garber and Maguire 2005; Nelson et al. 2014; Weiskittel et al. 2009).

**Table 2.1** Variables tested to fit branch and tree level foliage models

Variable	Definition	Formula
<b>Branch</b>		
$\omega_{ij}$ (Tree)	Random effect of tree (j) within site (i) on branch	
BD (mm)	Branch diameter at stem junction	
BA (mm <sup>2</sup> )	Branch cross sectional area at stem junction	$\pi BD^2 / 4$
HIC (cm)	Height into crown from crown base	CL – DIC
DIC (cm)	Depth into crown from stem apex	CL – HIC
RHIC	Relative height into crown from base	HIC / CL
RDIC	Relative depth into crown from apex	DIC / CL
FM (g)	Total foliar mass of branch	Table 2
<b>Tree</b>		
$\varphi_i$ (Site)	Random effect of site location (i) on tree	
TH (cm)	Tree height	HBLC + CL
HBLC (cm)	Height from bole to base of crown	TH – CL
CL (cm)	Length of the crown	TH – HBLC
DBLC (mm)	Diameter of stem at base of crown	
DBH (mm)	Diameter at breast height (@ 1.3m)	
CLR	Crown length ratio	CL / TH
MCLR	Modified crown ratio	CL / (TH – 1.3m)
HMC (cm)	Height to the midpoint of the crown	HBLC + CL / 2
CFM (g)	Total foliar mass in the tree crown	Table 3

In addition to previously published models, modified and original models were also fit to the branch FM data. The modified and original models were obtained by substituting equivalent variables (e.g., RDIC for RHIC) or by sequentially adding variables to base models. Variables that significantly improved model fit were retained. Models were fit and parameters recovered using maximum likelihood estimation with the “nlme” function in the “nlme” package of R (R Core Team 2017; Pinheiro et al. 2017), which allows incorporation

of hierarchical random effects and the ability to account for autocorrelation and to weight the variance. Starting parameter values specified in the “nlme” function were first obtained by least squares estimation from the “proc model” function in SAS (SAS Institute Inc. 2016).

Parameter estimates were screened for significance using a threshold  $p$ -value of 0.05, and non-significant parameters were considered to be zero and removed from the model. Once a set of models with all significant parameters was obtained, the relative explanatory power, or goodness of fit for each model was assessed using multiple selection criteria: likelihood ratio tests, adjusted and generalized  $R^2$ , Akaike information criterion (AIC), and root mean squared error (RMSE). Among the best-fitting models with statistically equivalent performance across fit statistics, the simplest model that showed a significant improvement in goodness of fit over a base model was retained and selected for estimation of foliage mass for the rest of the branches.

### *2.3.3 Crown foliar mass models*

The branch summation method (Monserud and Marshall 1996) was employed to obtain an estimate of total crown foliar mass. Of the original 64 trees, 14 were not included because they did not have height measurements for all the branches. Using the branch model, foliar mass was estimated for 7408 individual branches and summed across each of the remaining 50 tree crowns (Table A1). A variety of published, modified, and original linear and nonlinear mixed effects models (Table 1.2) were fit to the total crown foliar mass estimates to test the significance of tree and stand variables (Table 2.1) by examining the  $p$ -values of their parameters. The same model selection criteria employed to select the best branch foliage mass models were used to select the best crown foliar mass model. Variation due to unmeasured

**Table 2.2** *Branches sampled for branch foliar mass model*

Site	Trees	Branches		BD (mm)			RHIC			FM (g)		
	n	n	per tree	min	mean	max	min	mean	max	min	mean	max
Bandy	5	19	3.8	8.00	35.11	69.00	0.07	0.34	0.60	4.00	91.48	246.04
Carsc	6	36	6.0	3.82	10.78	24.38	0.06	0.48	0.87	0.57	38.02	148.47
Coram 2	1	8	8.0	7.00	13.25	17.00	0.17	0.25	0.41	4.50	19.91	37.50
Deer Creek	1	2	2.0	13.00	17.00	21.00	0.15	0.21	0.26	25.00	26.50	28.00
Fortine Sinclair	1	6	6.0	15.00	26.67	50.00	0.39	0.58	0.77	26.00	61.67	164.00
G-Man	2	10	5.0	7.00	22.00	31.00	0.15	0.40	0.62	3.00	73.80	132.00
Lubrecht Old Coloma	1	4	4.0	36.00	45.25	58.00	0.12	0.18	0.29	40.00	134.80	232.95
Lubrecht River Flats	11	47	4.3	5.00	29.49	63.00	0.01	0.40	0.76	2.10	104.38	486.00
McCall 1	2	13	6.5	20.32	41.42	58.42	0.15	0.42	0.86	30.50	201.23	435.00
McCall 3	3	11	3.7	20.32	36.02	50.80	0.29	0.56	0.82	51.50	186.55	317.00
McCall 4	5	25	5.0	7.62	33.22	63.50	0.16	0.48	0.84	6.00	185.88	833.50
McCall 5	1	4	4.0	15.24	19.68	22.86	0.42	0.59	0.77	55.00	67.88	78.50
Ninemile Edith Peak	2	9	4.5	10.00	17.89	25.00	0.39	0.54	0.67	11.00	43.56	88.00
Ninemile Petty Creek	3	19	6.3	7.00	33.63	45.00	0.20	0.43	0.71	10.00	146.05	310.00
Rexford Pinkham	7	25	3.6	6.00	13.92	50.00	0.05	0.34	0.62	2.00	23.01	265.19
Seeley Morrell Creek	2	13	6.5	14.00	34.77	51.00	0.28	0.52	0.84	17.00	94.12	194.45
St Maries	2	7	3.5	15.00	29.29	35.00	0.09	0.33	0.56	6.00	70.83	249.23
TMU	3	18	6.0	3.82	11.06	17.96	0.11	0.50	0.85	2.53	30.89	116.64
UI217	4	24	6.0	5.09	11.87	20.56	0.05	0.50	0.84	5.70	34.40	78.50
UI486	2	12	6.0	4.78	9.19	17.08	0.14	0.50	0.81	4.19	17.42	45.52
<b>All</b>	<b>64</b>	<b>312</b>	<b>4.9</b>	<b>3.82</b>	<b>23.67</b>	<b>69.00</b>	<b>0.01</b>	<b>0.44</b>	<b>0.87</b>	<b>0.57</b>	<b>84.97</b>	<b>833.50</b>

**Table 2.3** *Trees used to fit vertical foliar distribution models*

Site	n	DBH (mm)			TH (cm)			DBLC (mm)			CL (cm)		
		min	mean	max	min	mean	max	min	mean	max	min	mean	Max
Bandy	2	214.0	251.5	289.0	1849	1953	2056	170.0	196.5	223.0	1250	1257	1264
Carscallen	6	61.0	115.6	162.6	652	944	1137	71.1	149.9	246.4	585	879	1094
Coram 2	1	159.0	159.0	159.0	1894	1894	1894	94.0	94.0	94.0	827	827	827
Fortine Sinclair	1	317.0	317.0	317.0	2564	2564	2564	200.0	200.0	200.0	1307	1307	1307
Lubrecht River Flats	3	305.0	390.0	466.0	2887	2913	2954	220.0	255.0	309.0	2000	2089	2161
McCall 1	2	360.7	422.9	485.1	2993	3094	3194	233.7	265.4	297.2	1430	1599	1768
McCall 3	3	269.2	400.5	495.3	2478	2858	3072	208.3	312.4	388.6	1503	1681	1905
McCall 4	5	185.4	351.5	607.1	1948	2590	3423	81.3	268.2	533.4	951	1620	2359
McCall 5	1	264.2	264.2	264.2	2185	2185	2185	218.4	218.4	218.4	1722	1722	1722
Ninemile Edith Peak	2	164.0	174.5	185.0	1781	1997	2212	128.0	140.0	152.0	1397	1473	1549
Ninemile Petty Creek	3	307.0	388.0	443.0	2266	2481	2761	163.0	262.3	318.0	1354	1594	1762
Rexford Pinkham	7	118.0	170.6	206.0	1158	1573	1777	82.0	111.0	136.0	644	920	1201
Seeley Morrell Creek	2	380.0	394.0	408.0	3008	3011	3013	286.0	294.5	303.0	2263	2505	2746
St Maries	2	255.0	285.0	315.0	2490	2492	2493	134.0	144.5	155.0	742	924	1106
Tower Mixup	3	76.2	125.3	188.0	811	1079	1277	76.2	125.3	188.0	649	930	1140
UI-217	4	96.5	137.2	177.8	817	1058	1295	99.1	141.0	167.6	683	908	1055
UI-486	2	73.7	101.6	129.5	762	1012	1262	71.1	100.3	129.5	634	843	1052
<b>All</b>	<b>49</b>	<b>61.0</b>	<b>247.0</b>	<b>607.1</b>	<b>652</b>	<b>1951</b>	<b>3423</b>	<b>71.1</b>	<b>188.6</b>	<b>533.4</b>	<b>585</b>	<b>1294</b>	<b>2746</b>

site-level environmental variables and stand conditions were accounted for by including a random effect for site. Models were fit using maximum likelihood estimation with the “nlme” function in R (R Core Team 2017; Pinheiro et al. 2017) from starting parameter values obtained from “proc model” in SAS (SAS Institute Inc. 2016).

#### 2.3.4 Vertical distribution of foliage in the crown

Of the 50 trees for which foliage was estimated across all the branches, one was excluded as an outlier from the data used in vertical foliage distribution model testing because it only had 10 branches in the crown. Vertical distribution of FM estimated with the branch foliage mass model for all the branches in the crowns of the remaining 49 *L. occidentalis* trees (Table 2.3) were used to fit the left- and right-truncated [i] and un-truncated two-parameter Weibull, the  $\beta$ -distribution [ii], and the Johnson’s  $S_B$  [iii] functions. The general form of the PDFs are expressed as

$$[i] \quad p(X) = \frac{\beta X^{\beta-1} e^{-((X/\eta)^\beta - (\gamma/\eta)^\beta)}}{\eta^\beta}$$

$$[ii] \quad p(X) = \frac{X^c (1-X)^{d-1}}{\Gamma(c)\Gamma(d) / \Gamma(c+d)}$$

$$[iii] \quad p(X) = \frac{\tau e^{-\frac{1}{2}(\psi + \tau \ln \frac{X}{1-X})^2}}{\sqrt{2\pi} X(1-X)}$$

where  $X$  represents the position in the crown, and  $p(X)$  is the proportion of total crown FM at that position. Relative depth in the crown (RDIC, Table 2.1) was used for  $X$  to facilitate ease of comparison across crowns of different lengths (Weiskittel et al. 2009; Schneider et al.

2011; Nelson et al. 2014). Absolute values may be obtained by rescaling the interval of the fitted PDF from  $[0, 1]$  to the measured crown length of each tree and/or rescaling  $p(X)$  by total crown FM (Maguire and Bennet 1996; Garber and Maguire 2005). In the Weibull function [i],  $\beta$  is the skew (shape) parameter,  $\eta$  is the kurtosis (scale) parameter, and  $\gamma$  is the truncation point. In the  $\beta$ -distribution [ii],  $c$  and  $d$  are shape parameters, and  $\Gamma(x)$  is the gamma function. In Johnson's  $S_B$  [iii],  $\psi$  and  $\tau$  are shape parameters.

Relative to using RDIC or other branch position variables alone, the “binning” approach (e.g., Stenberg et al. 1993; Garber and Maguire 2005; Weiskittel et al. 2009) smooths data and improves the fit of density functions. Aggregating foliage into vertical strata of equal length reduces noise associated with variation in the size of branches (see Figure 3.2, Chapter 3, page 72 for an example). To improve fitting of PDFs, foliage in the crown was partitioned into 20 equal segments along the length of the stem in each crown.

Root mean square error (RMSE) and mean absolute bias (MAB) were calculated from observed data and predicted values summed across the bins for each tree. The distribution of error and bias across tree size was examined by plotting error and absolute bias against DBH. RMSE and overall MAB were also calculated across trees and used as model selection criteria to select the best-fitting PDF. Shape parameters were recovered for each tree from each PDF by maximum likelihood estimation (Weiskittel et al. 2009; Nelson et al. 2014). Tree vertical foliage distribution shape parameter estimates for the best-fitting PDF were then modeled as functions of tree variables to discern how the distribution changed with respect to intrinsic factors (Table 2.1). During model selection, published (Table 1.3), modified, and original equation forms were tested, and the simplest model (fewest parameters) among models that showed equivalent performance across a range of fit statistics was selected. Variation due to

unmeasured site-level variables were accounted for by including random effects for site. Models were fit and their parameters estimated by weighted least squares with fixed effects using the “nls” function and by maximum likelihood with mixed effects using the “nlme” function in R (R Core Team 2017; Pinheiro et al. 2017). Starting parameter values were obtained from the “proc model” function in SAS (SAS Institute Inc. 2016).

## 2.4 Results

### 2.4.1 Branch foliar mass model

A total of 91 branch FM models of a variety of forms borrowed and adapted from the literature were tested and compared (Table A2). A modified form of the Maguire and Bennet (1996) model (Eq. [2.1]) had the highest log likelihood score, the lowest Akaike information criterion (AIC) and root mean square error (RMSE), and the highest generalized and adjusted  $R^2$  for both fixed and combined fixed and random effects (Table 2.7). It was selected as the best model. Equation [2.1] includes random effects for site and tree within site in both the BD and RHIC terms, and a constant in the RHIC term. The model form was

$$[2.1] \quad FM = a_0 BD^{a_1 + \varphi_i + \omega_{ij}} (0.25 + RHIC)^{a_2 + \varphi_i' + \omega_{ij}' - 1} e^{a_3 CL}$$

where  $a_0$ ,  $a_1$ ,  $a_2$ , and  $a_3$  are parameters and  $\varphi_i$ ,  $\varphi_i'$ ,  $\omega_{ij}$ , and  $\omega_{ij}'$  are random effects from site  $i$  on BD, from site  $i$  on RHIC, from tree  $j$  within site  $i$  on BD, and from tree  $j$  within site  $i$  on RHIC, respectively. When applied to estimate foliar mass, the original form of the selected model (Eq. [2.5], Table A2) predicted zero foliar mass for the lowermost branches in the crowns. Since crown length was defined by live branches, an additional parameter was added to the relative height value before it was raised to its exponent to correct for the zero FM estimate obtained for the lowest branches. The additional parameter was estimated to be 0.25,

but was not significant ( $p > 0.05$ ). To keep all parameters significant, the actual value of 0.25 was substituted in Equation [2.1] as a constant. Substitution of a constant did not change the number of parameters, and therefore could not be tested in a log likelihood ratio test for a significant improvement in model fit; however, the log likelihood improved ( $\delta = 0.96$ ).

The exponential term for crown length significantly improved model fit over a base model that included only BD and RHIC (Eq. [2.5] over [2.12], Table A2) in a log likelihood ratio test ( $\chi^2 = 4.76$ ;  $df = 1$ ;  $0.025 < p < 0.05$ ). RHIC had more explanatory power than RDIC.

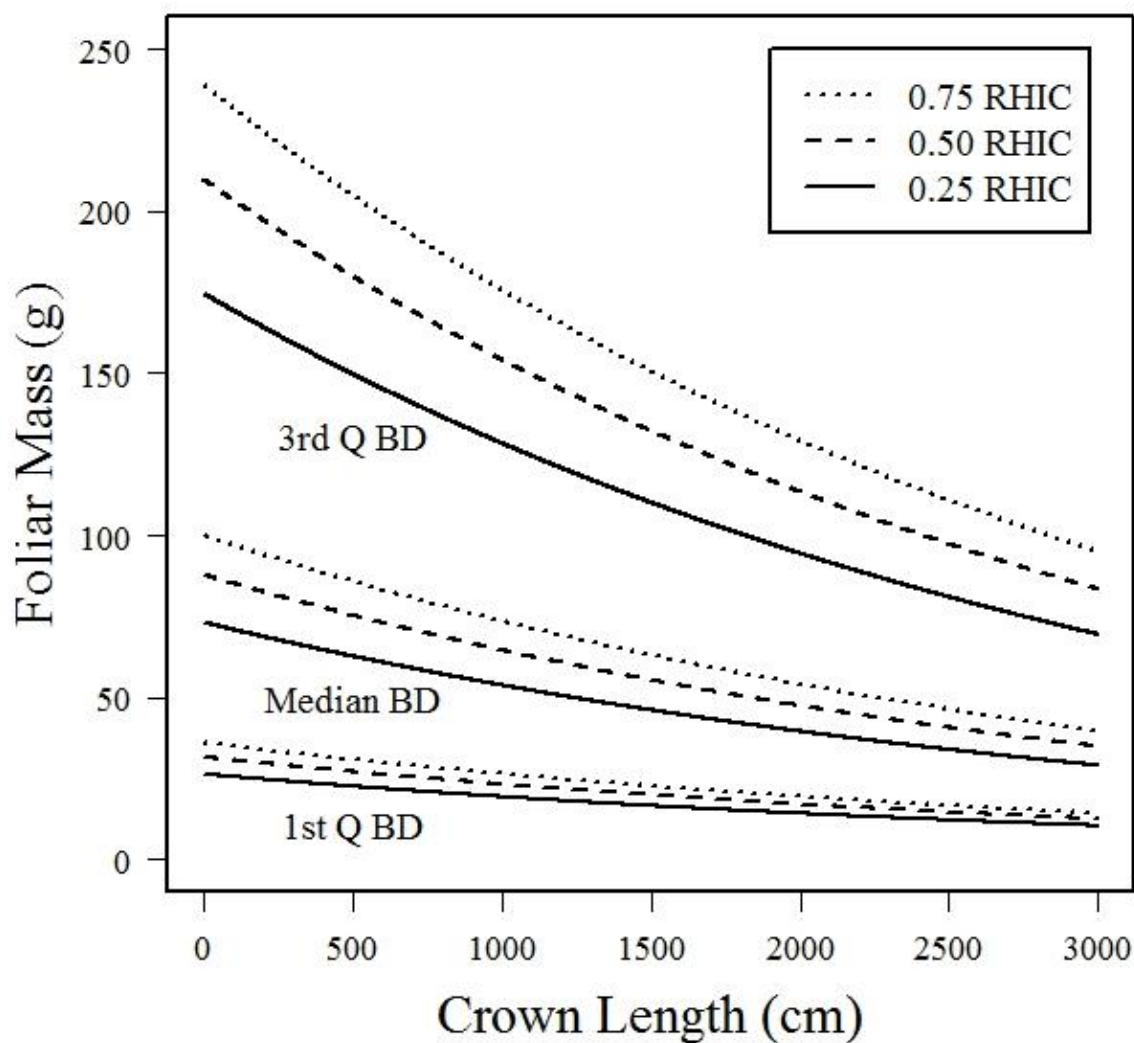


**Figure 2.2** Branch foliar mass predicted by Equation [2.1] by crown length (CL) for quartiles of relative height in the crown (RHIC) and branch diameter (BD)

Substituting RHIC for RDIC in the base model conferred a marginal reduction in error and increase in  $R^2$  and a substantial improvement in log likelihood ( $\delta = 3.56$ ; Eq. [2.15] over [2.12], Table A2). Random effects contributed to the  $R^2$  of Equation [2.1] (Table 2.7).

**Table 2.4** *Parameter estimates for branch and crown foliar mass models*

<b>Model</b>	<b>Par</b>	<b>Estimate</b>	<b>SD</b>	<b>p</b>
Branch FM Equation [2.1]	a0	0.602347	0.194738	0.002210
	a1	1.706984	0.101006	0.000000
	a2	1.452303	0.144354	0.000000
	a3	-0.000308	0.000126	0.015335
Crown FM Equation [2.2]	b1	38.380153	3.522708	0.000000
	b2	-3.155260	0.588623	0.000008

#### 2.4.2 Crown foliar mass model

In total, 26 different models for total crown foliage of a variety of forms borrowed and adapted from the literature were tested and compared (Table A3). Of the models tested with all significant parameters, the highest log likelihood, lowest AIC, and highest generalized and adjusted  $R^2$  for fixed effects (Table 2.7) were obtained from a modified form of the Kenefic and Seymour (1999) model for total crown foliage (Table 1.2), with random effects for site incorporated into coefficients for both DBH and HMC. The model form was

$$[2.2] \quad CFM = (b_1 + \varphi_i'')DBH + (b_2 + \varphi_i''')HMC$$

where  $b_1$  and  $b_2$  are parameters and  $\varphi_i''$  and  $\varphi_i'''$  are random effects from site  $i$  on DBH and HMC, respectively. In a simple linear model, absolute residuals from Equation [2.2] were positively correlated with DBH partitioned into 5 inch bins ( $F = 9.499$ ;  $df_1 = 1$ ;  $df_2 = 48$ ;  $p = 0.0034$ ;  $R^2 = 0.1652$ ). Like the original Kenefic and Seymour (1999) model (Eq. [2.112], Table A3), Equation [2.2] expresses total crown foliage as a linear function of DBH (Fig 2.3), but includes HMC instead of MCLR. There was a large improvement in the likelihood

between the original and modified forms ( $\delta = 7.77$ ). Overall, the lowest RMSE and highest generalized and adjusted  $R^2$  for combined fixed and random effects was obtained from an original form that was a mixed function with a power term for DBH and an exponential CL term (Eq. [2.111], Table A3), but inclusion of CL did not significantly improve model fit over a base model (Eq. [2.113], Table A3) in a likelihood ratio test ( $\chi^2 = 2.09$ ;  $df = 1$ ;  $0.1 < p < 0.9$ ). Inclusion of random effects improved the  $R^2$  of Equation [2.2] (Table 2.7).

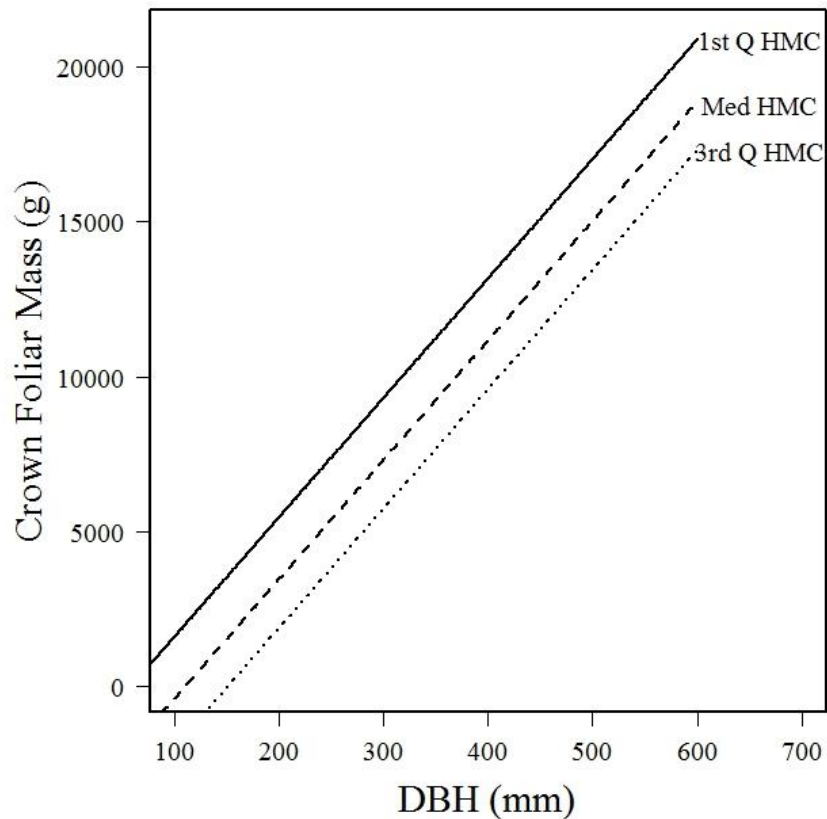


**Figure 2.3** Crown foliar mass predicted by Equation [2.2] by DBH for quartiles of height to middle of the crown (HMC)

#### 2.4.3 Vertical distribution of foliage in the crown

When fitting distribution models to the estimates of branch foliage for the branches of 49 trees (Tables A1 and 2.2), the right-truncated two-parameter Weibull gave the lowest root mean squared error (RMSE) and mean absolute bias (MAB) of the five probability density functions

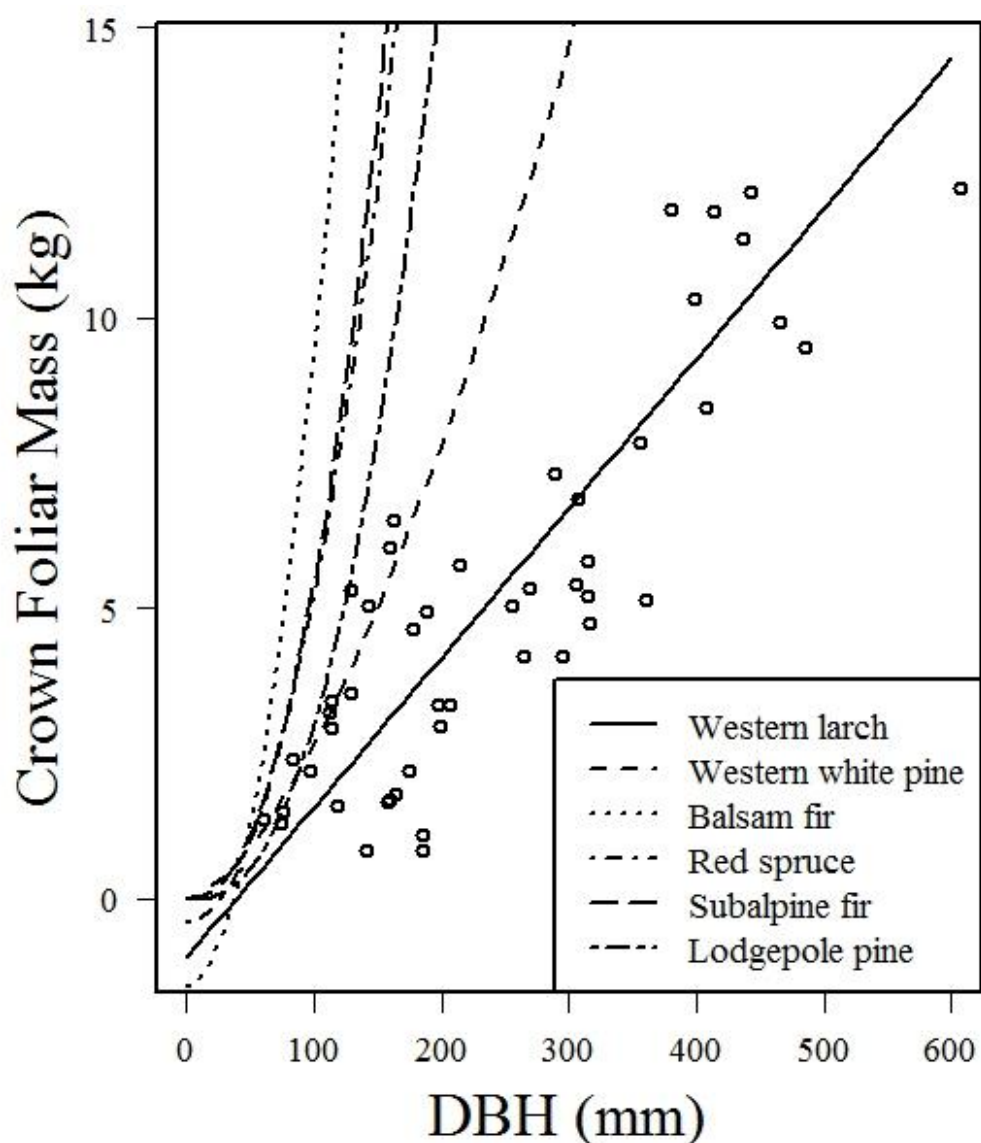


**Figure 2.4** Predicted and actual\* crown foliar mass by DBH<sup>†</sup> for *L. occidentalis* compared to predictions of models for other species<sup>‡</sup>

\*Actual values depicted as circles were estimated by branch summation from Equation [2.1].

<sup>†</sup>Height to the middle of the crown for Equation [2.2] was estimated using the linear model  $HMC = 316.8 + 3.9976DBH$  ( $F = 157.6$ ;  $df_1 = 1$ ;  $df_2 = 47$ ;  $p < 2.2E-16$ ;  $R^2 = 0.7702$ ).

<sup>‡</sup>Western white pine (Monserud and Marshall 1999); balsam fir and red spruce (Marchand 1983); subalpine fire (Smith and Long 1989); and lodgepole pine (Long and Smith 1989).

tested (Table 2.5). Both whole-tree RMSE and MAB of the Weibull estimates increased steadily with DBH (Figure 2.5). Across all trees, the maximum likelihood parameter

**Table 2.5** *Fit statistics for PDFs*

<b>Model</b>	<b>RMSE (g)</b>	<b>MAB (g)</b>
Weibull (right-truncated)	125.16	88.26
Weibull (no truncation)	126.17	88.84
Beta	134.53	95.68
Weibull (left-truncated)	135.86	95.21
Johnson's $S_B$	157.15	112.86

estimates for the right-truncated two-parameter Weibull had a mean of  $0.684 \pm 0.085$  and range of 0.448 to 0.858 for kurtosis ( $\eta$ ), and a mean of  $3.475 \pm 0.917$  and range of 2.064 to 6.362 for skew ( $\beta$ ). Overall, the majority of foliage was located in the lower crown. Peak foliage for the average values of the kurtosis and skew parameters occurred at RDIC = 0.62.

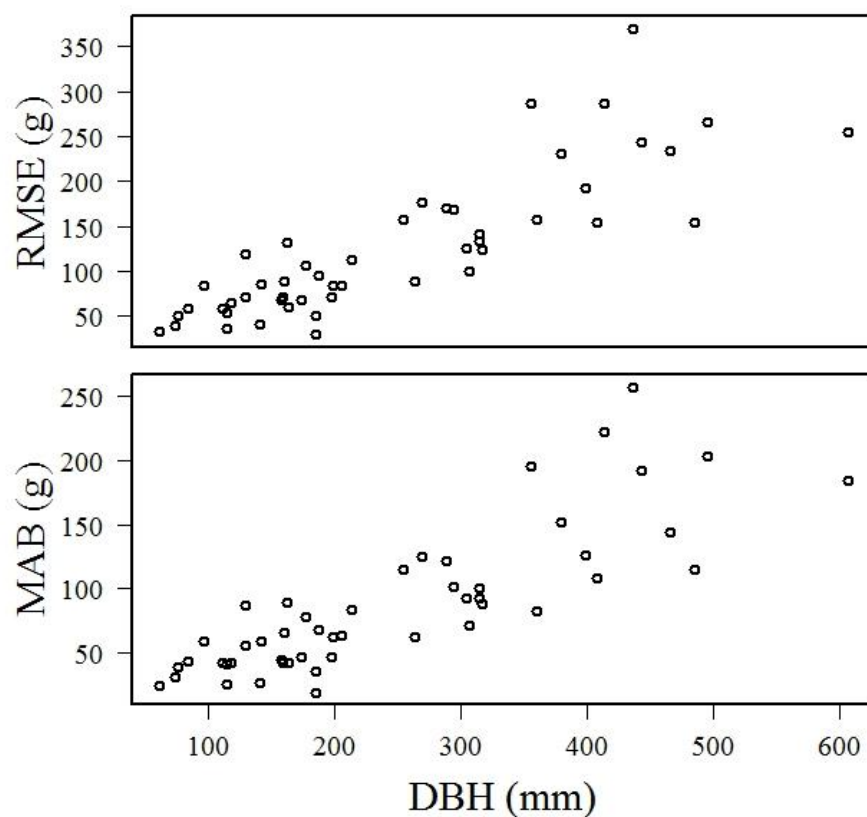


**Figure 2.5** *RMSE and MAB by tree size (DBH) of Weibull predictions of proportion of total FM in each bin*

A total of 28 different models of a variety of forms were fit to the kurtosis ( $\eta$ ) parameter estimates and compared (Table A4). The best-fitting model of the kurtosis parameter was a linear function of CL and DBLC, and had the form

$$[2.3] \quad \eta = g_0 + g_1 CL + g_2 DBLC$$

where  $g_0$ ,  $g_1$ , and  $g_2$  are parameters. No improvement in fit was observed by adding random effects for site (Eq. [2.121], Table A4), so random effects were not included. Equation [2.3] had the highest log likelihood, lowest AIC and RMSE, and highest generalized and adjusted fixed and combined fixed and random  $R^2$  among models tested (Table 2.7). In a likelihood ratio test, Eq. [2.3] showed significant improvement over a model expressing kurtosis as linear function of CL alone (Eq. [2.136], Table A4;  $\chi^2 = 6.19$ ;  $df = 1$ ;  $0.01 < p < 0.025$ ).

**Table 2.6** *Parameter estimates for models of vertical foliage distribution kurtosis and skew*

<b>Model</b>	<b>Par</b>	<b>Estimate</b>	<b>SD</b>	<b>p</b>
Weibull kurtosis ( $\eta$ )	g0	0.818712	0.023273	0.000000
Equation [2.3]	g1	-0.000204	0.000030	0.000000
	g2	0.000686	0.000162	0.000195
Weibull skew ( $\beta$ )	g3	2.632306	0.127060	0.000000
Equation [2.4]	g4	-0.883330	0.130914	0.000000
	g5	0.000043	0.000015	0.008123

A total of 18 different models of a variety of forms were fit to the skew ( $\beta$ ) parameter estimates and compared (Table A5). The best-fitting model of the skew parameter was a power function of CLR with the estimate of CFM obtained by branch summation with Equation [2.1] included in the exponent, with the form

$$[2.4] \quad \beta = g_3 CLR^{g_4 + \varphi_i''''} + g_5 CFM$$

where  $g_3$ ,  $g_4$ , and  $g_5$  are parameters and  $\varphi_i''''$  is the random effect from site  $i$  on CLR. Equation [2.4] had the highest log likelihood, the lowest AIC and RMSE, and highest

**Table 2.7** Fit statistics for models selected to estimate FM and its distribution

Model	LL	AIC	RMSE	Adjusted R <sup>2</sup>		Generalized R <sup>2</sup>	
				Fixed	Fixed + Rand	Fixed	Fixed + Rand
[2.1] Branch FM	-1653.52	3329.03	42.83	0.634	0.847	0.638	0.849
[2.2] Crown FM	-419.26	850.52	1032.05	0.832	0.934	0.835	0.935
[2.3] Kurtosis ( $\eta$ )	70.52	-131.04	0.057	0.516	0.516	0.536	0.536
[2.4] Skew ( $\beta$ )	-41.18	92.35	0.497	0.522	0.731	0.542	0.742

generalized and adjusted R<sup>2</sup> for fixed and combined fixed and random effects among models without all significant parameters. Equation [2.4] represented a significant improvement over a base model that was a power function of CLR alone (Eq. [2.154], Table A5) in a likelihood ratio test ( $\chi^2 = 8.09$ ; df = 1;  $p < 0.005$ ). Random effects contributed an improvement to the R<sup>2</sup> of Equation 2.4 (Table 2.7).

Based on parameter estimates for Equations [2.3-2.4] (Table 2.6), kurtosis ( $\eta$ ) increases as DBLC increases and as CL decreases. Skew ( $\beta$ ) increases as CFM increases and as CLR decreases (Figure 2.6). Substituting  $CLR = TH / CL$ , skew decreases as TH increases when CL is constant, and decreases as CL increases when TH is constant (Figure 2.7).

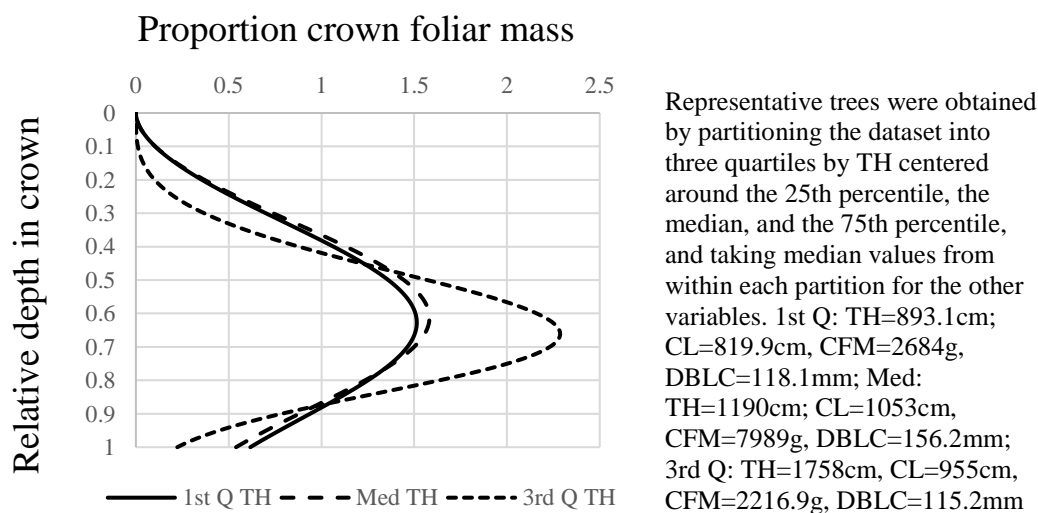


**Figure 2.6** Predicted vertical foliar mass distribution for representative *L. occidentalis* trees by height class under *L. occidentalis* model

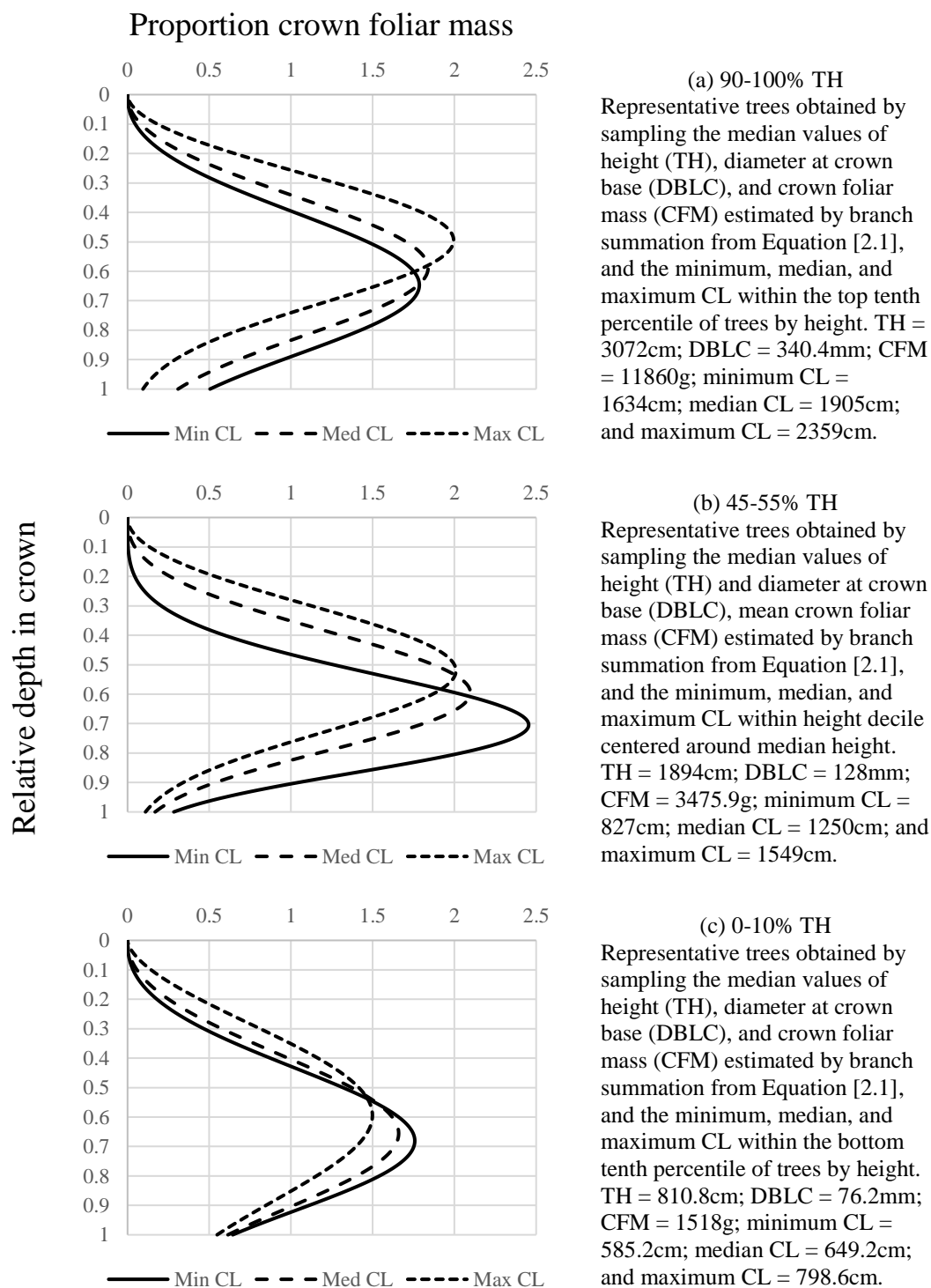


**Figure 2.7** Predicted vertical foliar mass distribution for representative *L. occidentalis* trees of minimum, median and maximum crown length (CL) within the bottom (c), middle (b), and top (a) deciles by height (TH)

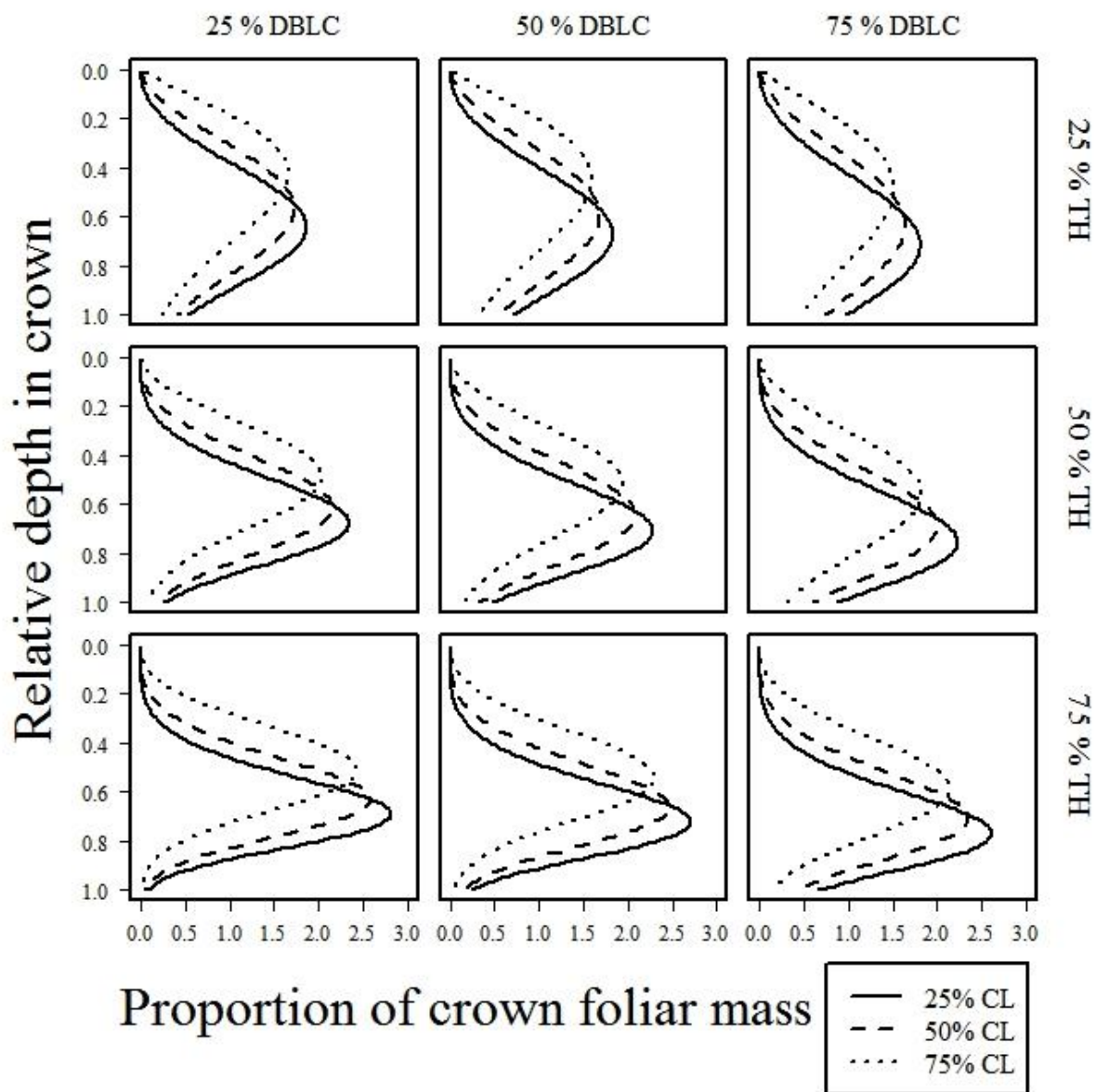


**Figure 2.8** Predicted vertical distribution of foliar mass in *L. occidentalis* at median CFM and quartiles of measured values of diameter at crown base (DBLC), tree height (TH), and crown length (CL), using the relationship  $CL = TH / CLR$

## 2.5 Discussion

### 2.5.1 Branch foliar mass

A combination of both branch- and tree-level variables provided the best predictive power to estimate branch foliar mass. Equation [2.1] resembles several branch foliage models selected for other species, but with notable exceptions. In previous models for the shade-tolerant *Picea rubens* Sarg. and the shade-intolerant *P. contorta* and *Pinus ponderosa* Dougl. ex Laws., branch leaf area increased with increasing depth into the crown (Maguire et al. 1998; Garber and Maguire 2005). In the shade-intolerant *Pinus sylvestris* L., whether branch foliar mass increased or decreased with branch depth was site-specific (Mäkelä and Vanninen 2001), suggesting the ability to adapt to light conditions. In another shade-intolerant species (*Pinus taeda* L.), branch foliar mass increased with increasing relative height in the crown (Gillespie et al. 1994; Xu and Harrington 1998), as it does in *L. occidentalis* according to Equation [2.1]. The light compensation point for photosynthesis is higher in shade-intolerant species like *P. taeda* and *L. occidentalis*. Thus, lower branches support less foliage because they are shaded by upper branches and unable to fix enough carbon to meet local respiratory demand.

Due to the exponential term in the model, branch foliar mass also depended on crown length. Whereas branch foliar mass increased positively with branch diameter and relative height, branches of similar diameter and height had less foliage in longer-crowned trees than short-crowned trees (Figure 2.2), most likely due to self-shading. Since *L. occidentalis* replaces all its foliage with a fresh cohort every year, where foliage is produced and how much can be supported by a branch both reflect immediate light conditions. Equation [2.1] is simpler than models for other species, which often include a second exponential term for relative branch position (Maguire et al. 1988; Xu and Harrington 1998; Kantola and Mäkelä

2004; Garber and Maguire 2005; Weiskittel et al. 2009; Nelson et al. 2014). Less plasticity in branch foliage production to absolute branch position and greater plasticity to overall crown size further indicate greater dependence of foliage biomass production on light conditions relative to hydraulic or structural constraints at the branch level.

### 2.5.2 Crown foliar mass

A simple linear model fit crown foliar mass for *L. occidentalis* as well as or better than nonlinear models. Because the range of tree sizes sampled for this study was within the range of previous studies, sampling scheme can be ruled out as a factor contributing to the selection of a linear over a nonlinear form. Kenefic and Seymour (1999) published a linear model to predict crown foliar mass from DBH and modified crown length ratio in *T. canadensis*. Ultimately, height to the middle of the crown was chosen as a superior substitute crown length ratio (see Table 2.1 for relationships). Cross-sectional area and height to the middle of the crown were also used to model total crown leaf area for *P. contorta* and *Abies lasiocarpa* (Hook.) Nutt., but fit a power series rather than a linear model (Smith and Long 1989; Long and Smith 1989).

Crown foliar mass was negatively correlated with height to the middle of the crown in *L. occidentalis* (Table 2.4; Figure 2.3). This finding adds to widespread and consistent observations that have shown larger trees to support more foliage, but less as the crown recedes (Dean and Long 1986; Maguire and Bennet 1996; Weiskittel et al. 2009; Monserud and Marshall 1999), although most previous models were non-linear. Crown foliar mass was also positively correlated with DBH but inversely related to height to middle of the crown in *P. taeda* (Jerez et al. 2005). In taller *L. occidentalis*, greater growth efficiency, per-unit-mass

photosynthetic capacity, hydraulic constraints, or spatial dependence of foliage production on immediate light conditions could be responsible for the lower relative rate of foliar space-filling observed in the crown compared to other species (Figure 2.4). Unlike deciduous conifers, evergreens accumulate more foliage by retaining cohorts from previous years, which may lead to higher observed rates of foliage biomass scaling (Marchand 1983; Long and Smith 1989; Smith and Long 1989; Monserud and Marshall 1999). The greater variance in crown foliar mass observed for larger trees could be due to branch shedding, epicormic sprouting, or cumulative deteriorative effects of disease and severe weather events on the crown over longer life-spans.

In contrast, in saplings with small DBH and height to the middle of the crown, crown foliar mass might increase as fast or faster in *L. occidentalis* than in other species. Evergreens whose crown foliar mass scales as a power or exponential function of DBH should accumulate foliage at a slower rate than *L. occidentalis* when young if the initial slope of the exponential crown foliar mass model is lower than the slope of the linear crown foliar mass model. The estimated linear coefficient for DBH in the linear crown foliar mass model for *L. occidentalis* (Table 2.4) is almost twice as high as the initial slope parameter estimate for allometric power series models of crown foliar mass for *P. ponderosa* and nearly eight times higher than the initial slope for *Pinus monticola* Dougl. ex D. Don in Idaho (Monserud and Marshall 1999). Much faster initial accumulation of foliage in young trees predicted for *L. occidentalis* compared to sympatric conifer species is consistent with the growth rate advantage observed for *L. occidentalis* saplings on open disturbed sites.

Besides being inconsistent with models for other species, the linear relationship between crown foliar mass and DBH and height to the middle of the crown in *L. occidentalis*

does not support the theory of allometric scaling of foliage with a power function of diameter across tree species life histories and niche space (Osawa et al. 1991; Enquist et al. 1999).

However, linear scaling of total crown foliar mass with DBH and height to the middle of the crown is consistent with the hypothesis that foliar crown volume-filling is limited by self-shading. *L. occidentalis* is among the most shade-intolerant species of conifers and its crown foliage scales with body mass with a fractal dimension well outside the distribution observed across most other conifer species (Duursma et al. 2010).

### 2.5.3 Vertical distribution of foliage in the crown

As expected based on previous findings (Maguire and Bennet 1996; Weiskittel et al. 2009), the vertical distribution of foliage in the crown depended on crown length, crown length ratio, and crown foliar mass. The positive correlation of DBH with RMSE and MAB (Figure 2.5) is likely due to larger absolute predicted and actual values of foliar mass per vertical bin in larger trees, since total crown foliar mass was positively correlated with DBH. Older trees also had a longer period of potential exposure to extrinsic factors such as shade and below-ground competition during stand development, as well as a higher cumulative probability of experiencing severe weather, pests, disease, etc. Extrinsic factors could have contributed to greater variation in the distribution that could not be accounted for with a model that only considered intrinsic factors.

Consistent with the exponential term for crown length in the branch foliage models used to generate foliage estimates for individual branches, crown length and crown length ratio had significant effects on the vertical foliage distribution of *L. occidentalis*. The downward shift and much more mono-layered foliage distribution predicted by our model for

taller *L. occidentalis* (Table 2.6; Figures 2.6-2.8) is similar to that of other shade-intolerant species (Van Hees and Bartelink 1993; Maguire and Bennet 1996). With respect to crown length, *L. occidentalis* has a more diffuse distribution of foliage centered at a higher position in longer-crowned relative to shorter-crowned trees (Figure 2.8), which is consistent with the hypothesis that self-shading acts as an important constraint on foliage allocation in this species. However, the tallest trees showed the opposite trend—a decrease in kurtosis as the crown lengthened—when the model was simulated on representative trees generated from summary statistics (Figure 2.7). Similar to these findings, *Pseudotsuga menzeisii* var. *menzeisii* (Mirb.) Franco vertical foliage distribution also shows increasing kurtosis and an upward shift under conditions of increasing shade competition (Maguire and Bennet 1996). In contrast to *L. occidentalis* and *P. menzeisii*, shade-tolerant evergreens shift foliage upward into a more monolayered distribution with increasing crown length even at young ages (Weiskittel et al. 2009).

The preferential allocation of foliage within a more condensed stratum lower in the crowns of taller shade-intolerant trees may reflect a balancing act between minimizing water loss while maximizing light capture. Vapor deficit is likely to be higher in the upper canopy of tall trees, and may exert more influence than stem water deficit on stomatal behavior in *L. occidentalis* and other *Larix* spp. (Higgins et al. 1987; Anfodillo et al. 1998). Soil water content may not be an important factor for *L. occidentalis* rooted deeply on moist sites, but low humidity occurs frequently in the west. By allocating foliage in a monolayer deep in the crowns of dominant and codominant trees, the stomata can remain open, and high levels of photosynthesis may be maintained as long as there is ample supply of water from the stem. Furthermore, the gravitational component of water potential is more negative in the

uppermost branches of the tallest trees, potentially limiting foliage production. It is also possible that the tallest trees were of dominant social position such that the lower portion of the crown received ample light, allowing more foliage to be supported on the lower branches.

Most other studies also found that a measure of total crown foliage significantly accounted for variance in its vertical distribution (Maguire and Bennett 1996; Utsugi et al 2006; Weiskittel et al. 2009). This widespread observation makes sense because greater amounts of total foliage are likely to lead to greater self-shading and hydraulic constraints on the vertical foliage distribution. However, unlike previous studies, our model of vertical foliage distribution also included diameter at the base of the crown (DBLC) as a significant component of the variance in the vertical foliage distribution. The strong correlation between DBLC and crown biomass across tree species is a well-explored relationship foundational to the pipe-model theory of tree growth (Shinozaki et al. 1964; Chiba et al. 1988; Osawa et al. 1990), and a functional consequence of the allometric scaling of metabolism with mass (Enquist et al. 1999), which is known to be constrained by self-shading (Duursma et al. 2010). The slightly more upward-shifted and more diffuse distribution of foliage associated with smaller values of DBLC under our model for *L. occidentalis* (Table 2.6; Figure 2.8) could be the consequence of less residual carbon available for diameter growth in light-limited growing environments such as dense stands where increased side shade has led to crown recession.

#### 2.5.4 Conclusions

*L. occidentalis* appears to exhibit dynamic patterns of biomass allocation and retention driven by immediate growing conditions. Preferential allocation of productive biomass to better-lit portions of the canopy drives the observed variation in foliar mass and its distribution. Shorter

crowns support more foliage per branch and higher densities of foliage in better-lit strata. Allocation of woody biomass in the crown, which determines where foliage can be produced, is also likely to be driven by immediate growing conditions. Notably, the representative trees from the 1st and 3rd quartile by height both had longer crowns than the representative tree of median height (Figure 2.6, caption). These observations may be due to branch shedding in median height-class trees in response to competition with neighboring trees, crown lengthening under dominant social position for tall trees, and open site conditions for the youngest trees. As a result, trees of intermediate height exhibited a more leptokurtic foliage distribution than the smallest or largest trees (Figures 2.6-2.7). The younger trees in the dataset had many more branches than the older trees (Table A1), indicating branches are shed at a high rate as the stand develops and side-shade increases.

The plasticity of the vertical foliage distribution of *L. occidentalis* to light availability, is likely facilitated by higher turnover of biomass and indeterminate development, in line with previously observed spatial correlation between biomass production and light intensity within the crowns of other *Larix* spp. (Kurachi et al. 1986; Osawa 1990). In another shade-intolerant conifer (*Pinus banksiana* Lamb.), observed variation in vertical distribution of foliage, though markedly opposite *L. occidentalis* with respect to crown length and height, could be accounted for primarily by variation in allocation of internodal foliage (Schneider et al. 2011). Shade intolerance has a physiological basis at the leaf level, such that new foliage produced in the spring is passively allocated to well-lit and more productive portions of the crown.

The intrinsic dynamics of vertical foliage distribution in *L. occidentalis* may arise from the interaction between light and hydraulic factors. Unlike broadleaf deciduous trees, which concentrate foliage in a monolayer at the top of the crown, *L. occidentalis* foliage has a

relatively diffuse distribution more similar to its coniferous relatives, with peak density closer to the crown base (Maguire and Bennet 1996; Weiskittel et al. 2009). A multilayered crown form is inferior in the understory but hydraulically advantageous on the exposed, disturbed sites where *L. occidentalis* prefers to regenerate (Horn 1971). Because *L. occidentalis* foliage is relatively unprotected, constraints from more negative water potentials and/or higher vapor deficits in the upper crown may impose some limit on the magnitude of the upward shift in the foliage distribution in response to shade. However, this study did not explicitly investigate the effect of water potential, social position, or stand density on vertical foliage allocation.

Shade-tolerant conifers have a characteristic capacity for adaptive morphological response to different stand conditions. When light is limiting, shade-tolerant species produce foliage with higher specific leaf area and thus higher photosynthetic rate per unit mass (Fry & Phillips 1977; Chen et al. 1996). Whereas evergreen species are able to flush new foliage in the upper part of the crown and the ends of branches while retaining older cohorts in the lower and inner crown (Wang et al. 1990; Kershaw and Maguire 1996; Weiskittel et al. 2008), *L. occidentalis* is limited in its ability to shift vertical foliage distribution to optimize photosynthesis when light becomes limiting. Despite the high level of plasticity afforded by annual turnover of crown foliage, indeterminate growth, and epicormic branching, *L. occidentalis* is maladapted to light and hydraulic limitations. The disadvantage exhibited by *L. occidentalis* in shade conditions may stem jointly from low light compensation point at the individual leaf level a passive and consequently less efficient characteristic pattern of intrinsic vertical foliage allocation.

## 2.6 Works cited

1. Anfodillo, T., Rento, S., Carraro, V., Furlanetto, L., Urbinati, C., and Carrer, M. 1998. Tree water relations and climatic variations at the alpine timberline: seasonal changes of sap flux and xylem water potential in *Larix decidua* Miller, *Picea abies* (L.) Karst. and *Pinus cembra* L. *Ann. Sci. Forest.* **55**(1-2): 159-172.
2. Arno, S.F., Smith, H.Y., and Krebs, M.A. 1997. Old Growth Ponderosa Pine and Western Larch Stand Structures: Influence of Pree-1900 Fires and Fire Exclusion. USDA For. Serv. Res. Pap. INT-RP-495.
3. Bidlake, W.R. and Black, R.A. 1989. Vertical distribution of leaf area in *Larix occidentalis*: a comparison of two estimation methods. *Can. J. For. Res.* **19**: 1131-1136.
4. Buckley, D.S., Zasada, J.C., Tappeiner, J.C., II, and Stone, D.M. 1997. Plant morphological characteristics as a tool in monitoring response to silvicultural activities. *In* Communicating the role of silviculture in managing the national forests: Proceedings of the National Silviculture Workshop. Warren, PA, 19-22 May 1997. UDSA For. Serv. Gen. Tech. Rep. NE-238: 37-41.
5. Chen, H.Y., Klinka, K., and Kayahara, G.J. 1996. Effects of light on growth, crown architecture, and specific leaf area for naturally established *Pinus contorta* var. *latifolia* and *Pseudotsuga menziesii* var. *glauca* saplings. *Can. J. For. Res.* **26**(7): 1149-1157.
6. Chiba, Y., Fujimori, T., and Kiyono, Y. 1988. Another interpretation of the profile diagram and its availability with consideration of the growth process of forest trees. *J. Jpn. For. Soc.* **70**(6): 245-254.
7. Dean, T.J., and Long, J.N. 1986. Variation in sapwood area—leaf area relations within two stands of lodgepole pine. *Forest Sci.* **32**(3): 749-758.
8. Duursma, R.A., Mäkelä, M., Reid, D.E.B., Jokela, E.J., Porte, A.J., and Roberts, S.D. 2010. Self-shading affects allometric scaling in trees. *Funct. Ecol.* **24**: 723 -730.
9. Enquist, B.J., West, G.B., Charnov, E.L., and Brown, J.H. 1999. Allometric scaling of production and life history variation in vascular plants. *Nature* **401**: 907-911
10. Fry, D.J., and Phillips, I.D.J. 1977. Photosynthesis of conifers in relation to annual growth cycles and dry-matter production. 2. Seasonal photosynthetic capacity and mesophyll ultrastructure in *Abies grandis*, *Picea sitchensis*, *Tsuga heterophylla* and *Larix leptolepis* growing in south west England. *Physiol. Plant.* **40**(4): 300-306.
11. Garber, S.M., and Maguire, D.A. 2005. The response of vertical foliage distribution to spacing and species composition in mixed conifer stands in central Oregon. *Forest Ecol. Manag.* **211**: 341-355.

12. Gillespie, A.R., Allen, H.L., and Vose, J.M. 1994. Amount and vertical distribution of foliage of young loblolly pine trees as affected by canopy position and silvicultural treatment. *Can. J. For. Res.* **24**(7): 1337-1344.
13. Goudie, J.W., Parish, R., and Antos, J.A. 2016. Foliage biomass and specific leaf area equations at the branch, annual shoot and whole-tree levels for lodgepole pine and white spruce in British Columbia. *Forest Ecol. Manag.* **361**: 286-297.
14. Gower, S.T., and Richards, J.H. 1990. Larches: Deciduous Conifers in an Evergreen World. *BioScience.* **40**(11): 818-826.
15. Higgins, S.S., Black, R.A., Rademaker, G.K., and Bidlake, W.R. 1987. Gas exchange characteristics and water relations of *Larix occidentalis*. *Can. J. For. Res.* **17**(11): 1364-1370.
16. Horn, H.S. 1971. *The Adaptive Geometry of Trees*. Princeton University Press, Princeton, N.J.
17. Jerez, M., Dean, T.J., Cao, Q.V., and Roberts, S.D. 2005. Describing Leaf Area Distribution in Loblolly Pine Trees with Johnson's SB Function. *Forest Sci.* **51**(2): 93-101.
18. Kantola A., and Mäkelä, A. 2004. Crown development in Norway spruce [*Picea abies* (L.) Karst.]. *Trees* **18**: 408-421.
19. Kenefic, L.S., and Seymour, R.S. 1999. Leaf area prediction models for *Tsuga canadensis* in Maine. *Can. J. For. Res.* **29**(10): 1574-1582.
20. Kershaw, J.A., and Maguire, D.A. 1996. Crown structure in western hemlock, Douglas-fir, and grand fir in western Washington: horizontal distribution of foliage within branches. *Can. J. For. Res.* **26**:128-142.
21. Kretschmann, D.E. 2010. Mechanical properties of wood (Chapter 5). *In Wood Handbook: Wood as an Engineering Material*. USDA For. Serv. Gen. Tech. Rep. FPL-GTR 190.
22. Kurachi, N., Hagihara, A., and Hozumi, K. 1986. Distribution of leaf- and branch-biomass density within a crown of Japanese larch and its relationship to primary production: analysis by sainome-cutting. *In Crown and Canopy Structure in Relation to Productivity*, Ibaraki, Japan, 14-20 October 1985. *Edited by* T. Fujimori and D. Whitehead. Forestry and Forest Products Research Institute, Ibaraki, Japan. pp. 308-322.
23. Lanner, R.M. 1995. The Role of Epicormic Branches in the Life History of Western Larch. *In Ecology and Management of Larix Forests: Proceedings of an International Symposium*, Whitefish, MT., 5-9 October 1992. *Edited by* W.C. Schmidt and K.J. McDonald. USDA For. Serv. Gen. Tech. Rep. GTR-INT-319. pp. 323-326.

24. Long, J.N., and Smith, F.W. 1989. Estimating leaf area of *Abies lasiocarpa* across ranges of stand density and site quality. *Can. J. For. Res.* **19**: 930-932.
25. Li, F. 2004. Modeling Crown Profile of *Larix olgensis* Trees. *Sci. Silv. Sin.* **40**(5): 16-24.
26. Maguire, D.A., Brissette, J. C., and Gu, L. 1998. Crown structure and growth efficiency of red spruce in uneven-aged, mixed-species stands in Maine. *Can. J. For. Res.* **28**(8), 1233-1240.
27. Maguire, D.A., and Bennett, W.S. 1996. Patterns in vertical distribution of foliage in young coastal Douglas-fir. *Can. J. For. Res.* **16**: 1991-2005.
28. Marchand, P.J. 1984. Sapwood area as an estimator of foliage biomass and projected leaf area for *Abies balsamea* and *Picea rubens*. *Can. J. For. Res.* **14**(1): 85-87.
29. Mäkelä, A., and Vanninen, P. 2001. Vertical structure of Scots pine crowns in different age and size classes. *Trees* **15**: 385-392.
30. McClelland, B.R., Frissell, S.S., Fischer, W.C., and Halvorson, C.H. 1979. Habitat management for hole-nesting birds in forests of western larch and Douglas-fir. *J. Forest.* **77**(8): 480-483.
31. Monserud, R.A., and Marshall, J.D. 1999. Allometric crown relations in three northern Idaho conifer species. *Can. J. For. Res.* **29**(5): 521-535.
32. Nelson, A.S., Wagner, R.G., Weiskittel, A.R., and Saunders, M.R. 2015. Effects of species composition, management intensity, and shade tolerance on vertical distribution of leaf area index in juvenile stands in Maine, USA. *Eur. J. Forest Res.* **134**: 281-291.
33. Nelson, A.S., Weiskittel, A.R., and Wagner, R.G. 2014. Development of branch, crown, and vertical distribution leaf area models for contrasting hardwood species in Maine, USA. *Trees* **28**: 17-30.
34. Niinemets, Ü., and Kull, K. 1994. Leaf weight per area and leaf size of 85 Estonian woody species in relation to shade tolerance and light availability. *For Ecol. Manag.* **70**: 1-10.
35. Oliver, C.D., and Larson, B.C. 1990. *Forest stand dynamics*. McGraw-Hill, NY, NY.
36. Osawa A., Ishizuka, M., and K. Yoichi. 1991. A profile theory of tree growth. *Forest Ecol. Manag.* **41**:33-63.
37. Osawa, A. 1990. Reconstructed development of stem production and foliage mass and its vertical distribution in Japanese larch. *Tree Physiol.* **7**: 189-200.

38. Pinheiro, J., Bates, D., DebRoy, S., Sarkar, D. and R Core Team. 2017. nlme: Linear and Nonlinear Mixed Effects Models. R package version 3.1-131. Available from <https://CRAN.R-project.org/package=nlme> [accessed 18 April 2017].
39. R Core Team. 2017. R: A language and environment for statistical computing. R Foundation for Statistical Computing, Vienna, Austria. Available from <https://www.R-project.org/> [accessed 18 April 2017].
40. Rehfeldt, G.E., and Jaquish, B.C. 2010. Ecological impacts and management strategies for western larch in the face of climate-change. *Mitig. Adapt. Strat. Gl.* **15**: 283-306.
41. Schmidt, W.C. and Shearer, R.C. 1990. Western larch (*Larix occidentalis*). In *Silvics of North America: Vol 1. Conifers. Edited by R.M. Burns and B. Honkala*. USDA For. Serv. Ag. Hand. No. 654.
42. Schneider, R., Fortin, M., Berninger, F., Ung, C. H., Swift, D.E., and Zhang, S.Y. 2011. Modeling Jack Pine (*Pinus banksiana*) Foliage Density Distribution. *Forest Sci.* **57**(3): 180-188.
43. Shinozaki, K., Yoda, K., Hozumi, K. and Kira, T. 1964. A quantitative analysis of plant form: the pipe model theory. 1. Basic analyses. *Jap. J. Ecol.* **14**(3): 97-105.
44. Smith, F.W., and Long, J.N. 1989. The influence of canopy architecture on stemwood production and growth efficiency of *Pinus contorta* var. *latifolia*. *J. Appl. Ecol.* **26**: 681-691.
45. Stenberg, P., Kuuluvainen, T., Kellomäki, S., Grace, J.C., Jokela, E.J., and Gholz, H.L. 1994. Crown Structure, Light Interception and Productivity of Pine Trees and Stands. *Ecol. Bull.* **43**: 20-34.
46. Stenberg, P., Smolander, H., and Kellomäki, S. 1993. Description of crown structure for light interception models: angular and spatial distribution of shoots in young Scots pine. *Stud. For. Suec.* **191**: 43-50.
47. Utsugi, H., Araki, M., Kawasaki, T., and Ishizuka, M. 2006. Vertical distributions of leaf area and inclination angle, and their relationship in a 46-year-old *Chamaecyparis obtusa* stand. *Forest Ecol. Manag.* **225**(1): 104-112.
48. Van Hees, A.F.M., and Bartelink, H.H. 1993. Needle area relationships of Scots pine in the Netherlands. *Forest Ecol. Manag.* **58**(1): 19-31.
49. Vose, J.M., Clinton, B.D., Sullivan, N.H., and Bolstad, P.V. 1995. Vertical leaf area distribution, light transmittance, and application of the Beer-Lambert law in four mature hardwood stands in the southern Appalachians. *Can. J. For. Res.* **25**(6): 1036-1043.
50. Wang, Y.P., Jarvis, P.G., and Benson, M.L. 1990. Two-dimensional needle-area density distribution within the crowns of *Pinus radiata*. *Forest. Ecol. Manag.* **32**:217-237.

51. Waring, R.H. 1983. Estimating forest growth and efficiency in relation to canopy leaf area. *Adv. Ecol. Res.* **13**: 327-354.
52. Weiskittel, A.R., Kershaw, J.A., Hofmeyer, P.V., and Seymour, R.S. 2009. Species differences in total and vertical distribution of branch- and tree-level leaf area for the five primary conifer species in Maine, USA. *Forest Ecol. Manag.* **258**: 1695-1703.
53. Weiskittel, A.R., Temesgen, H., Wilson, D.S., and Maguire, D.A. 2008. Sources of within- and between-stand variability in specific leaf area of three ecologically distinct conifer species. *Ann. Forest Sci.* **65**:103.
54. Xu, M., and Harrington, T.B. 1998. Foliage biomass distribution of loblolly pine as affected by tree dominance, crown size, and stand characteristics. *Can. J. For. Res.* **28**: 887-892.
55. Zhao, X., and Wang, X. 2004. Study on branching pattern plasticity of *Larix chinensis*. *Acta Bot. Bor.-Occ. Sin.* **25**(1): 113-117.

## Chapter III

### SPATIAL VARIATION IN SPECIFIC LEAF AREA AND HORIZONTAL DISTRIBUTION OF LEAF AREA IN JUVENILE WESTERN LARCH

#### 3.1 Abstract

Leaf area, specific leaf area (SLA), and their spatial distribution in the crown are important indicators of biological response to changes in growing conditions including light and water availability. Patterns of foliage allocation within the crown can be related to species life history differences. Western larch (*Larix occidentalis* Nutt.) is a deciduous coniferous pioneer species in the Inland Northwest (INW) known for its rapid growth, high-quality wood, and ecological importance. Analysis of nonlinear models revealed that SLA and horizontal leaf area distributions differ between cardinal quadrants of juvenile western larch crowns. Similar to other conifers, horizontal distributions of foliage in western larch also shifted further outward towards the branch tips with increasing depth in the crown. The horizontal distribution became more concentrated as the crown receded. The ability of western larch to concentrate foliage to more illuminated portions of the canopy derives passively from its extreme shade intolerance and annually-deciduous habit. However, the higher SLA observed on the more exposed, southern side of the crown and the proximal shift of horizontal distribution of leaf area observed in the southwest quadrant are likely due to hydraulic factors.

#### 3.2 Introduction

Among other things, gross photosynthesis depends on water and light availability and the distribution of leaf area within the canopy, including its horizontal distribution along branches (Horn 1971; Stenberg et al. 1993). As light penetrates deeper into the crown from both

vertical and horizontal directions, the amount of photosynthetically active radiation available to foliage is diminished (Stenberg et al. 1994). The size of gaps between trees in a stand and the amount of resulting side shade are major determinants of light interception, and horizontal distribution of foliage and lateral branch growth feedback on each other during canopy closure (Oliver and Larson 1990).

Leaf area (LA) and foliar mass (FM) differ in their distributions within the crown; their relative distributions can be related to one another through spatial variation in specific leaf area (SLA), the ratio of projected area to dry weight biomass. SLA is positively correlated with net photosynthesis on a leaf mass basis (Jurik 1986; Oren et al. 1986; Ellsworth and Reich 1993; Reich et al. 1997). SLA is generally higher for shade-tolerant species than shade-intolerant species, and has been observed to decrease with light availability (Niinemets and Kull 1994; Niinemets and Kull 1995; Niinemets 1996; Temesgen and Weiskittel 2006; Perrin and Mitchell 2013). The amount and components of SLA variance differ between species (Marshall and Monserud 2002; Goudie et al. 2016), with greater variance across light gradients reported for shade-tolerant relative to shade-intolerant species (Chen et al. 1996; Bond et al. 1999). SLA also decreases as leaves age and is negatively correlated with leaf lifespan (Gulmon and Chu 1981; Chabot and Hicks 1982; Reich et al. 1997; Ishii et al. 2002; Temesgen and Weiskittel 2006; Weiskittel et al. 2008).

In addition to light availability, hydraulic factors are also thought to underpin spatial variation in SLA. Functional limitation of SLA due to lower turgor pressure during initial leaf expansion is the basis for the hydraulic resistance and gravitational water potential hypotheses to explain observations of decreasing SLA with longer paths traveled by water to developing foliage (Tardieu et al. 1999; Phillips and Riha 1993; Ibrahim et al. 1998; Myers et al. 1998;

Marshall and Monserud 2003). Under this hypothetical framework, the degree of variation in SLA should also depend on stomatal conductance, which is more strongly linked to vapor deficit and/or stem water potential in some species than others (Anfodillo et al. 1998).

Western larch (*Larix occidentalis* Nutt.) is a shade-intolerant pioneer, and unique among mid-elevation mesic species of the Inland Northwest (INW) for its deciduous habit. As an important provider of wildlife habitat (McClelland et al. 1979) and the fastest growing and most fire-adapted species in the region (Schmidt and Shearer 1990), *L. occidentalis* is worthy of focus for research to improve management strategies. Due to past and projected declines precipitated by fire suppression (Arno et al. 1997) and climate change (Rehfeldt and Jaquish 2010), *L. occidentalis* has also been targeted by public-sector restoration efforts (Scott et al. 2013). While *L. occidentalis* has an advantage on disturbed sites due to high photosynthetic rate per unit mass of high-SLA foliage and sustained stomatal conductance through the growing season (Higgins et al. 1987), it suffers during stand competition. Side-shade is an important factor during stand competition (Oliver and Larson 1990). Thus, plasticity of horizontal distribution of leaf area defines the adaptive response to stand competition.

Previous studies have used probability density functions (PDFs) to model horizontal foliage distributions (Wang et al. 1990; Stenberg et al. 1993; Kershaw and Maguire 1996; Xu and Harrington 1998; Temesgen et al. 2003), and fixed and mixed effects models to describe spatial variation of SLA within the crowns of other species (Ishii et al. 2002; Marshall and Monserud 2002; Temesgen and Weiskittel 2006; Weiskittel et al. 2008; Fellner et al. 2016). In most species, horizontal distribution of foliage depends on relative vertical position in the crown and crown length (Stenberg et al. 1993; Kershaw and Maguire 1996; Xu and Harrington 1998; Temesgen et al. 2003). Through analysis of the sign and magnitude of

correlation of SLA and leaf area distribution with intrinsic variables and through comparison between species with contrasting life histories, spatial foliage distribution modeling permits the identification of morphological response factors underlying autoecological traits such as site preference, shade-intolerance, and growth rate. Development of baseline empirical leaf area and SLA distribution models can provide a framework for future research investigating the response of *L. occidentalis* to extrinsic variables such as management, natural disturbance, and climate change (Buckley et al. 1997). Baseline models will also allow inferences to be made about how light and hydraulic conditions constrain horizontal distribution of leaf area.

We employed a multilevel modeling approach to identify the major intrinsic components of variance of SLA and leaf area in crowns of juvenile *L. occidentalis*. The specific objectives of the study were: A) to develop spatial models of SLA as functions of intrinsic variables such as horizontal position along the branch, vertical position and dimensions of the branch, tree-level measurements, and random effects to account for extrinsic factors; B) to model the horizontal distribution of foliage along individual branches; and C) to model parameter estimates for the best-fitting PDFs to identify which intrinsic variables significantly influence the horizontal distribution of foliage along branches.

### **3.3 Materials and methods**

#### *3.3.1 Study site and data collection*

A total of 15 juvenile *L. occidentalis* trees were destructively sampled from 4 locations in Latah County of northern Idaho between June 29 and August 11 of 2016. Mean average temperature of the sites ranged from 7.7°C to 8.8°C and mean annual precipitation ranged from 658 mm to 688 mm. Elevation ranged from 957 m to 1330 m a.s.l. Latitude ranged from

46°49'48''N to 47°6'36''N. Age of the trees ranged from 10 to 14 years old. Between 2 and 6 trees were sampled from each site.

**Table 3.1** *Summary of trees destructively harvested for leaf area study*

Site	n	DBH (mm)			DBLC (mm)			TH (cm)			HBLC (cm)		
		min	mean	max	min	mean	Max	min	mean	max	min	mean	max
Carsc	6	61.0	115.6	162.6	71.1	149.9	246.4	652.3	943.9	1137.0	18.3	64.5	100.6
TMU	3	76.2	125.3	188.0	76.2	125.3	188.0	810.8	1079.0	1277.0	137.2	149.4	161.5
UI217	4	96.5	137.2	177.8	99.1	141.0	167.6	816.9	1058.4	1295.0	57.9	150.1	240.8
UI486	2	73.7	101.6	129.5	71.1	100.3	129.5	762.0	1011.9	1262.0	128.0	169.2	210.3

For every tree at each location, diameter at breast height (DBH), diameter at the base of the live crown (DBLC), height (TH), and vertical distance along the stem from the base of the bole to the base of the live crown (HBLC) were recorded (Table 3.1). For every branch on every tree, length from tip to bole (TBL), vertical distance along the stem from the base of the crown to the center of the junction (HIC), and diameter 5 cm from the junction (BD) were recorded (Table 3.2). The distance from the stem junction to the start of foliage (LTF) and the

**Table 3.2** *Summary of branches harvested for leaf area study*

Site	Tree	n	BD (mm)			HIC (cm)			TBL (cm)		
			min	mean	max	min	mean	max	min	mean	max
Carsc	1	6	4.60	8.13	11.08	133.66	402.30	646.70	71.00	124.67	161.00
Carsc	2	6	5.20	13.24	23.72	158.71	437.40	734.70	56.00	149.17	212.00
Carsc	3	6	7.52	11.38	15.36	143.42	493.20	762.40	88.00	145.83	172.00
Carsc	4	6	3.82	6.46	11.96	51.94	286.90	511.90	36.00	69.17	107.00
Carsc	5	6	6.72	15.33	24.38	127.57	502.40	871.60	67.00	142.00	237.00
Carsc	6	4	5.97	8.27	9.63	350.61	509.40	652.60	59.00	89.75	128.00
TMU	1	6	3.82	9.08	13.67	146.65	505.60	847.60	37.00	85.50	120.00
TMU	2	6	8.85	14.61	17.96	176.84	584.70	956.80	83.00	143.33	173.00
TMU	3	6	4.38	9.49	13.66	73.46	322.10	548.50	50.00	87.17	115.00
UI217	1	6	8.70	12.66	19.08	55.36	503.00	887.40	93.00	137.33	199.00
UI217	2	6	6.30	10.41	14.10	133.89	340.70	551.90	90.00	119.50	148.00
UI217	3	6	7.87	10.91	14.37	195.09	422.30	619.10	91.00	126.50	172.00
UI217	4	6	5.09	13.51	20.56	274.21	548.40	856.20	52.00	151.83	227.00
UI486	1	6	4.78	7.46	9.14	90.98	301.80	485.00	54.00	91.67	120.00
UI486	2	6	4.89	10.92	17.08	228.69	544.40	856.70	49.00	123.33	174.00

cardinal quadrant of the branch (NE, SE, SW, and NW) was also recorded. The main stem of each tree and all attached branches were divided into three equal vertical sections along the stem. Within each section of each tree, two random branches were selected for measurement of foliar biomass (FM), except one tree (Carsc 6), because only 4 branches were sampled in the crown for foliage. Each selected branch was divided into 10 cm horizontal segment along its length, and FM was measured separately for each segment (Table B1).

For leaf area analysis, initial measures of LA and SLA for each 10 cm segment revealed that SLA varied across the branch, but was consistently similar within 20-30 cm sections. Thus, to minimize processing time, 3 or 4 horizontal segments were randomly selected from each of the six branches measured for FM per tree as subsamples for SLA analysis. A subsample of approximately 50-100 needles were taken from each of the branch segments selected for LA analysis. Any remaining foliage from the branch segments selected for leaf area analysis were processed along with the rest of the branch segments for foliage biomass. Each needle SLA subsample was scanned and analyzed for projected one-sided area with WinSEEDLE™ (Regent Instruments Inc., Quebec CA) at the 800 dpi setting. The dry biomass of each needle subsample was processed separately from any remaining foliage from its corresponding branch segment to estimate SLA.

Foliage from the rest of the branch segments, from the needle LA subsamples and from the remainder of the segments from which the LA subsamples were taken were placed in an oven and allowed to dry for at least 72 hours at 65 °C. Foliage was then removed from each segment and weighed on a balance to the nearest 0.1 mg. LA from subsamples were divided by their FM to obtain SLA values for the subsampled branch segments.

### 3.3.2 Specific leaf area models

SLA values calculated for sampled segments (Table B2) were used to fit linear and nonlinear models of a variety of forms to estimate SLA across the crown as a function of an array of variables including vertical branch position (i.e., HIC, DIC, RHIC, or RDIC), horizontal position of the foliage along the branch (i.e., DAB, PAB, RDAB, RPAB, DAF, RPAF, or RDAF), and other branch and tree-level measurements (Table 3.3).

**Table 3.3** Variables to be tested in model fitting

Variable	Definition	Formula
<b>Segment</b>		
DAB (cm)	Distance along branch, distally from stem junction	
PAB (cm)	Distance along stem, proximally from branch tip	TBL-DAB
RDAB	Relative distal distance along branch from bole	DAB/FL
RPAB	Relative proximal distance along branch from tip	PAB/FL
DAF (cm)	Relative distal distance from start of foliage	DAB-DTF
RPAF	Relative proximal distance along branch from tip	PAB/FL
RDAF	Relative distal distance along branch from tip	DAF/FL
FM (g)	Foliar biomass of branch segment	
LA (cm <sup>2</sup> )	Leaf area of branch segment	
SLA (cm <sup>2</sup> g <sup>-1</sup> )	Specific leaf area of branch segment	LA/FM
<b>Branch</b>		
$\omega_{ij}$ (Tree)	Random effect of tree (j) within site (i) on branch	
BD (mm)	Branch diameter at stem junction	
DTF (cm)	Distance from stem junction to start of foliage	TBL-FL
FL (cm)	Length of foliated portion of branch	TBL-DTF
TBL (cm)	Branch length	
NW, NE, SW, and SE	Cardinal quadrant of branch	Dummy variable (equal 1 or 0)
HIC (cm)	Height into crown from crown base	CL – DIC
DIC (cm)	Depth into crown from stem apex	CL – HIC
RHIC	Relative height into crown from base	HIC / CL
RDIC	Relative depth into crown from apex	DIC / CL
<b>Tree</b>		
$\phi_i$ (Site)	Random effect of site location (i) on tree	
TH (cm)	Tree height	HBLC + CL
HBLC (cm)	Height from bole to base of crown	TH – CL
CL (cm)	Length of the crown	TH – HBLC
DBLC (mm)	Diameter of stem at base of crown	
DBH (mm)	Diameter at breast height (@ 1.3m)	
HMC (cm)	Height to the midpoint of the crown	HBLC+CL/2

Variation due to unmeasured tree-level factors such as age and extrinsic variables such as social position were accounted for by including random effects for site and tree within site. Models were fit and parameter estimates obtained by maximum likelihood estimate with the “nlme” function in the “nlme” package of R (R Core Team 2017; Pinheiro et al. 2017), which allows the incorporation of hierarchical random effects and the ability to account for autocorrelation and to weight the variance. Starting parameter values specified in the “nlme” function were obtained from the “proc model” function in SAS (SAS Institute Inc. 2016).

Parameter estimates were screened for significance using a threshold  $p$ -value of 5%, and non-significant parameters were considered to be zero and excluded from the model. Once a set of models with all significant parameters was obtained, the relative explanatory power, or goodness of fit of the models was assessed using multiple selection criteria: likelihood ratio tests, adjusted and generalized  $R^2$ , Akaike information criterion (AIC), and root mean squared error (RMSE). During model building, the simplest model that yielded a statistically significant improvement in a likelihood ratio test over a corresponding base model with one less parameter was selected. This process was repeated until no significant improvement in fit was obtained from the inclusion of additional variables. The final model retained was used to estimate leaf area for the rest of the branch segments (Table B1).

### *3.3.3 Horizontal distribution of leaf area along branches*

Data representing the horizontal distribution of leaf area along branches was obtained by estimating SLA for each branch segment with the SLA model and multiplying by the foliar mass measured for each segment on 88 branches from 15 trees (Table B1). The left- and right-truncated Weibull [i],  $\beta$ -distribution [ii], and Johnson’s  $S_B$  [iii] functions were fit to the LA

distribution along individual branches and parameters recovered using maximum likelihood estimation (Weiskittel et al. 2009). The forms of the PDFs are expressed as

$$[i] \quad p(X) = \frac{\beta X^{\beta-1} e^{-((X/\eta)^\beta - (\gamma/\eta)^\beta)}}{\eta^\beta}$$

$$[ii] \quad p(X) = \frac{X^c (1-X)^{d-1}}{\Gamma(c)\Gamma(d) / \Gamma(c+d)}$$

$$[iii] \quad p(X) = \frac{\tau e^{-\frac{1}{2}(\psi + \tau \ln \frac{X}{1-X})^2}}{\sqrt{2\pi} X(1-X)}$$

where  $X$  represents the horizontal position along the branch and  $p(X)$  is the relative leaf area density at that position. Relative proximal distance from branch tip to the bole (RPAB, Table 3.3) was used for  $X$  to facilitate comparison across branches and trees of different size, to permit comparison to past studies, and because it reflects light attenuation in the crown. In the Weibull function [i],  $\beta$  is the skew (shape) parameter,  $\eta$  is the kurtosis (scale) parameter, and  $\gamma$  is the truncation point. In the  $\beta$ -distribution [ii],  $c$  and  $d$  are shape parameters, and  $\Gamma(x)$  is the gamma function. In Johnson's  $S_B$  [iii],  $\psi$  and  $\tau$  are shape parameters.

To make the discrete data more amenable to fitting PDFs, LA estimates were divided into horizontal bins of equal length along the branch. The distribution of residuals and overall average root mean squared error (RMSE) and mean absolute bias (MAB) were compared among models and binning schemes to select the best model and number of bins. To assess model performance, the horizontal distribution of standard error and bias averaged for each bin across branch length was plotted to look for correlation. Once binning was optimized and the best-fitting PDF was selected, parameter estimates (i.e., Weibull  $\eta$  and  $\beta$ ) recovered for

individual branches were modeled as linear and nonlinear functions of branch and tree variables to analyze how the horizontal foliage distribution changes with respect to intrinsic factors. Model fitting was performed with the “nlme” package of R (R Core Team 2017; Pinheiro et al. 2017), using starting parameters obtained from “proc model” in SAS (SAS Institute Inc. 2016). Model building proceeded bottom-up as in Section 3.3.2.

### 3.4 Results

#### 3.4.1 Specific leaf area model

The young *L. occidentalis* trees in this study had an overall mean SLA of  $64.22 \pm 17.65 \text{ cm}^2 \text{ g}^{-1}$  and ranged from 15.62 to  $131.92 \text{ cm}^2 \text{ g}^{-1}$  across branches, trees, and sites (Table B2).

A total of 65 model forms were tested and compared for SLA of the 10cm branch segments, and 12 additional models obtained by substituting initial slope parameter estimates as constants were also tested to allow for non-significance of the initial slope parameter estimates in model comparisons (Table B3). Of the total 77 models, a mixed power and exponential function of HIC, HMC, RDAF, with dummy variables for SE and SW had the lowest likelihood, AIC, and RMSE, and highest generalized and adjusted  $R^2$  for combined fixed and random effects (Eq. [3.4], Table B3).

However, a model substituting RPAB for RDAF (Eq. [3.5], Table B3) had comparable scores for all goodness of fit criteria. RPAB was used because distance along the entire branch from the tip is more biologically informative in terms of light availability and the unfoliated portion of most branches was short. Use of RPAB also maintains consistency with the horizontal leaf area PDFs (Eqs. [i-iii]). Equation [3.1], which matched Equation [3.5] but retained the non-significant initial slope parameter (Table 3.4), was selected and had the form

$$[3.1] \quad SLA = m_0 HIC^{m_1 + \varphi_i + \omega_{ij}} HMC^{m_2 + m_3 RPAB + q_0} (SE + SW)$$

where  $m_0$ ,  $m_1$ ,  $m_2$ ,  $m_3$ , and  $q_0$  are parameters,  $\varphi_i$  and  $\omega_{ij}$  are random effects of site  $i$  and tree  $j$  within site  $i$  on HIC, and SE and SW are dummy variables (0 or 1) for branches in the southeast and southwest quadrants, respectively. The inclusion of a factor for whether the branches were on the south side of the tree significantly improved the model fit over a base model (Eq. [3.27], Table B3;  $\chi^2 = 5.61$ ;  $df = 1$ ;  $0.01 < p < 0.025$ ). Overall, SLA had an inverse relationships with HMC, HIC, and distance from the bole, and the southern quadrants (SW and SE) had higher SLA after accounting for the other variables (Figure 3.1; Table 3.4).

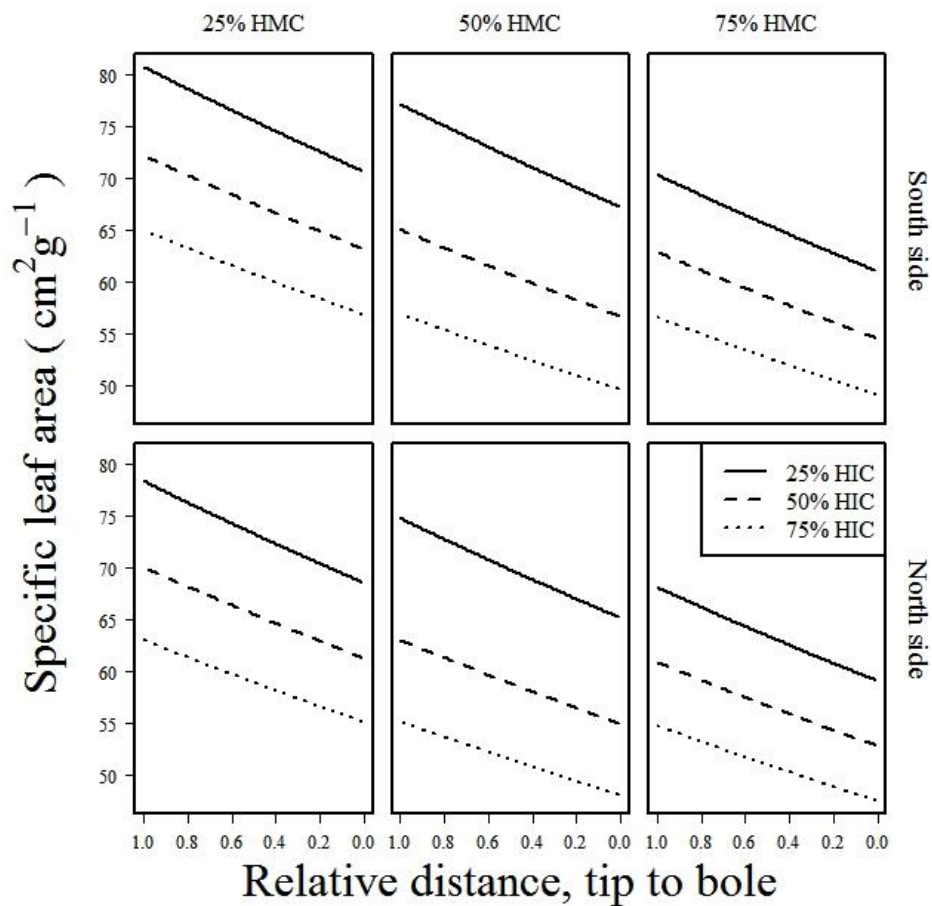


**Figure 3.1** Specific leaf area predicted by Equation [3.1] by quartile of relative distance from tip to bole (RPAB), height to the middle of the crown (HMC), height of the branch from crown base (HIC), and whether the branch is on the south or north side of the crown

**Table 3.4** *Parameter estimates for spatial SLA model*

<b>Model</b>	<b>Par</b>	<b>Estimate</b>	<b>SD</b>	<b>p</b>
SLA Equation [3.1]	m0	2634.114609	2022.226200	0.193360
	m1	-0.237192	0.012700	0.000000
	m2	-0.380581	0.122200	0.001963
	m3	0.021677	0.002900	0.000000
	q0	0.004882	0.002100	0.019141

### 3.4.2 Horizontal distribution of leaf area along branches

Across binning schemes and PDFs, RMSE and MAB reached local minimums with 13 bins (Figure 3.2). When fitting distribution models for aggregated estimates of LA along the branch lengths, the right-truncated two-parameter Weibull distribution had a marginally better RMSE than the other PDFs (Table 3.5). Across all branches, maximum likelihood parameter estimates for the right-truncated Weibull with 13 bins had a mean of  $0.672 \pm 0.169$  and range of 0.316 to 1.411 for kurtosis ( $\eta$ ), and a mean of  $2.99 \pm 0.700$  and range of 1.432 to 5.189 for skew ( $\beta$ ). Standard error of the Weibull model appeared to be normally distributed along the length of the branch and peaked in the eighth bin (Figure 3.3a). There was no apparent spatial directional trend in bias along the length of the branch (Figure 3.3b). By bin, absolute bias was strongly correlated with LA (Figure 3.4).

**Table 3.5** *Fit statistics for PDFs*

<b>Model (13 bins)</b>	<b>RMSE (mm<sup>2</sup>)</b>	<b>MAB (mm<sup>2</sup>)</b>
Weibull (right-truncated)	92.34	62.79
Beta	92.52	62.38
Johnson's S <sub>B</sub>	92.60	62.44
Weibull (no truncation)	94.10	63.74
Weibull (left-truncated)	118.43	81.41

A total of 42 different models of a variety of forms were fit to the Weibull kurtosis ( $\eta$ ) parameter estimates and compared (Table B4). A mixed power and exponential function of HBLC, TBL, RDIC, and a dummy variable for the SW quadrant (Eq. [3.2]) had the highest

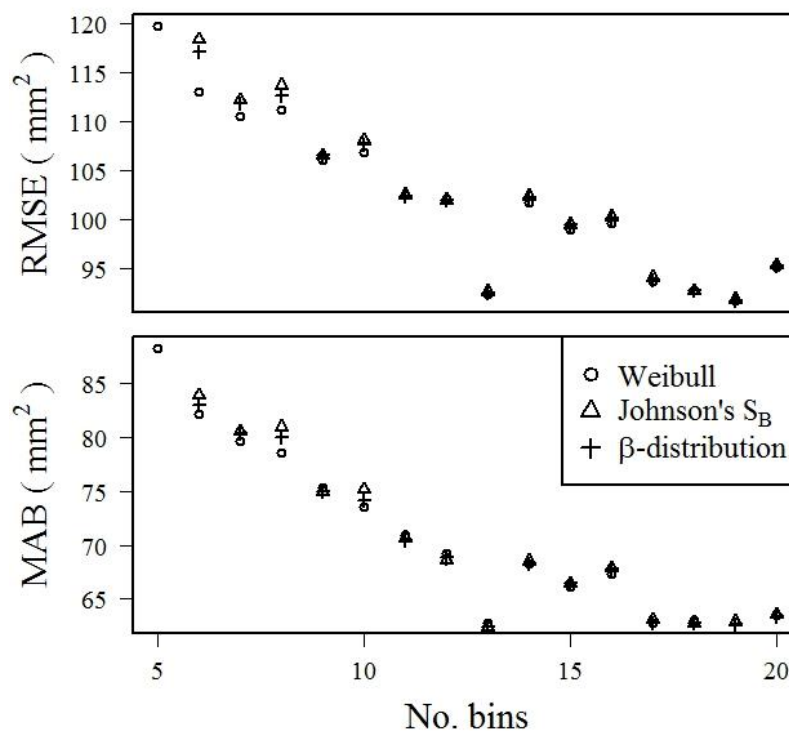


**Figure 3.2** Root mean squared error (RMSE) and mean absolute bias (MAB) of foliage estimates averaged across trees for binning schemes with different numbers of bins for the right-truncated Weibull, Johnson's  $S_B$  and  $\beta$ -distribution models

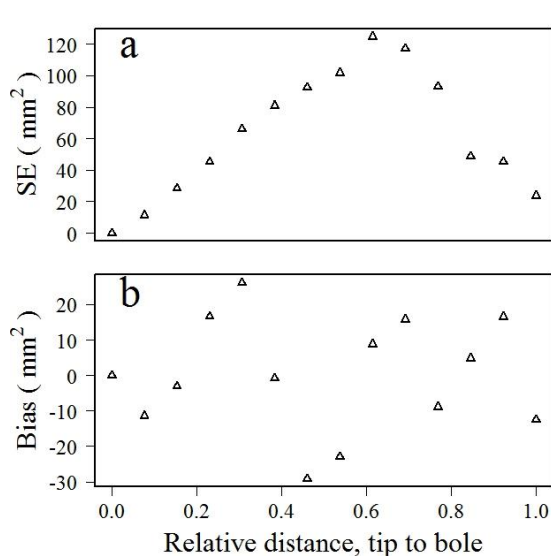


**Figure 3.3** Standard error and bias of fitted Weibull distribution with 13 bins averaged across trees for each bin, by RPAB

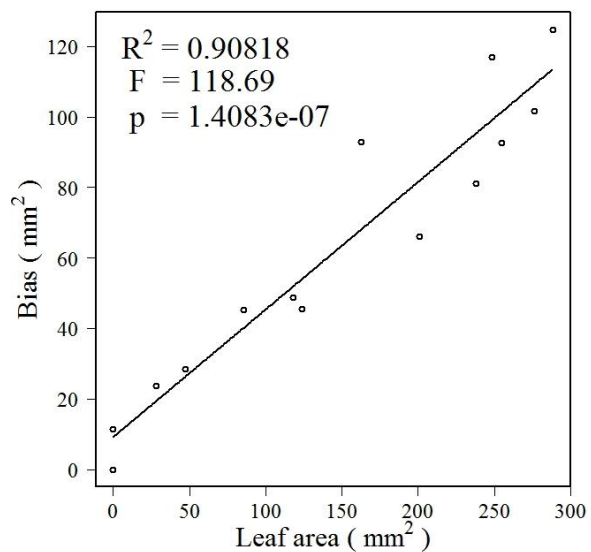


**Figure 3.4** Correlation between absolute bias and leaf area averaged across trees for each bin with 13 bins

likelihood, lowest AIC and RMSE, and highest generalized and adjusted fixed and combined fixed and random  $R^2$  among models tested. Equation [3.2] had the form

$$[3.2] \quad \eta = h_0 HBLC^{h_1 + q_1 SW} TBL^{h_2 + \omega_j} e^{h_3 RDIC}$$

where  $h_0$ ,  $h_1$ ,  $h_2$ ,  $h_3$ , and  $q_1$  are parameters,  $\omega_j$  is the random effect of tree  $j$  on total branch length, and SW is a dummy variable for whether the branch was in the southwest quadrant. The inclusion of a factor for whether the branch was in the southwest quadrant significantly improved the model fit over a base model (Eq. [3.83], Table B4;  $\chi^2 = 6.15$ ;  $df = 1$ ;  $0.01 < p < 0.025$ ). The random effect  $\omega_j$  did not improve the  $R^2$  of the kurtosis model (Table 3.6).

A total of 16 different models of a variety of forms were fit to the skew ( $\beta$ ) parameter estimates and compared (Table B5). A power series function of RDIC and BD (Eq. [3.3]) had the highest likelihood, lowest AIC and RMSE, and highest generalized and adjusted fixed and combined fixed and random  $R^2$  among models tested. Eq. [3.3] had form

$$[3.3] \quad \beta = (h_4 + \omega_j') RDIC^{h_5} (BD/10)^{h_6}$$

where  $h_4$ ,  $h_5$ , and  $h_6$  are parameters and  $\omega_j'$  is the random effect of tree  $j$ . Based on the maximum likelihood estimates for the parameters of the selected models fit to Weibull parameter estimates, the kurtosis ( $\eta$ ) parameter decreased with RDIC, HBLC, and TBL, and was higher on branches in the southwest (SW) quadrant (Table 3.7; Figures 3.5 and 3.8-3.9). Skew ( $\beta$ ) decreased with RDIC and increased with BD (Table 3.7; Figure 3.8).

**Table 3.6** *Fit statistics for SLA and horizontal LA distribution parameter models*

Model	LL	AIC	RMSE	Adjusted $R^2$		Generalized $R^2$	
				Fixed	Fixed + Rand	Fixed	Fixed + Rand
[3.1] SLA	-1715.53	3447.05	7.72	0.569	0.803	0.573	0.805
[3.2] Kurtosis ( $\eta$ )	50.56	-87.13	0.1325	0.346	0.346	0.378	0.378
[3.3] Skew ( $\beta$ )	-81.11	172.22	0.5952	0.105	0.319	0.127	0.335

In simple linear models, TBL was positively correlated with RDIC ( $F = 38.02$ ;  $df_1 = 1$ ;  $df_2 = 82$ ;  $p = 2.51E-8$ ;  $R^2 = 0.3168$ ), and so was BD ( $F = 20.98$ ;  $df_1 = 1$ ;  $df_2 = 82$ ;  $p = 1.64E-5$ ;  $R^2 = 0.2037$ ). When linear models are applied to predict TBL and BD from RDIC quantiles for estimation of horizontal leaf area distribution across absolute branch length with Equations [3.2] and [3.3], peak leaf area is distally shifted with increasing RDIC (Figure 3.9).

**Table 3.7** Parameter estimates for horizontal Weibull skew and kurtosis models

Model	Par	Estimate	s.d.	p
Weibull kurtosis ( $\eta$ ) Equation [3.2]	h0	3.619467	1.233611	0.004619
	h1	-0.078840	0.029589	0.009713
	h2	-0.259380	0.073316	0.000750
	h3	-0.253800	0.120454	0.038978
	q1	0.028475	0.011148	0.012992
Weibull skew ( $\beta$ ) Equation [3.3]	h4	2.513116	0.138704	0.000000
	h5	-0.207342	0.051235	0.000137
	h6	0.162248	0.075139	0.034410

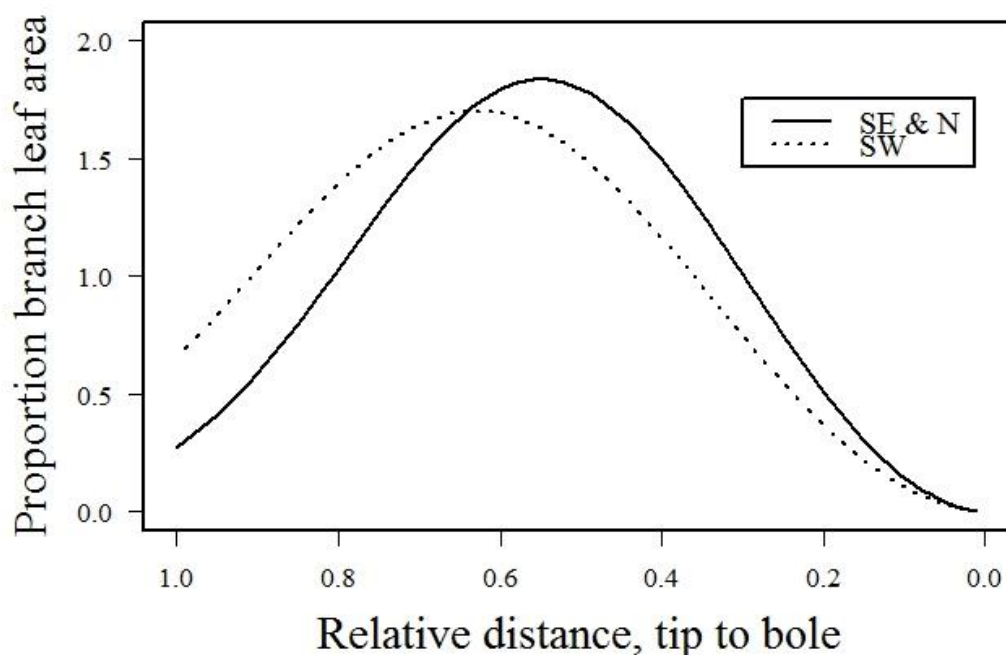


**Figure 3.5** Predicted horizontal distribution of leaf area density for southwest (SW) versus all other quadrants (SE and N) at median branch diameter, branch length, relative depth of branch in the crown, and height to base of the crown

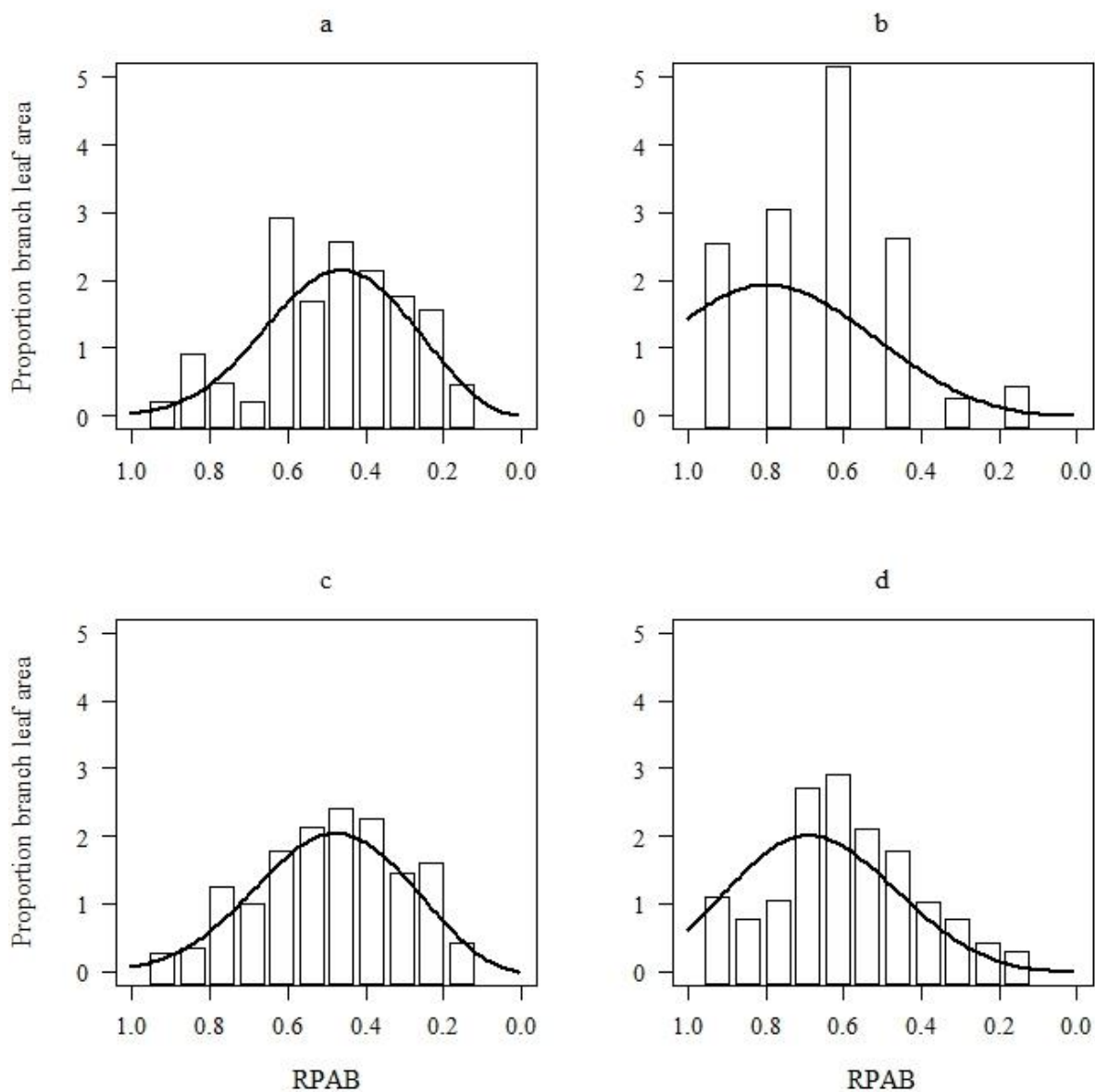


**Figure 3.6** Fitted Weibull curve and actual binned foliage measurements from four branches from the tallest tree in the dataset<sup>†</sup> for NW branches in the lower (a) and upper (b) crown and SW branches in the lower (c) and upper crown (d)<sup>‡</sup>

<sup>†</sup>(UI 217 Tree 4): DBH = 117.8 mm; TH = 1295.4 cm; HBLC = 240.8 cm. <sup>‡</sup>(a): RDIC = 0.74; TBL = 191 cm; BD = 10.6 mm. (b): RDIC = 0.19; TBL = 52 cm; BD = 5.1 mm. (c): RDIC = 0.73; TBL = 277 cm; BD = 20.6 mm. (d): RDIC = 0.26; TBL = 141 cm; BD = 10.3 mm.

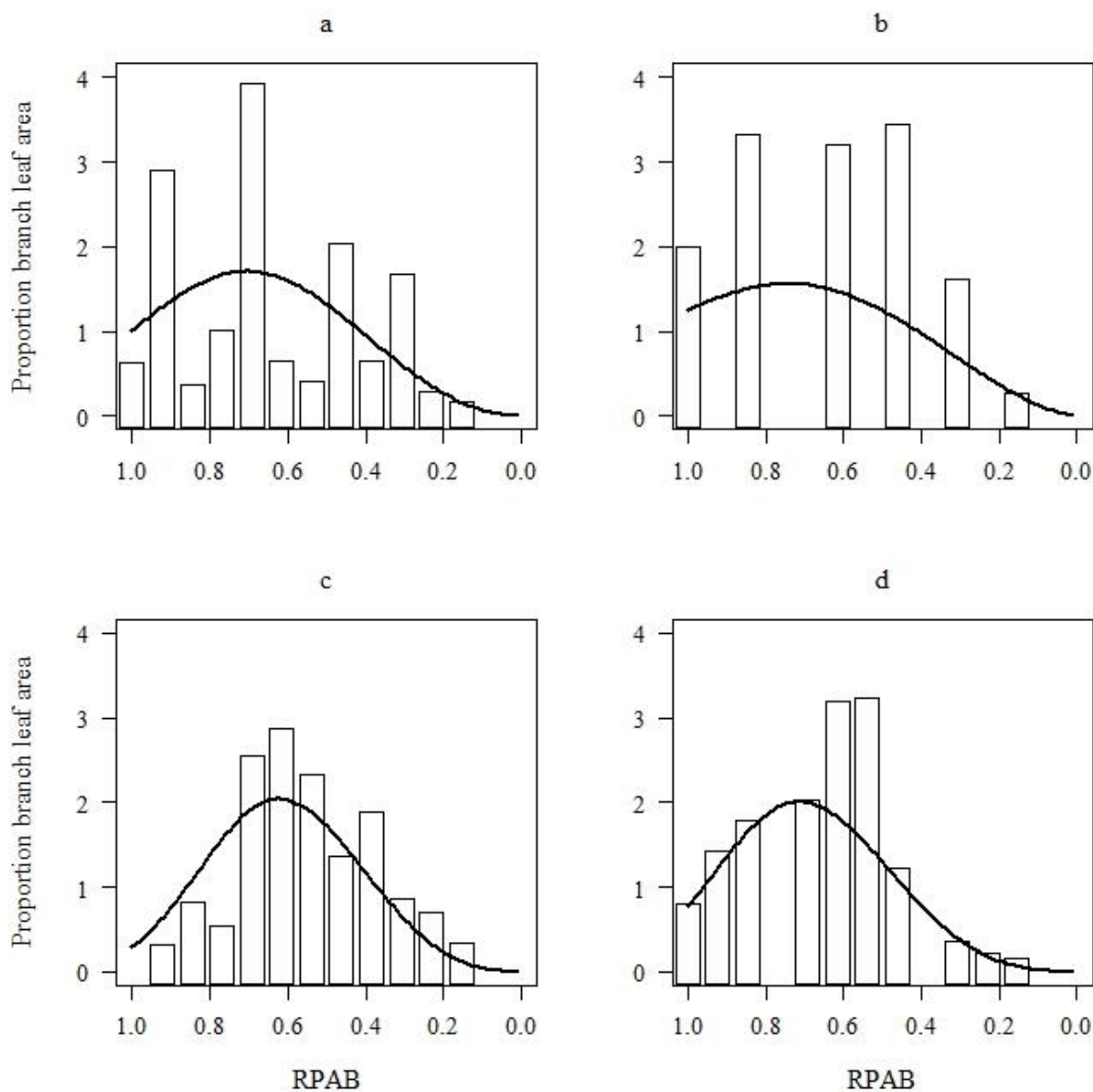


**Figure 3.7** Fitted Weibull curve and actual binned foliage measurements from four branches from a tree of intermediate height in the dataset<sup>†</sup> for SE branches in the lower and upper crown (a and b) and SW branches in the lower and upper crown (c and d)<sup>‡</sup>

<sup>†</sup>(Carscallen Tree 2): DBH = 129.5 mm; TH = 905.3 cm; HBLC = 18.3 cm. <sup>‡</sup>(a): RDIC = 0.70; TBL = 181 cm; BD = 14.4 mm. (b): RDIC = 0.23; TBL = 56 cm; BD = 5.2 mm. (c): RDIC = 0.82; TBL = 212 cm; BD = 23.7 mm. (d): RDIC = 0.17; TBL = 97 cm; BD = 8.4 mm.

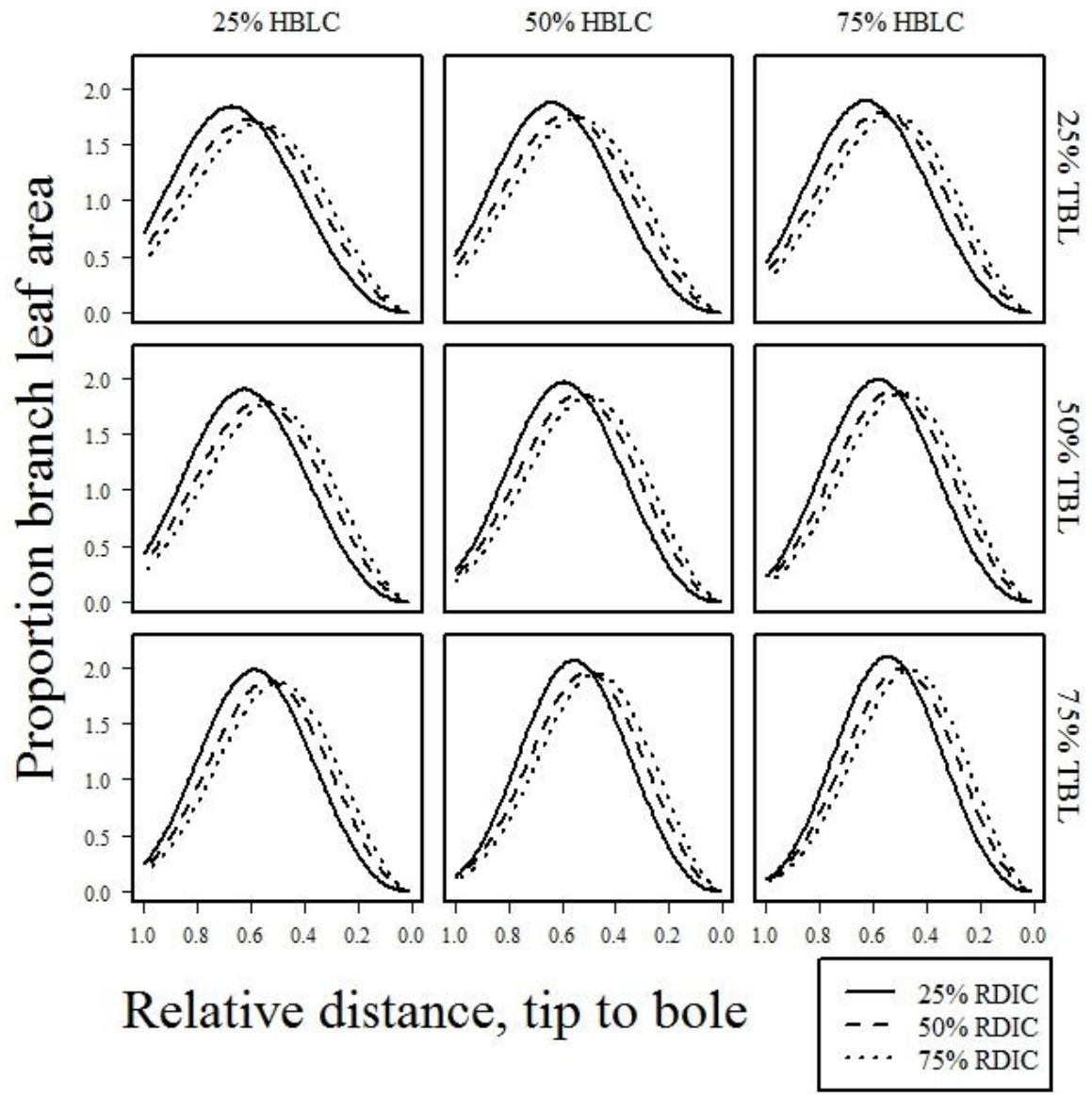


**Figure 3.8** Predicted horizontal distribution of percent branch leaf area at median branch diameter (BD) and quartiles by height to base of the crown (HBLC), branch length (TBL) and relative depth of branch in the crown (RDIC), for branches not in the SW quadrant

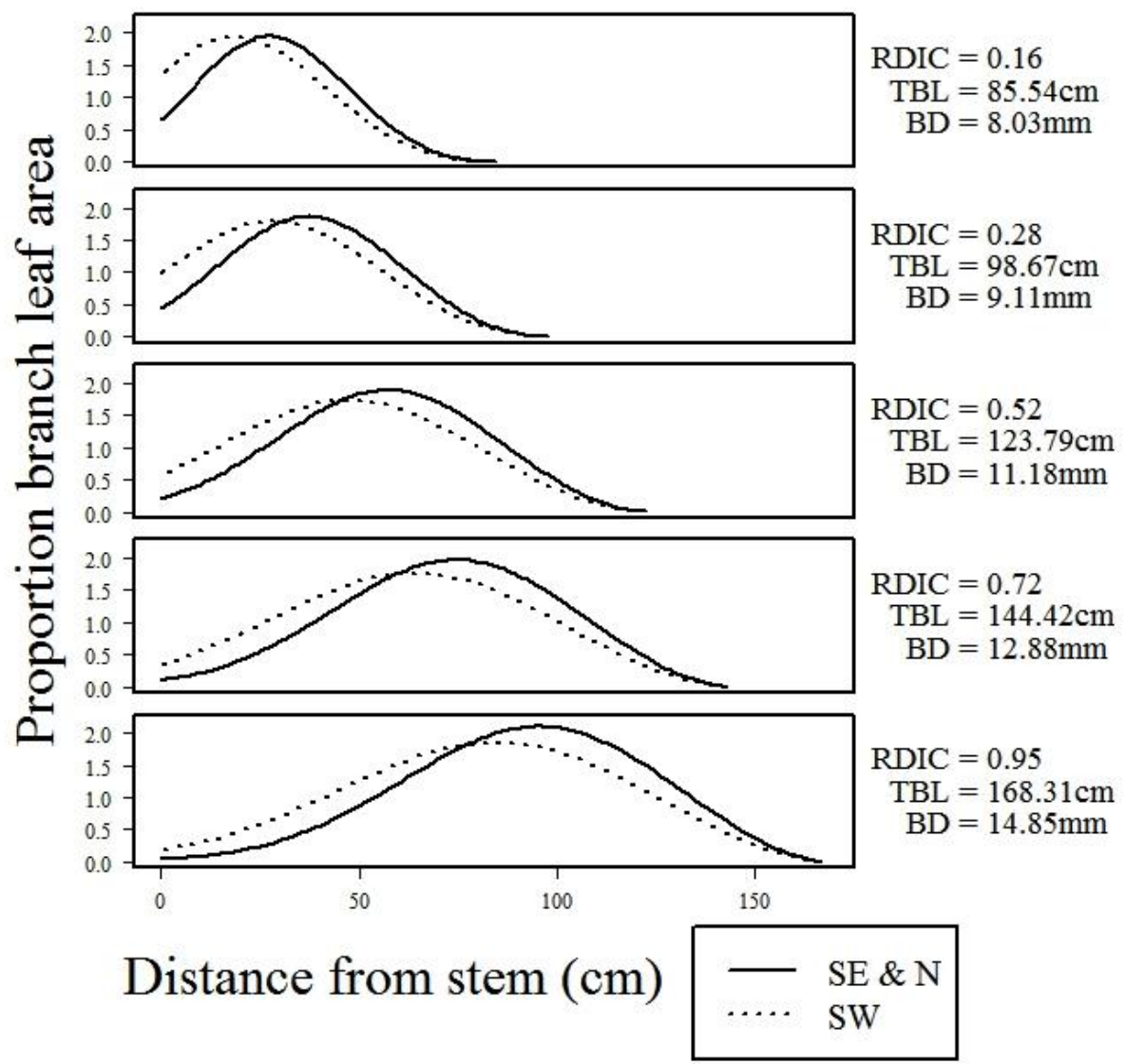


**Figure 3.9** Predicted horizontal distribution of percent crown leaf area by quadrant (SW vs others) at median height to base of the live crown (HBLC), minimum, first, second, and third quartile, and maximum relative depth of branch in the crown (RDIC), and corresponding expected branch length (TBL) and diameter (BD) predicted from linear models<sup>†</sup>

$$\begin{aligned} \dagger TBL &= 69.326 + 104.473RDIC \\ BD &= 6.689 + 8.615RDIC \end{aligned}$$

### 3.5 Discussion

#### 3.5.1 Specific leaf area

For its relative shade tolerance rank, *Larix occidentalis* has high average SLA at  $64 \text{ cm}^2 \text{ g}^{-1}$  (Gower and Richards 1990; Chen et al. 1996; Chen and Klinka 1998). Our measurements are close to those reported from field studies of *L. occidentalis* (e.g., Gower et al. 1987), but lower than those reported from the greenhouse (Higgins et al. 1987). Other studies have reported very high SLA of  $100\text{-}200 \text{ cm}^2 \text{ g}^{-1}$  for *Larix decidua* Mill., and  $200\text{-}275 \text{ cm}^2 \text{ g}^{-1}$  for other *Larix* spp. (Richards and Bliss 1986; Matyssek and Shulze 1987). Higher SLA in *Larix* spp. relative to evergreen conifers fits the trend of decreasing SLA with increased leaf lifespan (Reich et al. 1997).

The well-supported negative correlation between leaf lifespan and SLA has been demonstrated to underpin a number of other correlations between metabolism and N and P content observed across the leaf economics spectrum (Wright et al. 2004; Osnas et al. 2013). Thus, short-lived foliage yields a greater relative photosynthetic return on investment of limiting organic and mineral resources (Ellsworth and Reich 1993; Bond et al. 1999). As foliage ages, SLA and rate of photosynthesis per unit mass investment decrease together (Gower et al. 1993). By replacing the entire crown with a fresh cohort of foliage every year, *Larix* spp. are able to maintain high efficiency of resource use with less corresponding loss to respiratory demand of retained biomass relative to evergreens.

The negative correlations of SLA with height to the middle of the crown, height of the branch in the crown, and distance along the branch from the bole observed for *L. occidentalis* in this study (Table 3.4; Figure 3.1) are consistent with studies of many other species (Van Hees and Bartelink 1993; Ishii et al. 2002; Sellin and Kupper 2006; Temesgen and Weiskittel

2006) and with the hydraulic resistance and gravitational water potential hypothesis. Negative correlation between light availability and SLA is more pronounced in shade-tolerant species (Chen and Klinka 1996), whereas SLA plasticity in shade-intolerant species may be passively driven by hydraulic supply and demand during leaf development. Specifically, turgor pressure in expanding leaves is a function of stem water potential (supply) and stomatal conductance (demand) such that high SLA may be realized under conditions of high conductance, provided that leaf water status remains high throughout the course of leaf development (Tardieu et al. 1999; Weiskittel et al. 2008).

In support of the hypothesis that hydraulic supply and demand drive plasticity of SLA in *L. occidentalis*, an absolute measure of branch position (HIC) performed better than relative measures (RDIC, RHIC) in predicting SLA during model selection (Table B3), reflecting the influence of increasingly negative gravitational water potential. Because the trees were young, grew in the open, and had negligible crown recession, the negative correlation of SLA with height to the middle of the crown (Table 3.4) cannot be attributed to relative light availability. Decreasing SLA with increasing height could be a function of greater resistance and more negative water potential in taller trees. Chen and Klinka (1998) did not find a significant relationship between SLA and light availability in *L. occidentalis* seedlings.

To the best of the author's knowledge, only one other study has investigated the influence of cardinal branch direction on SLA, and did not report a significant effect for either *Pseudotsuga menzeisii* var. *menzeisii* (Mirb.) Franco or hybrid *Picea* (Weiskittel et al. 2008). Here, we report significantly higher SLA on the south side of crowns of *L. occidentalis* growing in the open on the west side of the Rocky Mountains after accounting for other

variables (Table 3.4). These results do not support a hypothesis of higher SLA with decreasing light availability in *L. occidentalis*, as inferred for *L. decidua* (Fellner et al. 2016) and reported for other species (Niinemets and Kull 1994; Chen et al. 1996).

Capacitance and hydraulic conductance was not likely to be a limiting factor during leaf expansion for the trees sampled in the present study. The trees were juvenile, grew on the ash cap, and were sampled in a year with higher than average precipitation. After accounting for other variables that serve as surrogates for the constraints of hydraulic resistance, the higher SLA observed on the south side of the trees relative to the less irradiated north side (Figures 3.5 and 3.9) may have been a consequence of increased transpiration due to higher vapor pressure deficit with little change in leaf water potential. In turn, higher turgor pressure sustained on the south side during leaf expansion would lead to higher SLA (Tardieu et al. 1999). *P. menzeisii* is much more isohydric than *L. occidentalis*, which may explain the lack of a significant effect from crown quadrant on SLA observed for that species (Weiskittel et al. 2008). High stomatal conductance and ample water supply during initial leaf expansion may also explain high SLA of *Larix* spp. relative to other conifers.

While the stomatal response of *L. occidentalis* is less sensitive to vapor deficit and xylem pressure potential than sympatric species within the range of this study (Higgins et al. 1987), its stomata do close before some other species under realistic field conditions (D.M. Johnson, personal communication). The combination of wetter growing conditions with lower humidity and consequently greater leaf turgor pressure may explain the higher SLA values observed for alpine *Larix* spp. (e.g., *Larix lyallii* Parl. and *L. decidua*; Richards and Bliss 1986; Matyssek and Schulze 1987) than *L. occidentalis*.

### 3.5.2 Horizontal distribution of leaf area

Judging from the degree of correlation between bias and position on the stem, the right-truncated Weibull function fit horizontal distribution of foliage along branches of *L. occidentalis* as well as or better than it did for other species. Unlike other studies in which residuals peaked in the proximal branch segments (Kershaw and Maguire 1996), there was no systemic bias associated with position along the branch (Figure 3.3b). The higher error rates near the center of the branch (Figure 3.3a) were likely due to positive correlation observed between the mean amount of foliage across all the branches in a given bin and the absolute bias in that bin (Figure 3.4).

Visually it is apparent that the distribution of leaf area along individual branches varies greatly within individual trees (Figures 3.7-3.8), and consequently the kurtosis and skew models had low  $R^2$  values (Table 3.6). In addition to irregularly-distributed sunflecks in the crown from the clumped allocation of foliage on short shoots characteristic of *Larix* spp., extrinsic factors that were not measured or tested could have contributed to variation not accounted for in the model. Defoliation due to water stress in trees growing on less ideal sites or from larch needle blight (*Hypodermella laricis* Tub.), which was present in some of the foliage samples, could have contributed to the unaccounted variation and resulted in the low  $R^2$  for the kurtosis and skew models.

The observed shift in leaf area distribution away from the bole with increasing crown depth (Figures 3.8-3.9) and branch diameter (Table 3.7) is similar to shade-tolerant conifers such as *Abies grandis* (Dougl. ex D. Don) Lindl. and *Tsuga canadensis* (L.) Carr., but more pronounced than in the intermediately shade-tolerant species *P. menzeisii* (Kershaw and

Maguire 1996). The outward shift in the distribution with increasing crown depth observed for *L. occidentalis* was more pronounced than in *Pinus sylvestris* L. (Stenberg et al. 1993). Based on the kurtosis ( $\eta$ ) model parameter estimates (Table 3.7), horizontal distribution of branch leaf area became slightly more leptokurtic (e.g., concentrated) in taller trees and shorter crowns, on longer branches, and on branches closer to the base of the crown (Figures 3.8-3.9), which was also similar to *T. canadensis* (Kershaw and Maguire 1996). The lack of a pronounced inward shift of the horizontal distribution of leaf area towards the bole as the crown receded contrasted with observations for another shade-intolerant evergreen, *Pinus taeda* L. (Xu and Harrington 1998), although there was minimal crown recession, as expected for juvenile trees. Similarities to a shade-tolerant species (*T. canadensis*) and differences from shade-tolerant species (*P. taeda* and *P. sylvestris*) highlight the uniqueness of the characteristic dynamics of *L. occidentalis* leaf allocation.

Like most species, the behavior of the horizontal leaf area distribution model indicates that as *L. occidentalis* grows upward and as its branches grow outward on open sites, leaf area shifts into a more concentrated layer (Figures 3.8-3.9), leaving a non-foliated space within the inner region of the crown along the proximal regions of the branches. Compared to uniform horizontal leaf area distributions, non-uniform distributions expose foliage to more light (Larsen and Kershaw 1996), suggesting the pattern of variation in horizontal leaf area distribution of *L. occidentalis* is adaptive. Alternatively, leaves may be difficult to produce and/or to maintain within the inner crown due to the high light-compensation point of shade-intolerant foliage, thereby passively generating the observed distribution.

Here, we report a significant effect of cardinal branch position on horizontal leaf area distribution (Figures 3.5 and 3.9). Zhao and Wang (2005) found a significant difference in

branch length and bifurcation ratio between southern and northern sides of the crown in *Larix chinensis* Beissn., which taken together with our findings suggests crown morphology is plastic to level of light and/or heat radiation in the genus *Larix*. Given our site location in the northern hemisphere and on the western slope of the Rocky Mountains, the southwest quadrant of the tree crown should receive more light and heat than the other quadrants.

A relatively more distally-shifted horizontal leaf area distribution could compensate for decreased light availability on north and eastern sides of the crown. However, this seems unlikely since on all other counts, environmental plasticity in spatial leaf allocation in *L. occidentalis* appears to be passively driven rather than adaptive. Alternatively, a more proximally-shifted distribution in the southwest quadrant may reduce water loss, or it may sustain transpiration and thus higher rates of photosynthesis late in the season under high irradiance by allowing the stomata to remain open. Under this hypothesis, lower rates of photosynthesis due to the closing of stomata would then prevent foliage generation and retention on the more distal portions of the southwest branches, where irradiance-related heat, and therefore vapor deficit, are highest.

### 3.5.3. Conclusions

In *L. occidentalis*, the distributions of leaf mass and leaf area are plastic to hydraulic forces and light availability. As a classic example of a pioneer species, *L. occidentalis* has a vertically multilayered crown and is adapted to intercept light from all sides. But unlike evergreen conifers, *L. occidentalis* replaces all of its crown foliage with a completely new cohort every year. Pioneer species also tend to be both shade and drought-tolerant (Horn 1971). Breaking from this generalization, *L. occidentalis* prefers mesic sites.

Evergreens retain older foliage in proximal regions of the crown while putting on new foliage in the distal regions (Kershaw and Maguire 1996). Shade-tolerant evergreens also optimize photosynthesis by varying specific leaf area with light level, and thus achieve higher rates of photosynthetic capacity per unit mass where light is limiting, and high photosynthetic returns where light is plentiful (Wang 1988; Gower et al. 1993; Kershaw and Maguire 1996; Chen et al. 1996; Osnas et al. 2013). In addition to light, hydraulic constraints also have demonstrable influence on the spatial foliage age structure realized by evergreen crowns (Linder et al. 1987). When *Pinus radiata* D. Don is subject to water and nutrient stress, older cohorts are shed from distal portions of the crown but retained proximally and on lower branches, while a flush of new foliage is produced in the lower canopy (Wang et al. 1990).

The peak in leaf area near the middle of the branch—the “sweet spot”—in juvenile *L. occidentalis* may reflect a balancing act between hydraulic and light constraints. Foliage cannot fix enough carbon to support itself proximal to the branch midpoint, but also encounters hydraulic stress near the branch tips. Foliage in the distal region of the branch is either difficult to produce due to increased hydraulic resistance and more negative water potential, or achieves low rates of photosynthesis due to decreased conductance if stomata close in response to higher vapor deficit.

In this shade-intolerant and drought-intolerant species, spatial variation in SLA and leaf area both appear to be a passively, environmentally-driven phenomena. Water-use efficiency of *L. occidentalis* foliage is also plastic to immediate growing conditions. It has been shown that other *Larix* spp. can recover from defoliation, but with a concomitant reduction in non-structural carbohydrate reserves (Vanderklein and Reich 1999). Thus, under scenarios of long-term changes in precipitation and temperature regimes in the INW (Rehfeldt

and Jaquish 2010) or competition for light with invading successional species following fire exclusion (Arno et al. 1997), *L. occidentalis* may eventually succumb to depletion of carbon reserves and ultimately be replaced.

However, this study and others like it are limited by the positive correlation between light availability and branch height in the crown or distance from the bole, which confounds analyses attempting to separate the hydraulic and light components of variance in SLA. The most distal segments of the highest branches in the crown have the most negative stem water potential and experience the highest vapor deficit, but also receive the most light, such that variation in SLA attributed to light conditions may also be accounted for by hydraulic constraints (e.g., Fellner et al. 2016). By detecting a difference in SLA between cardinal quadrants while accounting for distance from the bole and branch position and diameter, light and hydraulic components of SLA variance could be crudely partitioned and inferred in the present analysis. However, the observed effect of branch quadrant on SLA, though statistically significant, was small (Table 3.7).

The present study was also limited to juvenile trees between 10 and 14 years old, and did not capture variation in SLA and horizontal leaf area distribution across the full range of environmental conditions in which *L. occidentalis* grows. In addition to using more comprehensive sampling, future studies should examine multiple species across a factorial of isohydry/anisohydry and shade-tolerance within sites that span a gradient of environmental conditions or incorporate irrigation or other treatments. Such an expanded design will allow more complete partitioning of light intensity effects on spatial variation of SLA and leaf area from the effects of hydraulic supply and demand.

### 3.6 Works cited

1. Anfodillo, T., Rento, S., Carraro, V., Furlanetto, L., Urbinati, C., and Carrer, M. 1998. Tree water relations and climatic variations at the alpine timberline: seasonal changes of sap flux and xylem water potential in *Larix decidua* Miller, *Picea abies* (L.) Karst. and *Pinus cembra* L. *Ann. Sci. Forest.* **55**(1-2): 159-172.
2. Arno, S.F., Smith, H.Y., and Krebs, M.A. 1997. Old Growth Ponderosa Pine and Western Larch Stand Structures: Influence of Pree-1900 Fires and Fire Exclusion. USDA For. Serv. Res. Pap. INT-RP-495.
3. Bond, B.J., Farnsworth, B.T., Coulombe, R.A., and Winner, W.E. 1999. Foliage physiology and biochemistry in response to light gradients in conifers with varying shade tolerance. *Oecologia* **120**(2): 183-192.
4. Buckley, D.S., Zasada, J.C., Tappeiner, J.C., II, and Stone, D.M. 1997. Plant morphological characteristics as a tool in monitoring response to silvicultural activities. *In* Communicating the role of silviculture in managing the national forests: Proceedings of the National Silviculture Workshop. Warren, PA, 19-22 May 1997. UDSA For. Serv. Gen. Tech. Rep. NE-238: 37-41.
5. Chabot, B.F., and Hicks, D.J. 1982. The ecology of leaf life spans. *Annu. Rev. Ecol. Syst.* **13**(1): 229-259.
6. Chen, H.Y., and Klinka, K. 1998. Survival, growth, and allometry of planted *Larix occidentalis* seedlings in relation to light availability. *Forest Ecol. Manag.* **106**(2): 169-179.
7. Chen, H.Y., Klinka, K., and Kayahara, G.J. 1996. Effects of light on growth, crown architecture, and specific leaf area for naturally established *Pinus contorta* var. *latifolia* and *Pseudotsuga menziesii* var. *glauca* saplings. *Can. J. For. Res.* **26**(7): 1149-1157.
8. Ellsworth, D.S., and Reich, P.B. 1993. Canopy structure and vertical patterns of photosynthesis and related leaf traits in a deciduous forest. *Oecologia* **96**(2): 169-178.
9. Fellner, H., Dirnberger, G.F., and Sterba, H. 2016. Specific leaf area of European Larch (*Larix decidua* Mill.). *Trees* **30**: 1237-1244.
10. Goudie, J.W., Parish, R., and Antos, J.A. 2016. Foliage biomass and specific leaf area equations at the branch, annual shoot and whole-tree levels for lodgepole pine and white spruce in British Columbia. *Forest Ecol. Manag.* **361**: 286-297.
11. Gower, S. T., Reich, P. B., and Son, Y. 1993. Canopy dynamics and aboveground production of five tree species with different leaf longevities. *Tree Physiol.* **12**(4): 327-345.

12. Gower, S.T., Grier, C.C., Vogt, D.J., and Vogt, K.A. 1987. Allometric relations of deciduous (*Larix occidentalis*) and evergreen conifers (*Pinus contorta* and *Pseudotsuga menziesii*) of the Cascade Mountains in central Washington. *Can. J. For. Res.* **17**: 630-634.
13. Gulmon, S.L., and Chu, C.C. 1981. The effects of light and nitrogen on photosynthesis, leaf characteristics, and dry matter allocation in the chaparral shrub, *Diplacus aurantiacus*. *Oecologia.* **49**(2): 207-212.
14. Higgins, S.S., Black, R.A., Rademaker, G.K., and Bidlake, W.R. 1987. Gas exchange characteristics and water relations of *Larix occidentalis*. *Can. J. For. Res.* **17**(11): 1364-1370.
15. Horn, H.S. 1971. *The Adaptive Geometry of Trees*. Princeton University Press, Princeton, N.J.
16. Ibrahim, L., Proe, M.F., and Cameron, A.D. 1998. Interactive effects of nitrogen and water availabilities on gas exchange and whole-plant carbon allocation in poplar. *Tree Physiol.* **18**: 481-487.
17. Ishii, H., Ford, E.D., Boscolo, M.E., Manriquez, A.C., Wilson, M.E., and Hinckley, T.M. 2002. Variation in specific needle area of old-growth Douglas-fir in relation to needle age, within-crown position and epicormic shoot production. *Tree Physiol.* **22**(1): 31-40.
18. Jurik, T.W. 1986. Temporal and spatial patterns of specific leaf weight in successional northern hardwood tree species. *Am. J. Bot.* **73**(8): 1083-1092.
19. Kershaw, J.A., and Maguire, D.A. 1996. Crown structure in western hemlock, Douglas-fir, and grand fir in western Washington: horizontal distribution of foliage within branches. *Can. J. For. Res.* **26**:128-142.
20. Larsen, D. R., and Kershaw, J. A. 1996. Influence of canopy structure assumptions on predictions from Beer's law. A comparison of deterministic and stochastic simulations. *Agricultural and Forest Meteorology* **81**(1): 61-77.
21. Linder, S., Benson, M. L., Myers, B. J., and Raison, R. J. 1987. Canopy dynamics and growth of *Pinus radiata*: I. Effects of irrigation and fertilization during a drought. *Can. J. For. Res.* **17**(10): 1157-1165.
22. Marshall, J.D., and Monserud, R.A. 2003. Foliage height influences specific leaf area of three conifer species. *Can. J. For. Res.* **33**: 164-170.
23. Matyssek, R., and Schulze, E.D. 1987. Heterosis in hybrid larch (*Larix decidua* × *leptolepis*). *Trees* **1**(4): 225-231.

24. McClelland, B.R., Frissell, S.S., Fischer, W.C., and Halvorson, C.H. 1979. Habitat management for hole-nesting birds in forests of western larch and Douglas-fir. *J. Forest.* **77**(8): 480-483.
25. Myers, B.J., Benyon, R.G., Theiveyanathan, S., Criddle, R.S., Smith, C.J., and Falkiner, R.A. 1998. Response of effluent-irrigated *Eucalyptus grandis* and *Pinus radiata* to salinity and vapor pressure deficits. *Tree Physiol.* **18**: 565–573.
26. Niinemets, Ü. 1996. Plant growth-form alters the relationship between foliar morphology and species shade-tolerance ranking in temperate woody taxa. *Vegetatio.* **124**(2): 145-153.
27. Niinemets, Ü., and Kull, K. 1994. Leaf weight per area and leaf size of 85 Estonian woody species in relation to shade tolerance and light availability. *For Ecol. Manag.* **70**: 1-10.
28. Niinemets, Ü., and Kull, O. 1995. Effects of light availability and tree size on the architecture of assimilative surface in the canopy of *Picea abies*: variation in shoot structure. *Tree Physiol.* **15**(12): 791-798.
29. Oliver, C.D., and Larson, B.C. 1990. *Forest stand dynamics*. McGraw-Hill, NY, NY.
30. Oren, R., Schulze, E.D., Matyssek, R., and Zimmermann, R. 1986. Estimating photosynthetic rate and annual carbon gain in conifers from specific leaf weight and leaf biomass. *Oecologia* **70**(2), 187-193.
31. Osnas, J. L., Lichstein, J. W., Reich, P. B., and Pacala, S. W. 2013. Global leaf trait relationships: mass, area, and the leaf economics spectrum. *Science.* **340**(6133): 741-744.
32. Perrin, P.M., and Mitchell, F.J. 2013. Effects of shade on growth, biomass allocation and leaf morphology in European yew (*Taxus baccata* L.). *Eur. J. Forest. Res.* **132**(2): 211-218.
33. Phillips, J.G., and Riha, S.J. 1993. Canopy development and solar conversion efficiency in *Acacia auriculiformis* under drought stress. *Tree Physiol.* **12**: 137–149.
34. Pinheiro, J., Bates, D., DebRoy, S., Sarkar, D. and R Core Team. 2017. nlme: Linear and Nonlinear Mixed Effects Models. R package version 3.1-131. Available from <https://CRAN.R-project.org/package=nlme> [accessed 18 April 2017].
35. R Core Team. 2017. R: A language and environment for statistical computing. R Foundation for Statistical Computing, Vienna, Austria. Available from <https://www.R-project.org/> [accessed 18 April 2017].
36. Rehfeldt, G.E., and Jaquish, B.C. 2010. Ecological impacts and management strategies for western larch in the face of climate-change. *Mitig. Adapt. Strat. Gl.* **15**: 283-306.

37. Reich, P.B., Walters, M.B., & Ellsworth, D.S. 1997. From tropics to tundra: Global convergence in plant functioning. *PNAS* **94**(25): 13730-13734.
38. Richards, J.H., and Bliss, L.C. 1986. Winter water relations of a deciduous timberline conifer, *Larix lyallii* Parl. *Oecologia* **69**(1): 16-24.
39. Schmidt, W.C. and Shearer, R.C. 1990. Western larch (*Larix occidentalis*). In *Silvics of North America: Vol 1. Conifers. Edited by R.M. Burns and B. Honkala*. USDA For. Serv. Ag. Hand. No. 654.
40. Scott, G., Mahalovich, M.F., Rinehart, S., and Krueger, J. 2013. Reforestation-Revegetation Climate Change Primer for the Norther Region: Incorporating Climate Change Impacts into Reforestation and Revegetation Prescriptions. USDA For. Serv. Available from [http://ecoadapt.org/data/documents/Reforestation-Revegetation\\_Primer\\_Final.pdf](http://ecoadapt.org/data/documents/Reforestation-Revegetation_Primer_Final.pdf) [accessed 18 April 2017].
41. Sellin, A., and Kupper, P. 2006. Spatial variation in sapwood area to leaf area ratio and specific leaf area within a crown of silver birch. *Trees* **20**(3): 311-319.
42. Stenberg, P., Kuuluvainen, T., Kellomäki, S., Grace, J.C., Jokela, E.J., and Gholz, H.L. 1994. Crown Structure, Light Interception and Productivity of Pine Trees and Stands. *Ecol. Bull.* **43**: 20-34.
43. Stenberg, P., Smolander, H., and Kellomäki, S. 1993. Description of crown structure for light interception models: angular and spatial distribution of shoots in young Scots pine. *Stud. For. Suec.* **191**: 43-50.
44. Tardieu, F., Granier, C., and Muller, B. 1999. Modelling leaf expansion in a fluctuating environment: are changes in specific leaf area a consequence of changes in expansion rate? *New Phytol.* **143**: 33-43.
45. Temesgen, H., and Weiskittel, A.R. 2006. Leaf mass per area relationships across light gradients in hybrid spruce crowns. *Trees* **20**(4): 522-530.
46. Temesgen, H., and Weiskittel, A.R. 2006. Leaf mass per area relationships across light gradients in hybrid spruce crowns. *Trees* **20**(4): 522-530.
47. Van Hees, A.F.M., and Bartelink, H.H. 1993. Needle area relationships of Scots pine in the Netherlands. *Forest Ecol. Manag.* **58**(1): 19-31.
48. Vanderklein, D.W., and Reich, P.B. 1999. The effect of defoliation intensity and history on photosynthesis, growth and carbon reserves of two conifers with contrasting leaf lifespans and growth habits. *New Phytol.* **144**(1): 121-132.
49. Wang, Y.P., Jarvis, P.G., and Benson, M.L. 1990. Two-dimensional needle-area density distribution within the crowns of *Pinus radiata*. *Forest. Ecol. Manag.* **32**:217-237.

50. Weiskittel, A.R., Temesgen, H., Wilson, D.S., and Maguire, D.A. 2008. Sources of within- and between-stand variability in specific leaf area of three ecologically distinct conifer species. *Ann. Forest Sci.* **65**:103.
51. Wright, I. J., Reich, P. B., Westoby, M., Ackerly, D. D., Baruch, Z., Bongers, F., Flexas, J., et al. 2004. The worldwide leaf economics spectrum. *Nature*. **428**(6985): 821-827.
52. Xu, M., and Harrington, T.B. 1998. Foliage biomass distribution of loblolly pine as affected by tree dominance, crown size, and stand characteristics. *Can. J. For. Res.* **28**: 887-892.
53. Zhao, X., and Wang, X. 2004. Study on branching pattern plasticity of *Larix chinensis*. *Acta Bot. Bor.-Occ. Sin.* **25**(1): 113-117

## IV. APPENDIX

**Table A1** Summary statistics for branches used to predict foliar mass using Equation [2.1] to estimate crown foliar mass and to fit vertical foliage distribution models

	Site	Tree	n	BD			RHIC			
				min	mean	sd	max	mean	sd	max
1	Bandy	0010	172	2.00	13.83	11.09	47.00	0.54	0.21	0.84
2	Bandy	0013	171	2.00	13.68	7.00	29.00	0.50	0.20	0.80
3	Carsc	1	343	1.52	5.71	2.70	19.92	0.52	0.24	0.94
4	Carsc	2	343	2.92	8.22	3.84	23.72	0.50	0.26	0.95
5	Carsc	3	384	2.21	7.66	3.26	18.91	0.53	0.26	0.96
6	Carsc	4	159	1.80	5.67	2.28	11.98	0.48	0.27	0.92
7	Carsc	5	297	2.94	10.30	6.06	60.80	0.51	0.26	0.97
8	Carsc	6	217	1.49	6.62	3.03	15.08	0.50	0.25	0.91
9	Coram 2	3010	56	6.00	12.64	3.76	22.00	0.41	0.12	0.57
10	Fortine S.	0071	91	6.00	17.88	7.99	36.00	0.51	0.22	0.87
11	Lubrecht R. F.	0003	132	4.00	24.64	15.64	70.00	0.55	0.21	0.86
12	Lubrecht R. F.	0004	232	2.00	11.06	7.86	45.00	0.60	0.22	0.87
13	Lubrecht R. F.	0005	133	4.00	23.67	10.44	45.00	0.70	0.19	0.93
14	McCall 1	5005	59	7.62	25.31	15.23	55.88	0.28	0.15	0.51
15	McCall 1	5006	121	7.62	22.31	14.91	63.50	0.61	0.23	0.92
16	McCall 3	5009	102	7.62	17.88	8.26	38.10	0.51	0.19	0.75
17	McCall 3	5010	93	2.54	31.65	18.62	88.90	0.50	0.18	0.73
18	McCall 3	5019	121	7.62	32.77	12.02	58.42	0.52	0.21	0.86
19	McCall 4	5013	75	7.62	19.14	9.61	43.18	0.44	0.20	0.70
20	McCall 4	5014	100	7.62	17.63	9.21	43.18	0.51	0.23	0.81
21	McCall 4	5015	22	7.62	13.97	4.35	22.86	0.48	0.13	0.63
22	McCall 4	5016	82	7.62	28.22	11.72	76.20	0.43	0.18	0.65
23	McCall 4	5017	118	7.62	30.39	21.05	86.36	0.53	0.25	0.91
24	McCall 5	5020	102	7.62	15.91	7.62	60.96	0.58	0.21	0.84
25	Ninemile E. P.	0034	86	2.00	10.24	5.78	25.00	0.47	0.22	0.77
26	Ninemile E. P.	0035	39	5.00	11.90	6.51	25.00	0.46	0.24	0.78
27	Ninemile Petty	2064	136	6.00	25.89	11.20	49.00	0.48	0.24	0.88
28	Ninemile Petty	2066	133	6.00	25.36	13.01	52.00	0.56	0.24	0.92
29	Ninemile Petty	2067	99	7.00	21.14	8.38	43.00	0.54	0.20	0.84
30	Rexford Pinkh.	0038	84	6.00	10.19	1.94	14.00	0.36	0.16	0.61
31	Rexford Pinkh.	0039	10	6.00	8.60	1.35	10.00	0.13	0.08	0.22
32	Rexford Pinkh.	0041	93	5.00	13.23	4.73	24.00	0.55	0.17	0.78
33	Rexford Pinkh.	0042	91	5.00	14.28	5.18	25.00	0.49	0.18	0.73
34	Rexford Pinkh.	0043	85	7.00	11.80	2.44	18.00	0.42	0.17	0.65
35	Rexford Pinkh.	0044	32	5.00	11.78	3.08	20.00	0.32	0.14	0.51
36	Rexford Pinkh.	0060	61	6.00	12.05	3.31	20.00	0.40	0.16	0.60
37	Rexford Pinkh.	0061	105	4.00	12.90	4.60	25.00	0.51	0.17	0.72
38	Seeley Morrell	0026	181	4.00	19.81	11.27	48.00	0.68	0.23	0.93
39	Seeley Morrell	0030	123	6.00	28.62	13.40	56.00	0.65	0.22	0.90
40	St Maries	0094	61	5.00	21.48	9.58	38.00	0.59	0.20	0.81
41	St Maries	0097	77	6.00	20.64	9.15	48.00	0.45	0.18	0.72
42	TMU	1	351	1.84	6.09	2.89	17.81	0.52	0.25	0.95
43	TMU	2	251	1.91	9.56	5.55	24.72	0.57	0.25	0.96
44	TMU	3	121	1.63	6.87	3.10	16.17	0.58	0.27	0.96
45	UI217	1	394	1.76	8.17	4.34	23.68	0.56	0.25	0.98
46	UI217	2	176	2.22	6.87	2.86	15.53	0.53	0.25	0.95
47	UI217	3	225	1.99	7.93	4.01	22.64	0.53	0.25	0.93
48	UI217	4	253	1.61	8.87	5.72	23.26	0.56	0.22	0.91
49	UI486	1	128	2.24	6.31	2.55	12.84	0.49	0.27	0.90
50	UI486	2	288	2.20	6.94	4.31	29.25	0.58	0.22	0.91
	<b>All</b>		<b>7408</b>	<b>1.49</b>	<b>13.09</b>	<b>10.88</b>	<b>88.90</b>	<b>0.53</b>	<b>0.24</b>	<b>0.98</b>

**Table A2** Models evaluated for goodness of fit to branch foliar mass

Branch foliar mass model		Rand	LL	AIC	RMSE	Adjusted R <sup>2</sup>		Generalized R <sup>2</sup>	
						Fixed	Fixed + Rand	Fixed	Fixed + Rand
[2.1]	$a_0 * (BD^{a_1}) * ((0.25 + RHIC)^{(a_2 - 1)} * \exp(a_3 * CL))$	a1 + a2	-1653.5	3329.0	42.83	0.634	0.847	0.638	0.849
[2.5]	$a_0 * (BD^{a_1}) * (RHIC^{(a_2 - 1)} * \exp(a_3 * CL))$	a1 + a2	-1654.5	3330.9	43.04	0.631	0.845	0.634	0.847
[2.6]	$(BD^{a_1}) * (RHIC^{(a_2 - 1)} * (CL^{a_3}) * (HBLC^{a_4}))$	a1 + a2	-1655.3	3332.6	43.31	0.612	0.841	0.615	0.843
[2.7]	$(BD^{a_1}) * (RHIC^{(a_2 - 1)} * (CL^{a_3}))$	a1 + a2	-1655.5	3331.1	43.33	0.625	0.842	0.628	0.843
[2.8]	$(BD^{a_1}) * (RHIC^{(a_2 - 1)} * (TH^{a_3}))$	a1 + a2	-1656.1	3332.1	43.30	0.617	0.842	0.619	0.843
[2.9]	$(a_0 * BD^{a_1}) * (RHIC^{(a_2 - 1)} * (HBLC^{a_3}))$	a1 + a2	-1656.2	3334.3	42.92	0.589	0.847	0.593	0.848
[2.10]	$(a_0 * BD^{a_1}) * (RHIC^{(a_2 - 1)} * \exp(a_3 * HBLC))$	a1 + a2	-1656.7	3335.5	43.35	0.622	0.841	0.626	0.843
[2.11]	$(a_0 * BD^{a_1}) * (RHIC^{(a_2 - 1)} * (DBLC^{a_3}))$	a1 + a2	-1656.8	3335.7	43.41	0.619	0.841	0.623	0.843
[2.12]	$(a_0 * BD^{a_1}) * (RHIC^{(a_2 - 1)})$	a1 + a2	-1656.9	3333.7	43.41	0.617	0.841	0.619	0.842
[2.13]	$(a_0 * BA^{a_1}) * (RHIC^{(a_2 - 1)})$	a1 + a2	-1657.2	3334.4	43.43	0.616	0.841	0.619	0.842
[2.14]	$(a_0 * BD^{a_1}) * (RDIC^{(a_2 - 1)}) * (TH^{a_3})$	a1 + a2	-1657.8	3337.6	43.77	0.600	0.839	0.604	0.840
[2.15]	$(a_0 * BD^{a_1}) * (RDIC^{(a_2 - 1)})$	a1 + a2	-1660.4	3340.8	43.77	0.608	0.840	0.611	0.841
[2.16]	$a_0 * BA^{a_1} * RHIC^{a_2} * TH^{a_3} * CL^{a_4} * DBLC^{a_5}$	a1	-1661.4	3338.8	44.59	0.602	0.830	0.608	0.832
[2.17]	$a_0 * BA^{a_1} * RHIC^{a_2} * TH^{a_3} * CL^{a_4} * DBLC^{a_5}$	a1	-1661.4	3338.8	44.59	0.602	0.830	0.608	0.832
[2.18]	$a_0 * BD^{a_1} * RHIC^{a_2} * TH^{a_3} * CL^{a_4} * DBLC^{a_5}$	a1	-1661.5	3339.1	44.61	0.602	0.830	0.609	0.832
[2.19]	$a_0 * BA^{a_1} * DIC^{a_2} * (HBLC/BA)^{a_3}$	a1	-1662.3	3336.6	44.63	0.599	0.831	0.603	0.832
[2.20]	$a_0 * BA^{a_1} * DIC^{a_2} * (HBLC/BD)^{a_3}$	a1	-1662.3	3336.6	44.63	0.599	0.831	0.603	0.832
[2.21]	$a_0 * BD^{a_1} * DIC^{a_2} * (HBLC/BA)^{a_3}$	a1	-1662.4	3336.8	44.65	0.599	0.831	0.603	0.832
[2.22]	$a_0 * BA^{a_1} * DIC^{a_2} * (TH/BA)^{a_3}$	a1	-1663.2	3338.4	44.91	0.618	0.828	0.621	0.830
[2.23]	$a_0 * BA^{a_1} * DIC^{a_2} * (TH/BD)^{a_3}$	a1	-1663.2	3338.4	44.91	0.618	0.828	0.621	0.830
[2.24]	$a_0 * BD^{a_1} * DIC^{a_2} * (TH/BA)^{a_3}$	a1	-1663.3	3338.6	44.92	0.618	0.828	0.621	0.830
[2.25] <sup>a</sup>	$a_0 * BD^{a_1} * DIC^{a_2} * (TH/BD)^{a_3}$	a1	-1663.3	3338.6	44.92	0.618	0.828	0.621	0.830
[2.26]	$a_0 * BA^{a_1} * RDIC^{a_2} * (TH/BA)^{a_3}$	a1	-1663.5	3339.1	44.76	0.600	0.830	0.604	0.832
[2.27]	$a_0 * BA^{a_1} * RDIC^{a_2} * (TH/BD)^{a_3}$	a1	-1663.5	3339.1	44.76	0.600	0.830	0.604	0.831
[2.28]	$a_0 * BD^{a_1} * RDIC^{a_2} * (TH/BA)^{a_3}$	a1	-1663.7	3339.3	44.77	0.600	0.830	0.604	0.831

**Table A2 cont.** Models evaluated for goodness of fit to branch foliar mass

Branch foliar mass model	Rand	LL	AIC	RMSE	Adjusted R <sup>2</sup>		Generalized R <sup>2</sup>	
					Fixed	Fixed + Rand	Fixed	Fixed + Rand
[2.29] a0 * BA^a1 * RDIC^a2 * (HBLC/BA)^a3	a1	-1663.8	3341.7	44.54	0.567	0.832	0.571	0.833
[2.30] a0 * BA^a1 * RHIC^a2 * (TH/BA)^a3	a1	-1663.9	3339.8	44.84	0.602	0.829	0.606	0.831
[2.31] a0 * BA^a1 * RHIC^a2 * (TH/BA)^a3	a1	-1663.9	3339.8	44.84	0.602	0.829	0.606	0.831
[2.32] a0 * BD^a1 * RHIC^a2 * (TH/BA)^a3	a1	-1664.0	3340.0	44.85	0.602	0.829	0.606	0.831
[2.33] a0 * BA^a1 * RDIC^a2 * (HBLC/BA)^a3	a1	-1664.5	3341.1	44.56	0.565	0.832	0.569	0.834
[2.34] a0 * BA^a1 * RDIC^a2 * (HBLC/BD)^a3	a1	-1664.5	3341.1	44.56	0.565	0.832	0.569	0.834
[2.35] a0 * BD^a1 * RDIC^a2 * (HBLC/BA)^a3	a1	-1664.7	3341.3	44.57	0.565	0.832	0.569	0.834
[2.36] a0 * BA^a1 * RHIC^a2 * (HBLC/BA)^a3	a1	-1664.9	3341.8	44.61	0.564	0.832	0.569	0.833
[2.37] a0 * BA^a1 * RHIC^a2 * (HBLC/BA)^a3	a1	-1664.9	3341.8	44.61	0.565	0.832	0.569	0.833
[2.38] a0 * BA^a1 * HIC^a2 * (TH/BA)^a3	a1	-1664.9	3341.9	44.79	0.584	0.830	0.588	0.832
[2.39] a0 * BA^a1 * HIC^a2 * (TH/BA)^a3	a1	-1664.9	3341.9	44.79	0.584	0.830	0.588	0.832
[2.40] a0 * BD^a1 * RHIC^a2 * (HBLC/BA)^a3	a1	-1665.1	3342.1	44.63	0.565	0.832	0.569	0.833
[2.41] a0 * BD^a1 * HIC^a2 * (TH/BA)^a3	a1	-1665.1	3342.1	44.80	0.584	0.830	0.588	0.832
[2.42] a0 * (HIC^a1) * (BA^a2)	a1 + a2	-1666.3	3352.7	44.08	0.596	0.839	0.599	0.840
[2.43] a0 * (HIC^a1) * (BD^a2)	a1 + a2	-1666.6	3353.2	44.09	0.596	0.839	0.599	0.840
[2.44] a0 * BA^a1 * HIC^a2 * (HBLC/BA)^a3	a1	-1667.1	3346.2	44.67	0.535	0.832	0.540	0.833
[2.45] a0 * BA^a1 * HIC^a2 * (HBLC/BA)^a3	a1	-1667.1	3346.2	44.67	0.535	0.832	0.540	0.833
[2.46] a0 * BD^a1 * HIC^a2 * (HBLC/BA)^a3	a1	-1667.3	3346.5	44.69	0.536	0.832	0.540	0.833
[2.47] (BA^a1) * (RHIC^(a2 - 1))	a1	-1668.7	3347.5	45.46	0.614	0.825	0.615	0.826
[2.48] a0 * (DIC^a1) * (BD^a2)	a1	-1668.9	3349.7	45.38	0.628	0.826	0.630	0.827
[2.49] a0 * (DIC^a1) * (BA^a2)	a1	-1668.9	3349.7	45.38	0.628	0.826	0.630	0.827
[2.50] BA^a1 * RDIC^a2 * TH^a3 * DBLC^a4	a4	-1668.9	3351.8	45.27	0.629	0.827	0.632	0.828
[2.51] (BD^a1) * (DIC^a2)	a2	-1669.7	3349.5	45.40	0.625	0.827	0.626	0.827
[2.52] a0 * (DIC^a1) * (BD^a2)	a1	-1669.9	3349.8	45.63	0.628	0.825	0.630	0.826
[2.53] <sup>b</sup> a0 * (DIC^a1) * (BA^a2)	a1	-1669.9	3349.8	45.63	0.628	0.825	0.630	0.826

**Table A2 cont. Models evaluated for goodness of fit to branch foliar mass**

Branch foliar mass model		Rand	LL	AIC	RMSE	Adjusted R <sup>2</sup>		Generalized R <sup>2</sup>	
						Fixed	Fixed + Rand	Fixed	Fixed + Rand
[2.54]	$(a_0 * BD^{a_1}) * (RDIC^{a_2}) * \exp(a_3 * RHIC)$	a3	-1670.1	3354.1	46.19	0.622	0.817	0.626	0.819
[2.55]	$(a_0 * BD^{a_1}) * (RHIC^{a_2}) * \exp(a_3 * RHIC)$	a3	-1670.2	3354.5	46.21	0.619	0.817	0.623	0.819
[2.56]	$(a_0 * BD^{a_1}) * \exp(a_2 * RHIC)$	a2	-1670.4	3352.8	46.23	0.620	0.818	0.623	0.819
[2.57]	$\exp(a_0) * BD^{a_1} * RHIC^{a_2} * \exp(a_3 * RHIC)$	a3	-1670.7	3353.3	46.36	0.618	0.816	0.622	0.818
[2.58]	$\exp(a_0) * BA^{a_1} * RHIC^{a_2} * \exp(a_3 * RHIC)$	a3	-1670.7	3353.3	46.36	0.618	0.816	0.622	0.818
[2.59]	$\exp(a_0) * BA^{a_1} * RDIC^{a_2} * \exp(a_3 * RHIC)$	a3	-1670.8	3353.5	46.37	0.621	0.816	0.625	0.818
[2.60]	$(a_0 * BD^{a_1}) * (\exp(a_2 * (RHIC)))$	a2	-1670.9	3351.8	46.39	0.620	0.816	0.623	0.817
[2.61]	$(a_0 * BA^{a_1}) * (\exp(a_2 * (RHIC)))$	a2	-1670.9	3351.8	46.39	0.620	0.816	0.623	0.817
[2.62] <sup>c</sup>	$(BD^{a_1}) * (DIC^{a_2})$	a2	-1671.2	3350.4	45.71	0.625	0.825	0.626	0.825
[2.63]	$(BA^{a_1}) * (DIC^{a_2})$	a2	-1671.9	3351.8	45.78	0.622	0.824	0.623	0.824
[2.64]	$BA^{a_1} * RDIC^{a_2}$	a1	-1672.4	3354.9	46.14	0.603	0.820	0.604	0.821
[2.65]	$a_0 * (HIC^{a_1}) * (BA^{a_2})$	a1	-1673.3	3356.5	45.71	0.598	0.824	0.601	0.825
[2.66]	$a_0 * (HIC^{a_1}) * (BD^{a_2})$	a1	-1673.3	3356.5	45.71	0.598	0.824	0.601	0.825
[2.67]	$(a_0 * BD^{a_1}) * (RDIC^{a_2}) * (DBLC^{a_3})$	a2	-1675.8	3365.7	47.31	0.607	0.807	0.611	0.809
[2.68]	$(a_0 * BA^{a_1}) * (RDIC^{(a_2 - 1)})$	a2	-1675.9	3361.8	47.39	0.613	0.807	0.615	0.809
[2.69]	$\exp(a_0) * BA^{a_1} * RDIC^{a_2} * \exp(a_3 * RDIC)$	a3	-1683.3	3378.7	47.24	0.617	0.812	0.621	0.814
[2.70] <sup>d</sup>	$\exp(a_0) * BD^{a_1} * RDIC^{a_2} * \exp(a_3 * RDIC)$	a3	-1683.3	3378.7	47.24	0.617	0.812	0.621	0.814
[2.71]	$(BA^{a_1}) * (HIC^{a_2})$	a2	-1685.3	3378.6	48.16	0.596	0.805	0.597	0.805
[2.72]	$(BD^{a_1}) * (HIC^{a_2})$	a2	-1687.6	3383.1	48.55	0.592	0.802	0.593	0.802
[2.73]	$\exp(a_0) * BA^{a_1} * RHIC^{a_2} * \exp(a_3 * RDIC)$	a3	-1687.9	3387.8	47.95	0.609	0.806	0.612	0.808
[2.74]	$\exp(a_0) * BD^{a_1} * RHIC^{a_2} * \exp(a_3 * RDIC)$	a3	-1687.9	3387.8	47.95	0.609	0.806	0.612	0.808
[2.75]	$(a_0 * BD^{a_1}) * (\exp(a_2 * (RDIC)))$	a2	-1687.9	3385.8	47.95	0.610	0.807	0.612	0.808
[2.76]	$(a_0 * BA^{a_1}) * (\exp(a_2 * (RDIC)))$	a2	-1687.9	3385.8	47.95	0.610	0.807	0.612	0.808
[2.77]	$(a_0 + a_1 * (BA^{(1/3)})) + a_2 * (RDIC^{(1/3)})^3$	a0	-1690.4	3392.8	48.58	0.603	0.804	0.605	0.805
[2.78]	$(a_0 + a_1 * (BA^{(1/3)})) + a_2 * (RHIC^{(1/3)})^3$	a0	-1690.8	3391.6	48.66	0.608	0.803	0.610	0.805

**Table A2 cont. Models evaluated for goodness of fit to branch foliar mass**

Branch foliar mass model	Rand	LL	AIC	RMSE	Adjusted R <sup>2</sup>		Generalized R <sup>2</sup>	
					Fixed	Fixed + Rand	Fixed	Fixed + Rand
[2.79] $(a_0 + a_1 * (BA^{(1/3)}) + a_2 * (RDIC^{(1/3)}))^3$	a0	-1691.1	3392.3	48.69	0.604	0.803	0.606	0.804
[2.80] $(a_0 + a_1 * (BD^{(1/3)}) + a_2 * (RDIC^{(1/3)}))^3$	a0	-1691.2	3392.3	48.49	0.600	0.805	0.602	0.806
[2.81] $(a_0 + a_1 * (BD^{(1/3)}) + a_2 * (RHIC^{(1/3)}))^3$	a0	-1691.3	3392.7	48.56	0.603	0.804	0.606	0.805
[2.82] $a_0 * BA^{a_1} * RDIC^{a_2} * TH^{a_3} * CL^{a_4} * DBLC^{a_5}$	a0	-1728.7	3473.4	61.66	0.638	0.638	0.644	0.644
[2.83] $(a_0 * BA^{a_1}) * (RDIC^{(a_2 - 1)}) * (\exp(a_3 * (RHIC^{a_4})))$	a4	-1731.1	3476.2	62.14	0.633	0.633	0.638	0.638
[2.84] $BA * (a_0 * RHIC + a_1 * (RHIC^2) + a_2) + a_3$	a3	-1732.3	3476.5	58.76	0.620	0.702	0.623	0.705
[2.85] $BA * (a_0 * RDIC + a_1 * (RDIC^2) + a_2) + a_3$	a3	-1732.3	3476.5	58.76	0.620	0.702	0.623	0.705
[2.86] <sup>e</sup> $(a_0 * BD^{a_1}) * (RDIC^{(a_2 - 1)}) * (\exp(a_3 * (RDIC^{a_4})))$	a3	-1733.2	3482.4	62.57	0.628	0.628	0.633	0.633
[2.87] <sup>f</sup> $(a_0 * BD^{a_1}) * (\exp(a_2 * (RDIC^{a_3})))$	a2	-1736.8	3485.7	63.30	0.621	0.621	0.624	0.624
[2.88] $(a_0 * BA^{a_1}) * (RHIC^{(a_2 - 1)})$	a0	-1738.7	3487.3	63.67	0.618	0.618	0.620	0.620
[2.89] $BD * (a_0 * RHIC + a_1 * (RHIC^2) + a_2) + a_3$	a3	-1739.3	3490.5	59.27	0.595	0.702	0.598	0.705
[2.90] $BD * (a_0 * RDIC + a_1 * (RDIC^2) + a_2) + a_3$	a3	-1739.3	3490.5	59.27	0.595	0.702	0.598	0.705
[2.91] $(a_0 * BD^{a_1}) * (RDIC^{(a_2 - 1)})$	a0	-1739.7	3489.5	63.89	0.615	0.615	0.617	0.617
[2.92] $(a_0 * BD^{a_1}) * (RDIC^{(a_2 - 1)})$	a0	-1739.7	3489.5	63.89	0.615	0.615	0.617	0.617
[2.93] $(a_0 * BD^{a_1}) * (\exp(a_2 * (RDIC^{a_3})))$	a2	-1745.3	3504.6	65.04	0.600	0.600	0.604	0.604
[2.94] $(a_0 * BD^{a_1})$	a0	-1745.5	3500.9	65.07	0.602	0.602	0.603	0.603

<sup>a</sup>Ek 1979; <sup>b</sup>Monserud and Marshall 2001; <sup>c</sup>Gillespie et al. 1994; <sup>d</sup>Maguire et al. 1998; <sup>e</sup>Maguire and Bennett 1996; <sup>f</sup>Xu and Harrington 1998

**Table A3** Models evaluated for goodness of fit to crown foliar mass

Crown foliar mass model	Rand	LL	AIC	RMSE	Adjusted R <sup>2</sup>		Generalized R <sup>2</sup>	
					Fixed	Fixed + Rand	Fixed	Fixed + Rand
[2.2] (b1 * DBH) + (b2 * HMC)	b1 + b2	-419.3	850.5	1032.18	0.832	0.934	0.835	0.935
[2.95] <sup>a</sup> b0 * (DBH^(b1 + (b2 * CL) + b3 * (TH/DBH)))	b3	-419.4	850.8	1012.20	0.814	0.935	0.825	0.939
[2.96] (b0 * (HMC^b1) * DBH^(b2 + b3 * (TH/DBH)))	b3	-419.8	851.7	1047.76	0.818	0.929	0.830	0.933
[2.97] (b0 * DBH^(b1 + b2 * (TH/DBH)))	b2	-419.9	849.8	1060.21	0.825	0.928	0.833	0.931
[2.98] b0 * (DBH^b1) * (CLR^b2) * (CL^b3)	b3	-420.9	853.8	1100.29	0.821	0.919	0.832	0.924
[2.99] (b0 * DBH^(b1 + b2 * (HMC/DBH)))	b2	-420.9	851.8	1105.98	0.825	0.920	0.832	0.923
[2.100] b0 * DBH^b1 * HMC^b2	b1	-422.0	854.0	1143.83	0.821	0.913	0.828	0.917
[2.101] b0 + (b1 * DBH) + (b2 * MCLR) + (b3 * HMC)	b0	-422.2	856.5	1132.57	0.827	0.916	0.838	0.922
[2.102] b0 + (b1 * DBH) + (b2 * HMC)	b0	-422.3	854.5	1132.61	0.830	0.918	0.837	0.922
[2.103] <sup>b</sup> (1/HMC) * ((DBH/b1)^b2)	b2	-422.8	853.7	1184.20	0.823	0.908	0.827	0.909
[2.104] b0 + (b1 * DBH) + (b2 * MCLR)	b0	-423.7	857.3	1126.76	0.814	0.921	0.822	0.925
[2.105] b0 * (DBH^b1) * exp(b2 * (DBH/HMC))	b2	-424.5	858.9	1195.39	0.802	0.905	0.810	0.909
[2.106] b0 * DBH^b1 * exp(MCLR * b2)	b1	-425.9	861.8	1159.85	0.779	0.915	0.788	0.919
[2.107] b0 * DBH^b1 * MCLR^b2	b1	-426.2	862.3	1132.79	0.772	0.921	0.781	0.924
[2.108] b0 * DBH^b1 * exp(HMC * b2)	b1	-426.5	863.0	1186.47	0.790	0.910	0.798	0.914
[2.109] b0 * DBH^b1 * CLR^b2	b1	-426.6	863.1	1125.82	0.767	0.922	0.777	0.925
[2.110] b0 * DBH^b1 * exp(CLR * b2)	b1	-426.7	863.3	1152.46	0.772	0.917	0.781	0.921
[2.111] DBH^b1 * exp(CL * b2)	b1	-426.9	861.7	956.52	0.688	0.949	0.694	0.950
[2.112] <sup>c</sup> b0 + b1 * (DBH + MCLR)	b0	-427.0	862.1	1094.91	0.721	0.932	0.727	0.933
[2.113] b0 * DBH^b1	b1	-427.9	863.8	1046.51	0.734	0.937	0.740	0.939
[2.114] (DBH^b1) * (CLR^b2) * (CL^b3)	b3	-428.4	866.7	1047.17	0.676	0.936	0.690	0.939
[2.115] <sup>d</sup> b0 * (DBH^b1) * exp(b2 * (DBH/CL))	b2	-428.5	867.0	1026.00	0.712	0.938	0.724	0.941
[2.116] <sup>e</sup> b0 * (CL^b1) * exp(b2 * (DBH/TH))	b2	-428.7	867.5	1335.36	0.772	0.879	0.781	0.884
[2.117] DBH^b1 * CL^b2	b1	-429.1	866.1	1043.10	0.679	0.938	0.686	0.940
[2.118] DBH^b1	b1	-429.9	865.7	1020.69	0.611	0.943	0.611	0.943
[2.119] (DBH^(b1 + b2 * (TH/DBH)))	b2	-430.4	868.7	1032.20	0.626	0.941	0.634	0.943

<sup>a</sup>Weiskittel et al 2009; <sup>b</sup>Jerez et al. 2005; <sup>c</sup>Kenefic and Seymour 1999; <sup>d</sup>Nelson et al. 2014; <sup>e</sup>Maguire and Bennett 1996;

**Table A4** Models evaluated for goodness of fit to Weibull kurtosis parameter estimates

Weibull kurtosis model		Rand	LL	AIC	RMSE	Adjusted R <sup>2</sup>		Generalized R <sup>2</sup>	
						Fixed	Fixed + Rand	Fixed	Fixed + Rand
[2.120]	$\exp(g_0 + (CL * g_1) + (DBLC * g_2) + (CFM * g_3))$	g1	72.6	-133.3	0.0549	0.546	0.546	0.574	0.574
[2.3]	$g_0 + g_1 * CL + g_2 * DBLC$	NA	70.5	-133.0	0.0592	0.516	NA	0.536	NA
[2.121]	$g_0 + (CL * g_1) + (DBLC * g_2)$	g1	70.5	-131.0	0.0574	0.516	0.516	0.536	0.536
[2.122]	$g_0 * (CL^{(g_1 + (DBLC * g_2) + (CFM * g_3))})$	g1	70.0	-128.1	0.0579	0.495	0.495	0.527	0.527
[2.123]	$g_0 * (CL^{(g_1 + (g_2 * DBLC))})$	g1	68.8	-127.6	0.0594	0.480	0.480	0.502	0.502
[2.124]	$g_0 * (CL^{g_1}) * (DBLC^{g_2})$	g1	68.1	-126.2	0.0592	0.464	0.502	0.486	0.523
[2.125]	$\exp(g_0 + (CL * g_1) + (DBH * g_2) + (CFM * g_3))$	g1	64.2	-116.4	0.0653	0.359	0.359	0.399	0.399
[2.126]	$g_0 + g_1 * CL + g_2 * DBH + g_3 * CFM$	NA	64.1	-118.3	0.0682	0.357	NA	0.397	NA
[2.127]	$g_0 + g_1 * CL + g_2 * DBH$	NA	64.0	-119.9	0.0677	0.367	NA	0.394	NA
[2.128]	$g_0 * (CL^{g_1}) * \exp(DBH * g_2)$	g1	63.5	-117.1	0.0662	0.356	0.356	0.383	0.383
[2.129]	$g_0 * (CL^{(g_1 + (DBH * g_2))})$	g1	63.5	-117.0	0.0662	0.354	0.354	0.381	0.381
[2.130]	$g_0 * (CL^{g_1}) * (DBH^{g_2})$	g1	63.4	-116.8	0.0663	0.353	0.353	0.379	0.379
[2.131]	$g_0 * (CL^{g_1}) * (CFM^{g_2})$	g1	63.3	-116.7	0.0664	0.351	0.351	0.378	0.378
[2.132]	$g_0 * (CL^{(g_1 + (g_2 * CL))})$	g1	62.6	-115.1	0.0675	0.330	0.330	0.358	0.358
[2.133]	$g_0 * (CL^{g_1}) * (TH^{g_2})$	g1	62.5	-115.0	0.0675	0.329	0.329	0.357	0.357
[2.134]	$g_0 * (CL^{g_1}) * (HMC^{g_2})$	g1	62.5	-115.0	0.0676	0.328	0.328	0.356	0.356
[2.135]	$g_0 + (CL * g_1)$	g1	62.4	-116.9	0.0677	0.340	0.340	0.354	0.354
[2.136]	$g_0 + CL * g_1$	NA	62.4	-118.9	0.0691	0.340	NA	0.354	NA
[2.137]	$g_0 * (CL^{g_1})$	NA	62.3	-118.6	0.0693	0.337	NA	0.350	NA
[2.138]	$g_0 * (CL^{g_1})$	g1	62.3	-116.6	0.0679	0.337	0.337	0.350	0.350
[2.139]	$CL^{(g_1 + (DBH * g_2) + (CFM * g_3))}$	g1	58.4	-106.9	0.0716	0.204	0.281	0.237	0.311
[2.140]	$g_0 * (TH^{g_1})$	g1	57.3	-106.5	0.0726	0.179	0.288	0.196	0.303
[2.141]	$g_0 + TH * g_1$	NA	57.2	-108.4	0.0769	0.183	NA	0.200	NA
[2.142]	$CL^{(g_1 + (g_2 * DBLC))}$	g1	57.1	-106.2	0.0704	0.156	0.364	0.174	0.378
[2.143]	$CL^{(g_1 + (g_2 * DBLC))}$	g1	57.1	-106.2	0.0704	0.156	0.364	0.174	0.378
[2.144]	$CL^{(g_1 + (g_2 * DBLC))}$	NA	56.7	-107.4	0.0777	0.166	NA	0.184	NA

**Table A4 cont.** Models evaluated for goodness of fit to Weibull kurtosis parameter estimates

Weibull kurtosis model		Rand	LL	AIC	RMSE	Adjusted R <sup>2</sup>		Generalized R <sup>2</sup>	
						Fixed	Fixed + Rand	Fixed	Fixed + Rand
[2.145]	g0 * (DBH^g1)	g1	56.6	-105.2	0.0734	0.157	0.276	0.175	0.291
[2.146]	g0 * (HMC^g1)	g1	55.9	-103.7	0.0727	0.117	0.315	0.135	0.330

**Table A5** Models evaluated for goodness of fit to Weibull skew parameter estimates

Weibull skew model		Rand	LL	AIC	RMSE	Adjusted R <sup>2</sup>		Generalized R <sup>2</sup>	
						Fixed	Fixed + Rand	Fixed	Fixed + Rand
[2.147]	g0 * (CLR^(g1 + (CFM * g2)))	g1 + g2	-36.7	87.3	0.387	0.411	0.852	0.436	0.858
[2.148]	g0 * (CLR^(g1 + (CFM * g2) + (HBLC * g3)))	g1 + g3	-37.9	91.7	0.459	0.236	0.763	0.284	0.778
[2.4]	g0 * (CLR^(g1 + (CFM * g2)))	g1	-41.2	92.4	0.497	0.522	0.731	0.542	0.742
[2.149]	g0 + (CL * g1) + (g2 * HBLC) + (g3 * CL * HBLC)	g2 + g3	-41.8	99.6	0.483	0.384	0.749	0.423	0.765
[2.150]	g0 * (CLR^g1) * (CFM^g2)	g1 + g2	-41.8	97.7	0.505	0.487	0.718	0.508	0.730
[2.151]	g0 * (CLR^g1) * (CFM^g2)	g1	-42.5	95.1	0.515	0.496	0.710	0.517	0.722
[2.152]	g0 * (CLR^(g1 + (CFM * g2)) * (CFM^g3))	g2	-42.8	97.6	0.535	0.501	0.669	0.532	0.690
[2.153]	g0 * (CLR^(g1 + (CFM * g2)))	g2	-43.0	95.9	0.539	0.514	0.669	0.534	0.683
[2.154]	g0 * (CLR^g1)	g1	-45.2	98.4	0.541	0.418	0.687	0.430	0.694
[2.155]	g0 + (CLR * g1) + (g2 * HBLC)	g2	-48.4	106.9	0.616	0.447	0.559	0.470	0.578
[2.156]	g0 * (CFM^g1) * (HBLC^g2)	g2	-48.8	107.6	0.641	0.456	0.500	0.478	0.521
[2.157] <sup>a</sup>	g0 * (CL^(g1 + (CFM * g2) + (TH * g3)))	g1 + g3	-49.6	115.3	0.602	0.373	0.592	0.412	0.617
[2.158]	g0 + (CFM * g1) + (g2 * HBLC)	g0	-49.9	109.8	0.660	0.431	0.464	0.455	0.486
[2.159]	g0 * HBLC^(g1 + (g2 * CL))	g1	-50.1	110.3	0.619	0.403	0.577	0.428	0.594
[2.160]	g0 + CLR * g1	NA	-50.8	107.6	0.697	0.423	NA	0.435	NA
[2.161]	g0 * (CL^g1) * (HBLC^g2)	g1	-51.6	113.3	0.673	0.387	0.459	0.412	0.481
[2.162]	g0 + (CL * g1) + (g2 * HBLC)	g0	-52.9	115.8	0.667	0.337	0.497	0.364	0.518
[2.163]	g0 * (HBLC^g1)	g1	-56.9	121.7	0.719	0.232	0.431	0.248	0.443

<sup>a</sup>Weiskittel et al. 2009

**Table B1** Summary of branch segments sampled for foliar mass

Site/Tr <sup>a</sup> /Sect <sup>b</sup> /Br <sup>c</sup>	n	Foliage (mg)		
		min	mean	max
Carsc 1 1 1	16	0.0	375.5	2449.5
Carsc 1 1 2	10	0.0	440.2	1009.4
Carsc 1 2 1	12	0.0	537.6	1236.9
Carsc 1 2 2	15	0.0	1774.2	3618.1
Carsc 1 3 1	10	0.0	717.0	1349.5
Carsc 1 3 2	7	0.0	700.6	1524.2
Carsc 2 1 1	20	3.8	6602.7	19135.3
Carsc 2 1 2	17	0.0	4371.1	15139.9
Carsc 2 2 1	20	30.3	6867.2	26905.3
Carsc 2 2 2	16	0.0	2327.4	9530.5
Carsc 2 3 1	6	54.0	822.1	1286.5
Carsc 2 3 2	10	14.3	1449.3	3508.4
Carsc 3 1 1	15	8.9	800.2	2454.1
Carsc 3 1 2	16	12.2	1754.8	4286.0
Carsc 3 2 1	18	69.4	3498.3	8339.6
Carsc 3 2 2	17	123.0	4612.9	9960.4
Carsc 3 3 1	14	89.3	4523.6	13024.1
Carsc 3 3 2	10	0.0	1509.5	5726.3
Carsc 4 1 1	11	47.1	1266.3	3317.4
Carsc 4 1 2	6	0.0	78.8	282.1
Carsc 4 2 1	8	79.3	1380.3	4937.8
Carsc 4 2 2	9	17.0	1077.5	2624.9
Carsc 4 3 1	6	54.0	591.1	1157.6
Carsc 4 3 2	4	0.0	77.1	195.9
Carsc 5 1 1	24	332.3	4871.6	13499.5
Carsc 5 1 2	19	0.0	7780.6	27133.4
Carsc 5 2 1	10	146.0	2010.0	5691.1
Carsc 5 2 2	17	327.2	6616.2	17709.3
Carsc 5 3 1	7	0.0	1171.2	2317.6
Carsc 5 3 2	10	85.2	3155.0	10801.8
Carsc 6 2 1	13	148.0	1600.1	3186.0
Carsc 6 2 2	10	393.7	1768.9	4613.9
Carsc 6 3 1	8	180.1	1758.9	7025.1
Carsc 6 3 2	6	188.4	1142.0	1734.6
TMU 1 1 1	12	0.0	2768.8	6735.7
TMU 1 1 2	12	0.0	2680.5	7008.3
TMU 1 2 1	9	17.1	1859.8	4155.3
TMU 1 2 2	8	104.8	1297.1	3456.5
TMU 1 3 1	8	55.1	2794.1	10176.6
TMU 1 3 2	4	92.1	549.7	965.4
TMU 2 1 1	18	0.0	2423.2	5413.2
TMU 2 1 2	17	0.0	2292.5	6537.0
TMU 2 2 1	17	0.0	3292.0	6782.5
TMU 2 2 2	16	0.0	6974.3	15333.3
TMU 2 3 1	13	0.0	4054.6	8196.6
TMU 2 3 2	9	0.0	2644.0	7734.5
TMU 3 1 1	8	41.8	987.4	2167.6
TMU 3 1 2	9	2.2	534.6	1885.0

**Table B1 cont.** Summary of branch segments sampled for foliar mass

Site/Tr <sup>a</sup> /Sect <sup>b</sup> /Br <sup>c</sup>	n	Foliage (mg)		
		min	mean	max
TMU 3 2 1	12	245.3	2414.1	6088.5
TMU 3 2 2	10	35.3	1660.9	5791.1
TMU 3 3 1	9	470.2	2285.1	5907.0
TMU 3 3 2	5	43.1	888.5	1687.0
UI217 1 1 1	16	0.0	441.3	1373.2
UI217 1 1 2	22	0.0	2340.5	5770.7
UI217 1 2 1	16	0.0	1144.1	5511.2
UI217 1 2 2	16	6.1	3530.4	13304.4
UI217 1 3 1	11	8.9	2634.0	5714.2
UI217 1 3 2	10	97.1	2413.1	9595.0
UI217 2 1 1	15	36.9	1488.3	3153.7
UI217 2 1 2	12	0.0	1456.1	3142.0
UI217 2 2 1	13	149.0	3858.2	10870.4
UI217 2 2 2	16	0.0	918.9	3984.7
UI217 2 3 1	9	67.9	1690.8	4173.0
UI217 2 3 2	12	118.6	3161.1	9037.2
UI217 3 1 1	18	0.0	2259.8	6032.6
UI217 3 1 2	13	0.0	725.4	1629.2
UI217 3 2 1	12	0.0	1592.8	2857.4
UI217 3 2 2	15	33.2	3986.0	8433.3
UI217 3 3 1	10	0.0	1066.7	2727.8
UI217 3 3 2	10	0.0	3262.4	14456.6
UI217 4 1 1	25	0.0	3122.5	8064.9
UI217 4 1 2	20	0.0	1867.5	6900.0
UI217 4 2 1	15	297.1	3316.3	8048.3
UI217 4 2 2	15	4.6	3831.4	10805.2
UI217 4 3 1	15	189.7	3752.9	11833.8
UI217 4 3 2	6	33.8	848.1	1966.2
UI486 1 1 1	12	23.3	405.9	1105.4
UI486 1 1 2	11	73.6	1170.5	2574.4
UI486 1 2 1	12	34.3	1496.3	4920.3
UI486 1 2 2	9	62.7	1582.6	5029.0
UI486 1 3 1	6	46.1	619.8	1153.1
UI486 1 3 2	7	256.2	1028.9	1993.7
UI486 2 1 1	18	0.0	1146.9	4304.1
UI486 2 1 2	16	0.0	1209.4	5660.6
UI486 2 2 1	13	0.0	1966.8	7232.2
UI486 2 2 2	16	0.0	2501.9	9094.3
UI486 2 3 1	5	0.0	733.0	1520.5
UI486 2 3 2	10	0.0	1483.5	3291.0
<b>Overall</b>	<b>1090</b>	<b>0.0</b>	<b>2535.6</b>	<b>27133.4</b>

<sup>a</sup>Tree within site<sup>b</sup>Vertical section along the main stem<sup>c</sup>Branch within vertical stem section

**Table B2.** Summary of branch segments sampled for specific leaf area

Site/Tr <sup>a</sup> /Sect <sup>b</sup> /Br <sup>c</sup>	Segs.	RPAB			LA (mm <sup>2</sup> )			FM (mg)			SLA (cm <sup>2</sup> g <sup>-1</sup> )					
		n	min	mean	max	min	mean	max	min	mean	max	min	mean	max		
Carsc	1	1	1	14	0.00	0.41	0.88	147.7	1241.1	1838.8	13.1	152.5	435.8	30.52	93.29	117.12
Carsc	1	1	2	8	0.00	0.43	0.98	821.4	1624.0	2146.6	74.0	176.2	243.3	82.32	93.81	111.01
Carsc	1	2	1	12	0.00	0.50	0.99	1686.7	1877.1	2143.6	189.7	227.7	266.0	68.34	82.78	92.11
Carsc	1	2	2	15	0.00	0.50	0.99	1351.7	1802.0	2072.3	209.5	281.0	564.3	32.70	66.65	78.31
Carsc	1	3	1	9	0.00	0.54	1.00	1172.5	1704.9	2057.7	193.2	274.5	330.3	54.69	62.50	71.10
Carsc	1	3	2	7	0.00	0.50	1.00	861.2	1804.8	2114.8	137.6	287.3	337.8	61.02	62.82	64.96
Carsc	3	1	1	4	0.07	0.45	0.84	496.3	591.9	677.1	52.7	72.3	82.5	72.82	83.00	94.18
Carsc	3	1	2	4	0.13	0.52	0.91	553.0	740.3	896.4	60.1	100.2	139.6	64.21	76.67	92.01
Carsc	3	2	1	4	0.12	0.55	0.98	553.9	708.0	865.2	82.8	107.2	137.6	54.20	66.67	81.39
Carsc	3	2	2	4	0.00	0.41	0.84	704.9	783.2	868.7	121.7	131.6	150.3	46.90	60.14	71.33
Carsc	3	3	1	4	0.07	0.43	0.81	711.8	751.9	802.7	137.6	142.2	149.5	50.31	52.88	54.65
Carsc	3	3	2	3	0.10	0.44	0.71	609.8	654.1	686.3	106.8	118.1	131.1	52.35	55.56	57.25
Carsc	4	1	1	4	0.10	0.53	0.97	362.3	488.3	663.9	30.2	46.3	62.4	97.98	106.85	119.97
Carsc	4	1	2	3	0.00	0.43	0.74	288.6	377.7	475.1	28.0	32.6	40.2	97.84	115.98	131.92
Carsc	4	2	1	3	0.14	0.56	0.99	640.8	729.5	775.1	67.2	86.5	97.5	79.50	85.48	95.36
Carsc	4	2	2	3	0.12	0.41	0.74	719.9	795.2	850.6	76.2	105.3	127.5	66.72	77.97	94.47
Carsc	4	3	1	3	0.20	0.59	0.98	811.2	951.9	1102.0	115.0	139.4	155.5	60.61	68.59	74.61
Carsc	4	3	2	3	0.00	0.44	1.00	606.5	1051.3	1296.5	114.1	183.2	243.0	53.15	57.17	65.01
Carsc	5	1	1	4	0.13	0.50	0.88	817.0	951.1	1062.6	104.5	140.1	178.6	59.50	69.61	86.18
Carsc	5	1	2	4	0.10	0.46	0.82	741.1	939.9	1043.5	113.4	157.4	177.3	55.39	60.25	65.35
Carsc	5	2	1	3	0.22	0.56	0.89	1041.4	1152.5	1257.2	178.5	199.6	215.3	53.83	57.82	61.30
Carsc	5	2	2	4	0.12	0.48	0.81	845.8	865.6	913.1	169.3	177.0	188.1	45.37	49.00	53.37
Carsc	5	3	1	3	0.16	0.60	0.98	1150.7	1236.8	1388.9	259.5	282.7	299.0	40.43	43.74	46.45
Carsc	5	3	2	3	0.33	0.65	0.98	916.2	970.3	1059.3	195.7	224.1	254.2	41.67	43.51	46.82
Carsc	6	2	1	3	0.17	0.63	0.99	598.9	636.3	696.3	89.7	106.0	123.7	56.29	60.60	66.77
Carsc	6	2	2	3	0.33	0.59	0.88	607.7	657.2	717.8	110.9	118.2	129.8	54.80	55.61	56.72
Carsc	6	3	1	3	0.14	0.62	1.00	674.5	790.5	960.7	137.1	155.7	192.3	48.98	50.88	53.70
Carsc	6	3	2	3	0.00	0.45	0.96	811.8	847.0	870.6	165.0	176.5	186.1	46.78	48.04	49.20
TMU	1	2	1	3	0.13	0.50	0.88	439.7	513.1	640.9	82.5	99.3	123.3	47.80	51.79	55.60
TMU	1	2	2	3	0.14	0.42	0.69	390.4	600.1	735.8	80.9	116.5	143.1	48.26	51.12	53.68
TMU	1	3	1	3	0.28	0.61	0.99	614.5	644.0	685.0	132.1	139.2	145.5	45.18	46.26	47.08
TMU	1	3	2	3	0.31	0.63	0.94	544.4	552.2	560.2	106.3	108.7	111.0	49.73	50.82	52.70
TMU	2	1	1	15	0.00	0.42	0.94	596.0	1421.1	1799.7	126.4	264.2	329.5	47.15	53.50	59.89

**Table B2 cont.** *Summary of branch segments sampled for specific leaf area*

Site/Tr <sup>a</sup> /Sect <sup>b</sup> /Br <sup>c</sup>	Segs. n	RPAB			LA (mm <sup>2</sup> )			FM (mg)			SLA (cm <sup>2</sup> g <sup>-1</sup> )		
		min	mean	max	min	mean	max	min	mean	max	min	mean	max
TMU 2 1 2	13	0.00	0.37	0.89	23.7	1053.0	1773.3	2.3	199.7	339.8	43.53	56.39	102.86
TMU 2 2 1	16	0.00	0.52	0.99	590.9	1312.7	1987.9	134.9	306.7	484.3	40.35	43.04	46.79
TMU 2 2 2	16	0.00	0.50	0.99	473.0	1263.4	2051.6	115.0	315.7	510.1	15.62	40.21	43.41
TMU 2 3 1	13	0.00	0.50	1.00	510.6	1579.0	2159.9	123.6	405.7	562.9	36.94	39.02	41.31
TMU 2 3 2	9	0.00	0.49	0.99	265.6	1165.3	2272.8	63.2	299.8	598.0	37.61	39.25	42.02
TMU 3 1 1	3	0.25	0.63	1.00	289.0	401.0	470.9	34.7	59.6	73.1	60.62	70.07	83.27
TMU 3 1 2	3	0.12	0.44	0.71	381.4	416.9	473.3	47.0	60.9	73.6	63.66	69.70	81.15
TMU 3 2 1	4	0.09	0.52	0.99	488.8	536.2	645.6	87.4	93.5	109.2	55.36	57.24	59.12
TMU 3 2 2	3	0.11	0.43	0.76	489.0	574.1	623.0	87.5	103.2	114.5	53.30	55.70	57.90
TMU 3 3 1	2	0.00	0.18	0.37	705.6	745.8	786.0	130.5	132.3	134.0	54.07	56.36	58.65
TMU 3 3 2	3	0.00	0.41	0.98	741.0	1004.4	1205.6	148.0	206.0	251.9	47.86	48.94	50.07
UI217 1 1 1	4	0.00	0.26	0.58	442.9	491.4	570.3	41.9	47.1	54.5	99.74	104.36	110.10
UI217 1 1 2	4	0.05	0.40	0.78	723.5	738.0	748.8	77.2	85.6	94.2	79.50	86.66	95.80
UI217 1 2 1	4	0.07	0.31	0.66	535.2	801.7	978.9	74.1	92.0	101.8	72.22	86.34	97.04
UI217 1 2 2	4	0.20	0.52	0.87	512.4	749.3	871.5	58.6	101.5	123.1	70.79	75.51	87.43
UI217 1 3 2	4	0.11	0.50	0.89	871.2	985.4	1292.3	123.4	141.9	191.6	67.45	69.76	72.89
UI217 2 1 1	4	0.14	0.52	0.91	633.2	674.9	766.0	66.1	72.7	82.9	90.61	92.88	95.79
UI217 2 1 2	4	0.00	0.31	0.71	662.3	793.3	947.0	72.2	97.9	123.9	76.43	82.39	91.73
UI217 2 2 1	4	0.08	0.47	0.78	722.5	837.7	969.7	98.5	117.9	140.9	62.13	71.72	83.74
UI217 2 2 2	4	0.13	0.37	0.60	799.8	866.8	1043.8	90.3	106.6	137.2	75.80	82.23	89.82
UI217 2 3 1	3	0.00	0.52	0.96	663.9	707.7	777.7	103.7	112.8	126.6	53.83	63.26	71.94
UI217 2 3 2	4	0.00	0.50	0.91	759.2	951.1	1088.9	112.5	161.9	202.2	53.85	59.73	67.48
UI217 3 1 1	17	0.00	0.46	0.97	161.3	1417.5	2025.7	27.9	191.4	264.1	57.82	73.34	82.61
UI217 3 1 2	13	0.00	0.48	0.97	998.7	1364.9	1693.9	117.2	173.2	219.6	70.93	79.30	86.04
UI217 3 2 1	11	0.00	0.48	0.99	750.5	1450.4	1839.3	116.0	186.3	249.6	64.69	77.41	86.47
UI217 3 2 2	13	0.07	0.52	1.00	1335.2	1740.2	1880.7	194.5	249.8	333.6	55.65	70.29	77.91
UI217 3 3 1	10	0.00	0.49	0.99	119.2	1445.5	1881.4	20.9	229.8	313.3	48.60	62.66	73.88
UI217 3 3 2	10	0.00	0.54	1.00	798.9	1755.3	2057.1	161.2	285.2	383.1	49.56	61.66	69.78
UI217 4 1 1	4	0.04	0.40	0.81	616.3	725.0	809.7	90.1	110.4	142.5	56.82	66.86	79.12
UI217 4 1 2	4	0.10	0.43	0.80	615.4	737.7	814.8	98.6	116.3	129.6	59.41	63.64	69.39
UI217 4 2 1	4	0.14	0.55	0.96	738.2	862.9	1026.2	110.8	138.9	170.3	56.31	62.37	66.87
UI217 4 2 2	4	0.07	0.43	0.83	701.5	985.2	1199.7	135.0	170.4	193.3	51.96	57.38	62.07
UI217 4 3 1	4	0.07	0.50	0.93	963.6	1199.1	1332.9	176.2	228.5	255.8	47.46	52.74	57.13

**Table B2 cont.** Summary of branch segments sampled for specific leaf area

Site/Tr <sup>a</sup> /Sect <sup>b</sup> /Br <sup>c</sup>	Segs.	RPAB			LA (mm <sup>2</sup> )			FM (mg)			SLA (cm <sup>2</sup> g <sup>-1</sup> )		
		n	min	mean	max	min	mean	max	min	mean	max	min	mean
UI217 4 3 2	3	0.20	0.53	0.80	987.0	1102.3	1284.5	186.3	203.4	229.7	52.98	54.08	55.92
UI486 1 1 1	4	0.00	0.35	0.80	346.4	490.3	606.0	34.7	54.1	67.0	84.91	91.60	99.83
UI486 1 1 2	4	0.10	0.59	0.98	621.4	751.2	821.8	58.6	84.5	106.5	77.17	90.97	106.04
UI486 1 2 1	4	0.18	0.52	0.91	812.0	897.1	998.9	105.6	117.2	130.8	73.53	76.61	78.90
UI486 1 2 2	3	0.25	0.63	1.00	925.0	1013.4	1115.4	120.1	148.0	186.7	59.74	69.88	77.02
UI486 1 3 1	3	0.20	0.67	1.00	901.9	938.7	974.3	142.8	157.2	170.0	57.31	59.88	63.16
UI486 1 3 2	3	0.00	0.28	0.67	1006.0	1098.7	1252.5	183.7	205.8	233.7	51.91	53.42	54.76
UI486 2 1 1	14	0.00	0.38	0.81	61.4	1330.3	1695.9	6.9	197.9	265.6	61.03	69.56	88.97
UI486 2 1 2	14	0.00	0.43	0.87	953.6	1491.6	1719.2	149.3	254.4	469.9	33.04	60.67	66.97
UI486 2 2 1	13	0.00	0.48	0.96	1278.9	1520.2	1768.9	238.0	271.9	330.6	49.82	56.09	62.16
UI486 2 2 2	16	0.00	0.48	0.96	477.6	1697.2	3485.8	103.2	343.1	712.2	41.25	49.25	56.79
UI486 2 3 1	5	0.00	0.50	1.00	1227.0	1824.3	2279.1	264.6	368.6	464.6	46.37	49.30	52.87
UI486 2 3 2	10	0.00	0.49	0.99	750.4	1927.8	2716.5	197.9	416.1	620.9	37.92	45.98	49.90
<b>Overall Values</b>	<b>485</b>	<b>0.00</b>	<b>0.48</b>	<b>1.00</b>	<b>23.7</b>	<b>1222</b>	<b>3485.8</b>	<b>2.3</b>	<b>208</b>	<b>712.2</b>	<b>15.62</b>	<b>64.22</b>	<b>131.92</b>

<sup>a</sup>Tree within site

<sup>b</sup>Vertical section along the main stem

<sup>c</sup>Branch within vertical stem section

**Table B3** Models evaluated for goodness of fit to specific leaf area

SLA model	Rand	LL	AIC	RMSE	Adjusted R <sup>2</sup>		Generalized R <sup>2</sup>	
					Fixed	Fixed + Rand	Fixed	Fixed + Rand
[3.4] (1122.0953 * HIC <sup>m1</sup> ) * (HMC <sup>(m2 + (RDAF * m3) + q0 * (SE + SW))</sup> )	m1 + m2	-1708.39	3438.78	7.71	0.554	0.815	0.556	0.816
[3.1] (m0 * HIC <sup>m1</sup> ) * (HMC <sup>(m2 + (RPAB * m3) + q0 * (SE + SW))</sup> )	m1 + m2	-1709.03	3442.07	7.72	0.548	0.815	0.552	0.816
[3.5] (1096.3052 * HIC <sup>m1</sup> ) * (HMC <sup>(m2 + (RPAB * m3) + q0 * (SE + SW))</sup> )	m1 + m2	-1709.04	3440.07	7.72	0.551	0.815	0.553	0.816
[3.6] (m0 * HIC <sup>m1</sup> ) * (HMC <sup>(m2 + (RDmF * m3) + q0 * SE + q1 * SW + q2 * NW)</sup> )	m1	-1712.00	3444.00	7.85	0.579	0.805	0.584	0.807
[3.7] (3182.855 * HIC <sup>m1</sup> ) * (HMC <sup>(m2 + (RDAF * m3) + q0 * SE + q1 * SW + q2 * NW)</sup> )	m1	-1712.00	3442.00	7.85	0.579	0.805	0.584	0.807
[3.8] (m0 * HIC <sup>m1</sup> ) * (HMC <sup>(m2 + (RDAF * m3) + q0 * (SE + SW) + q1 * NW)</sup> )	m1	-1712.10	3442.19	7.85	0.576	0.805	0.580	0.807
[3.9] (3133.4338 * HIC <sup>m1</sup> ) * (HMC <sup>(m2 + (RDAF * m3) + q0 * (SE + SW) + q1 * NW)</sup> )	m1	-1712.10	3440.19	7.85	0.576	0.806	0.580	0.807
[3.10] (m0 * HIC <sup>(m1 + q0 * SE + q1 * SW + q2 * NW)</sup> ) * (HMC <sup>(m2 + (RDAF * m3))</sup> )	m1	-1712.72	3445.45	7.86	0.574	0.804	0.580	0.807
[3.11] (3077.8926 * HIC <sup>(m1 + q0 * SE + q1 * SW + q2 * NW)</sup> ) * (HMC <sup>(m2 + (RDAF * m3))</sup> )	m1	-1712.72	3443.45	7.86	0.575	0.805	0.580	0.807
[3.12] (m0 * HIC <sup>(m1 + q0 * (SE + SW) + q1 * NW)</sup> ) * (HMC <sup>(m2 + (RDAF * m3))</sup> )	m1	-1712.73	3443.46	7.86	0.574	0.805	0.579	0.807
[3.13] (3072.5735 * HIC <sup>(m1 + q0 * (SE + SW) + q1 * NW)</sup> ) * (HMC <sup>(m2 + (RDAF * m3))</sup> )	m1	-1712.73	3441.46	7.86	0.575	0.805	0.579	0.807
[3.14] (m0 * HIC <sup>m1</sup> ) * (HMC <sup>(m2 + (RDAF * m3) + q0 * (SE + SW))</sup> )	m1	-1714.87	3445.73	7.89	0.572	0.804	0.575	0.805
[3.15] (2720.3161 * HIC <sup>m1</sup> ) * (HMC <sup>(m2 + (RDAF * m3) + q0 * (SE + SW))</sup> )	m1	-1714.87	3443.73	7.89	0.573	0.804	0.575	0.805
[3.16] m0 * HIC <sup>(m1 + q0 * (SE + SW))</sup> * (HMC <sup>(m2 + (RDAF * m3))</sup> )	m1	-1715.43	3446.86	7.90	0.572	0.803	0.575	0.805
[3.17] 2786.5374 * HIC <sup>(m1 + q0 * (SE + SW))</sup> * (HMC <sup>(m2 + (RDAF * m3))</sup> )	m1	-1715.43	3444.86	7.90	0.573	0.804	0.575	0.805
[3.18] (m0 * HIC <sup>m1</sup> ) * (HMC <sup>(m2 + (RDAB * m3) + q0 * (SE + SW))</sup> )	m1	-1715.53	3447.05	7.90	0.569	0.803	0.573	0.805

**Table B3 cont.** Models evaluated for goodness of fit to specific leaf area

SLA Model	Rand	LL	AIC	RMSE	Adjusted R <sup>2</sup>		Generalized R <sup>2</sup>	
					Fixed	Fixed + Rand	Fixed	Fixed + Rand
[3.19] (m0 * HIC^m1) * (HMC^(m2 + (RPAB * m3) + q0 * (SE + SW)))	m1	-1715.53	3447.05	7.90	0.569	0.803	0.573	0.805
[3.20] (1177.39008344619 * HIC^m1) * (HMC^(m2 + (RPAB * m3) + q0 * (SE + SW)))	m1	-1716.05	3446.11	7.92	0.553	0.803	0.556	0.804
[3.21] m0 * HIC^(m1 + q0 * (SE + SW)) * (HMC^(m2 + (RDAB * m3)))	m1	-1716.11	3448.22	7.91	0.569	0.803	0.573	0.804
[3.22] m0 * HIC^(m1 + q0 * (SE + SW)) * (HMC^(m2 + (RPAB * m3)))	m1	-1716.11	3448.22	7.91	0.569	0.803	0.573	0.804
[3.23] (m0 * HIC^(m1 + (m4 * (BD/10)))) * (HMC^(m2 + (RDAF * m3)))	m1	-1717.33	3450.66	7.94	0.571	0.801	0.574	0.803
[3.24] (m0 * HIC^m1) * (HMC^(m2 + (RDAF * m3)))	m1	-1717.61	3449.22	7.94	0.568	0.802	0.571	0.803
[3.25] 2457.9909 * (HIC^m1) * (HMC^(m2 + (RDAF * m3)))	m1	-1717.61	3447.22	7.94	0.569	0.802	0.571	0.803
[3.26] (m0 * HIC^m1) * (DBH^(m2 + (RDAF * m3)))	m1	-1717.84	3449.68	7.94	0.528	0.802	0.531	0.803
[3.27] (m0 * HIC^m1) * (HMC^(m2 + (RPAB * m3)))	m1	-1718.33	3450.66	7.95	0.565	0.801	0.568	0.802
[3.28] (2377.89121267239 * HIC^m1) * (HMC^(m2 + (RPAB * m3)))	m1	-1718.33	3448.66	7.95	0.566	0.802	0.568	0.802
[3.29] (m0 * HIC^m1) * (DBH^(m2 + (RPAB * m3)))	m1	-1718.48	3450.95	7.95	0.527	0.801	0.530	0.802
[3.30] m0 * HMC^(m1 + q0 * (SE + SW)) * (HIC^(m2 + (RPAB * m3)))	m1	-1721.55	3459.11	8.02	0.547	0.797	0.551	0.799
[3.31] m0 * HMC^(m1 + q0 * (SE + SW)) * (HIC^(m2 + (RDAB * m3)))	m1	-1721.55	3459.11	8.02	0.547	0.797	0.551	0.799
[3.32] (m0 * HMC^m1) * (HIC^(m2 + (RDAF * m3) + q0 * (SE + SW)))	m1	-1721.61	3459.22	8.02	0.549	0.797	0.553	0.799
[3.33] (1196.4444 * HMC^m1) * (HIC^(m2 + (RDAF * m3) + q0 * (SE + SW)))	m1	-1721.61	3457.22	8.02	0.550	0.797	0.553	0.799
[3.34] (m0 * HIC^m1) * (HMC^(m2 + (PAB * m3) + q0 * (SE + SW)))	m1	-1721.79	3459.57	8.01	0.573	0.798	0.577	0.800
[3.35] m0 * HIC^(m1 + q0 * (SE + SW)) * (HMC^(m2 + (PAB * m3)))	m1	-1722.15	3460.30	8.01	0.573	0.798	0.576	0.799

**Table B3 cont.** *Models evaluated for goodness of fit to specific leaf area*

SLA Model	Rand	LL	AIC	RMSE	Adjusted R <sup>2</sup>		Generalized R <sup>2</sup>	
					Fixed	Fixed + Rand	Fixed	Fixed + Rand
[3.36] (m0 * HMC^m1) * (HIC^(m2 + (RDAB * m3) + q0 * (SE + SW)))	m1	-1722.40	3460.79	8.04	0.547	0.796	0.551	0.798
[3.37] (m0 * HMC^m1) * (HIC^(m2 + (RPAB * m3) + q0 * (SE + SW)))	m1	-1722.40	3460.79	8.04	0.547	0.796	0.551	0.798
[3.38] m0 * HMC^(m1 + q0 * (SE + SW)) * (HIC^(m2 + (PAB * m3)))	m1	-1724.67	3465.34	8.07	0.554	0.795	0.557	0.796
[3.39] (m0 * HMC^m1) * (HIC^(m2 + (PAB * m3) + q0 * (SE + SW)))	m1	-1725.26	3466.51	8.08	0.553	0.794	0.557	0.796
[3.40] (m0 * HIC^m1) * ((RDAF + 1e-04)^m2) * (HMC^m3) * (ATBL^m4)	m1	-1728.99	3473.99	8.13	0.562	0.792	0.565	0.793
[3.41] (m0 * HIC^m1) * ((RPAB + 1e-04)^m2) * (DBH^m3)	m1	-1729.08	3472.16	8.13	0.518	0.792	0.521	0.793
[3.42] (m0 * HIC^m1) * ((RDAF + 1e-04)^m2) * (HMC^m3) * (FL^m4)	m1	-1729.15	3474.30	8.13	0.560	0.792	0.563	0.793
[3.43] (m0 * HIC^m1) * ((RPAB + 1e-04)^m2) * (HMC^m3)	m1	-1729.25	3472.49	8.14	0.561	0.792	0.563	0.793
[3.44] (3058.77057036259 * HIC^m1) * ((RPAB + 1e-04)^m2) * (HMC^m3)	m1	-1729.25	3470.49	8.14	0.562	0.792	0.563	0.793
[3.45] (m0 * HIC^m1) * ((RDAF + 1e-04)^m2) * exp(DBH * m3)	m1	-1729.61	3473.21	8.14	0.535	0.792	0.538	0.793
[3.46] (2698.23 * HIC^m1) * ((RDAF + 1e-04)^m2) * (HMC^m3) * exp((BD/10) * m4)	m1	-1729.75	3473.50	8.14	0.558	0.791	0.561	0.793
[3.47] (m0 * HIC^m1) * ((RDAF + 1e-04)^m2) * (DBH^m3)	m1	-1729.91	3473.83	8.14	0.513	0.791	0.516	0.793
[3.48] (2698.23 * HIC^m1) * ((RDAF + 1e-04)^m2) * (HMC^m3) * ((BD/10)^m4)	m1	-1729.93	3473.86	8.15	0.555	0.791	0.557	0.793
[3.49] (m0 * HIC^m1) * ((RDAF + 1e-04)^m2) * (HMC^m3)	m1	-1729.93	3473.87	8.15	0.555	0.791	0.558	0.793
[3.50] (2698.23 * HIC^m1) * ((RDAF + 1e-04)^m2) * (HMC^m3)	m1	-1729.93	3471.87	8.15	0.556	0.792	0.558	0.793

**Table B3 cont.** *Models evaluated for goodness of fit to specific leaf area*

SLA Model	Rand	LL	AIC	RMSE	Adjusted R <sup>2</sup>		Generalized R <sup>2</sup>	
					Fixed	Fixed + Rand	Fixed	Fixed + Rand
[3.51] (m0 * HIC^m1) * ((RDAF + 1e-04)^m2) * (DBLC^m3)	m1	-1729.97	3473.94	8.16	0.485	0.790	0.488	0.792
[3.52] (m0 * HIC^m1) * ((RDAF + 1e-04)^m2) * (TH^m3)	m1	-1730.12	3474.24	8.15	0.545	0.791	0.548	0.792
[3.53] (m0 * HIC^m1) * ((RDAF + 1e-04)^m2) * (CL^m3)	m1	-1730.71	3475.42	8.16	0.523	0.790	0.526	0.792
[3.54] (m0 * HIC^m1) * ((RDAF + 1e-04)^m2) * (HBLC^m3)	m1	-1734.12	3482.24	8.21	0.489	0.788	0.492	0.789
[3.55] (m0 * HIC^m1) * ((RPAB + 1e-04)^m2)	m1	-1734.30	3480.60	8.22	0.457	0.788	0.459	0.789
[3.56] (m0 * HIC^m1) * ((RDAF + 1e-04)^m2)	m1	-1734.51	3481.02	8.22	0.464	0.788	0.466	0.789
[3.57] (m0 * HIC^m1) * ((DAF + 1e-04)^m2)	m1	-1737.16	3486.33	8.27	0.464	0.785	0.466	0.786
[3.58] (m0 * HIC^m1) * ((PAB + 1e-04)^m2)	m1	-1737.59	3487.18	8.27	0.452	0.785	0.454	0.786
[3.59] (m0 * HIC^m1) * ((RDAB + 1e-04)^m2)	m1	-1738.81	3489.62	8.30	0.461	0.784	0.463	0.785
[3.60] (m0 * HIC^m1) * ((DAB + 1e-04)^m2)	m1	-1743.38	3498.76	8.38	0.459	0.779	0.461	0.780
[3.61] (m0 * HIC^m1) * exp(m2 * (BD/10))	m1	-1747.99	3507.97	8.47	0.471	0.775	0.473	0.775
[3.62] (m0 * HIC^m1) * ((BD/10)^m2)	m1	-1748.73	3509.47	8.48	0.459	0.774	0.461	0.775
[3.63] (m0 * HIC^m1)	m1	-1748.95	3507.89	8.48	0.450	0.775	0.451	0.775
[3.64] (m0 + HIC * m1) + (DAF * m2)	m0	-1753.84	3519.68	8.56	0.490	0.770	0.492	0.771
[3.65] (m0 + HIC * m1) + (DAB * m2)	m0	-1754.20	3520.39	8.56	0.487	0.770	0.489	0.771
[3.66] (m0 + HIC * m1) + (RDAF * m2)	m0	-1760.39	3532.79	8.67	0.454	0.764	0.456	0.765
[3.67] (m0 + HIC * m1) + (RDAB * m2)	m0	-1761.18	3534.36	8.68	0.453	0.763	0.455	0.764
[3.68] (m0 + HIC * m1) + (RPAB * m2)	m0	-1761.18	3534.36	8.68	0.453	0.763	0.455	0.764
[3.69] (m0 + HIC * m1) + (PAB * m2)	m0	-1769.34	3550.69	8.83	0.423	0.755	0.426	0.756
[3.70] (m0 + HIC * m1) + (RDAF * m2) + (HMC * m3) + (NE * q0) + (SE * q1) + (NW * q2)	m1	-1786.54	3593.07	9.10	0.393	0.738	0.400	0.741
[3.71] (m0 * HIC^m1) * ((RDAF + 1e-04)^m2) * (1 + q0 * NE) * (1 + q1 * SE) * (1 + q2 * NW)	m1	-1796.31	3608.62	9.64	0.472	0.700	0.478	0.704

**Table B3 cont.** Models evaluated for goodness of fit to specific leaf area

SLA Model	Rand	LL	AIC	RMSE	Adjusted R <sup>2</sup>		Generalized R <sup>2</sup>	
					Fixed	Fixed + Rand	Fixed	Fixed + Rand
[3.72] $(m_0 * HIC^{m_1}) * ((DAF + 1e-04)^{m_2}) * (1 + q_0 * NE) * (1 + q_1 * SE) * (1 + q_2 * NW)$	m1	-1796.51	3609.02	9.65	0.473	0.700	0.478	0.703
[3.73] $(m_0 + HIC * m_1) + (RDAF * m_2) + (NE * q_0) + (SE * q_1) + (NW * q_2)$	m1	-1838.42	3694.83	10.35	0.513	0.661	0.518	0.664
[3.74] $(m_0 * RHIC^{m_1}) * ((BD/10)^{m_2})$	m1	-1843.08	3698.15	10.36	0.359	0.662	0.362	0.664
[3.75] $(m_0 * RHIC^{m_1})$	m1	-1847.08	3704.17	10.42	0.300	0.659	0.302	0.660
[3.76] $(m_0 + HIC * m_1) + (RPAF * m_2)$	m1	-1853.25	3718.50	10.66	0.470	0.642	0.472	0.644
[3.77] $(m_0 * RDIC^{m_1})$	m1	-1886.87	3783.74	11.35	0.293	0.596	0.294	0.597
[3.78] $(m_0 * RHIC^{m_1}) * ((RDAF + 1e-04)^{m_2}) * (1 + q_0 * NE) * (1 + q_1 * SE) * (1 + q_2 * NW)$	m1	-1901.56	3819.11	12.00	0.301	0.536	0.308	0.541
[3.79] $(m_0 * HIC^{m_1}) * (RPAF^{m_2})$	m1	-2129.70	4271.39	19.01	-0.461	-0.140	-0.455	-0.135

**Table B4** Models evaluated for goodness of fit to Weibull kurtosis parameter estimates

Weibull kurtosis model	Rand	LL	AIC	RMSE	Adjusted R <sup>2</sup>		Generalized R <sup>2</sup>	
					Fixed	Fixed + Rand	Fixed	Fixed + Rand
[3.2] $h_0 * (HBLC^{(h_1 + (q_0 * SW))}) * (TBL^{h_2}) * \exp(RDIC * h_3)$	h2	50.56	-87.13	0.1325	0.346	0.346	0.378	0.378
[3.80] $h_0 * (HBLC^{(h_1)}) * (TBL^{(h_2)}) * \exp((RDIC * h_3) + (q_0 * SW))$	h2	49.98	-85.96	0.1335	0.337	0.337	0.369	0.369
[3.81] $(h_0 * (1 + (q_0 * SW))) * (HBLC^{(h_1)}) * (TBL^{(h_2)}) * \exp(RDIC * h_3)$	h2	49.98	-85.96	0.1335	0.337	0.337	0.369	0.369
[3.82] $h_0 * (HBLC^{(h_1)}) * (TBL^{(h_2 + (q_0 * SW))}) * \exp(RDIC * h_3)$	h2	49.80	-85.59	0.1338	0.334	0.334	0.366	0.366
[3.83] $h_0 * (HBLC^{h_1}) * (TBL^{h_2}) * \exp(RDIC * h_3)$	h2	47.49	-82.98	0.1375	0.305	0.305	0.331	0.331
[3.84] $h_0 * (TBL^{(h_1 + (h_2 * (BD/10))})) * \exp(RDIC * h_3)$	h2	46.24	-80.49	0.1390	0.284	0.296	0.310	0.321

**Table B4 cont.** Models evaluated for goodness of fit to Weibull kurtosis parameter estimates

Weibull kurtosis model		Rand	LL	AIC	RMSE	Adjusted R <sup>2</sup>		Generalized R <sup>2</sup>	
						Fixed	Fixed + Rand	Fixed	Fixed + Rand
[3.85]	$h_0 * (TBL^{h1}) * \exp((RDIC * h2) + (CLR * h3))$	h2	46.17	-80.34	0.1385	0.283	0.307	0.309	0.332
[3.86]	$h_0 * (CLR^{h1}) * (TBL^{h2}) * \exp(RDIC * h3)$	h2	46.04	-80.08	0.1391	0.281	0.296	0.307	0.321
[3.87]	$h_0 * (TBL^{h1}) * \exp((RDIC * h2) + ((BD/10) * h3))$	h2	45.81	-79.63	0.1397	0.277	0.289	0.303	0.314
[3.88]	$h_0 * (TBL^{h1}) * (RHIC^{h2})$	h2	45.01	-80.02	0.1410	0.272	0.285	0.290	0.302
[3.89]	$h_0 * (TBL^{h1}) * \exp(RDIC * h2)$	h2	44.97	-79.95	0.1375	0.267	0.348	0.285	0.363
[3.90]	$h_0 * (TBL^{h1}) * \exp(RHIC * h2)$	h2	44.75	-79.50	0.1407	0.267	0.294	0.285	0.311
[3.91]	$h_0 * (TBL^{h1}) * (RVD^{h2})$	h2	44.53	-79.06	0.1369	0.252	0.362	0.270	0.377
[3.92]	$h_0 * (TBL^{h1}) * (RDIC^{h2})$	h2	44.07	-78.14	0.1432	0.256	0.256	0.274	0.274
[3.93]	$h_0 * (TBL^{h1}) * \exp(RVD * h2)$	h2	44.01	-78.01	0.1419	0.254	0.283	0.272	0.300
[3.94]	$h_0 * (TBL^{h1}) * (VD^{h2})$	h2	43.84	-77.68	0.1399	0.248	0.322	0.266	0.338
[3.95]	$h_0 * (TBL^{h1}) * \exp(DIC * h2)$	h2	43.66	-77.32	0.1378	0.236	0.358	0.254	0.373
[3.96]	$h_0 * (TBL^{h1}) * (DIC^{h2})$	h2	43.49	-76.97	0.1393	0.238	0.336	0.256	0.352
[3.97]	$h_0 * (TBL^{h1}) * \exp(VD * h2)$	h2	43.24	-76.48	0.1446	0.241	0.241	0.259	0.259
[3.98]	$h_0 * (TBL^{h1}) * \exp((BD/10) * h2)$	h2	42.58	-75.17	0.1454	0.229	0.237	0.248	0.255
[3.99]	$h_0 * (ATBL^{h1})$	h0	41.82	-75.64	0.1449	0.223	0.268	0.232	0.277
[3.100]	$h_0 * (TBL^{h1}) * ((BD/10)^{h2})$	h2	41.55	-73.10	0.1476	0.210	0.210	0.229	0.229
[3.101]	$h_0 * (TBL^{h1})$	h0	41.26	-74.53	0.1462	0.213	0.252	0.223	0.261
[3.102]	$h_0 * \exp(RDIC * h1)$	h0	40.95	-73.90	0.1486	0.208	0.208	0.218	0.218
[3.103]	$h_0 * \exp(RHIC * h1)$	h0	40.95	-73.90	0.1486	0.208	0.208	0.218	0.218
[3.104]	$h_0 * (DIC^{h1})$	h0	40.74	-73.49	0.1448	0.198	0.285	0.207	0.294
[3.105]	$h_0 * (RHIC^{h1})$	h0	40.60	-73.20	0.1435	0.189	0.308	0.199	0.317
[3.106]	$h_0 * (RDIC^{h1})$	h0	40.47	-72.95	0.1495	0.199	0.199	0.209	0.209
[3.107]	$h_0 * \exp(DIC * h1)$	h0	40.36	-72.71	0.1497	0.197	0.197	0.207	0.207
[3.108]	$h_0 * (RVD^{h1})$	h0	40.05	-72.11	0.1434	0.173	0.317	0.183	0.325
[3.109]	$h_0 * \exp(RVD * h1)$	h1	40.04	-72.07	0.1502	0.191	0.191	0.201	0.201

**Table B4 cont.** *Models evaluated for goodness of fit to Weibull kurtosis parameter estimates*

Weibull kurtosis model	Rand	LL	AIC	RMSE	Adjusted R <sup>2</sup>		Generalized R <sup>2</sup>	
					Fixed	Fixed + Rand	Fixed	Fixed + Rand
[3.110] h0 * (FL^h1)	h0	39.98	-71.97	0.1483	0.188	0.232	0.198	0.242
[3.111] h0 * exp(ATBL * h1)	h0	39.14	-70.28	0.1518	0.173	0.173	0.183	0.183
[3.112] h0 * exp(TBL * h1)	h0	38.63	-69.27	0.1528	0.163	0.163	0.173	0.173
[3.113] h0 * exp(HIC * h1)	h0	38.36	-68.73	0.1437	0.118	0.328	0.128	0.336
[3.114] h0 * exp(FL * h1)	h0	37.44	-66.88	0.1549	0.139	0.139	0.150	0.150
[3.115] h0 * ((BD/10)^h1)	h0	37.38	-66.76	0.1551	0.138	0.138	0.148	0.148
[3.116] h0 * (HIC^h1)	h0	37.34	-66.67	0.1551	0.137	0.137	0.147	0.147
[3.117] h0 * (VD^h1)	h0	35.42	-62.84	0.1587	0.097	0.097	0.108	0.108
[3.118] h0 * exp(VD * h1)	h1	35.28	-62.56	0.1590	0.094	0.094	0.105	0.105
[3.119] h0 * exp((BD/10) * h1)	h0	34.86	-61.72	0.1598	0.085	0.085	0.096	0.096
[3.120] h0 * ((LTF + 1e-04)^h1)	h0	34.57	-61.14	0.1603	0.078	0.078	0.089	0.089

**Table B5** Models evaluated for goodness of fit to Weibull skew parameter estimates

Weibull skew model	Rand	LL	AIC	RMSE	Adjusted R <sup>2</sup>		Generalized R <sup>2</sup>	
					Fixed	Fixed + Rand	Fixed	Fixed + Rand
[3.121] $(h_0 * (1 + (q_0 * SW))) * (RDIC^{h_1}) * ((BD/10)^{h_2})$	h0	-79.9	171.73	0.5931	0.133	0.307	0.165	0.332
[3.122] $(h_0) * (RDIC^{h_1}) * ((BD/10)^{h_2}) * \exp(q_0 * SW)$	h0	-79.9	171.73	0.5931	0.133	0.307	0.165	0.332
[3.3] $h_0 * (RDIC^{h_1}) * ((BD/10)^{h_2})$	h0	-81.1	172.22	0.5952	0.105	0.319	0.127	0.335
[3.123] $(h_0 * (1 + (q_0 * SW))) * (RDIC^{h_1})$	h0	-82.3	174.56	0.6144	0.101	0.259	0.122	0.277
[3.124] $h_0 * \exp(HIC * h_1)$	h0	-82.4	172.9	0.6058	0.090	0.302	0.101	0.310
[3.125] $h_0 * \exp(VD * h_1)$	h0	-82.9	173.74	0.6060	0.075	0.305	0.086	0.313
[3.126] $h_0 * (RDIC^{h_1})$	h0	-83.1	174.15	0.6127	0.081	0.283	0.092	0.292
[3.127] $h_0 * \exp(RDIC * h_1)$	h0	-83.3	174.61	0.6128	0.072	0.285	0.083	0.293
[3.128] $h_0 * \exp(RHIC * h_1)$	h0	-83.3	174.62	0.6131	0.073	0.284	0.084	0.292
[3.129] $h_0 * \exp(RVD * h_1)$	h0	-83.4	174.75	0.6119	0.068	0.289	0.079	0.297
[3.130] $h_0 * \exp(DIC * h_1)$	h0	-83.5	174.95	0.6078	0.053	0.304	0.064	0.312
[3.131] $h_0 * (RVD^{h_1})$	h0	-83.8	175.68	0.6149	0.057	0.282	0.068	0.291
[3.132] $h_0 * (RHIC^{h_1})$	h0	-84.4	176.72	0.6201	0.048	0.268	0.059	0.277
[3.133] $h_0 * (VD^{h_1})$	h0	-85.6	179.17	0.6703	0.060	0.060	0.071	0.071
[3.134] $h_0 * (HIC^{h_1})$	h0	-85.8	179.53	0.6334	0.022	0.233	0.034	0.242
[3.135] $h_0 * (DIC^{h_1})$	h0	-86.1	180.17	0.6743	0.049	0.049	0.060	0.060